
# POLITECNICO DI MILANO

## MASTER OF SCIENCE

**In**

**Civil Engineering for Risk Mitigation**

## ANALYSIS OF SEDIMENT PARTICLE MOTION ON A SMOOTH BED

A Master thesis
by

**Md. Sazadul Hasan**

Supervisor:

**Dr. Alessio RADICE**

Co-supervisor:

**Dr. Jenny CAMPAGNOL**

OCTOBER 2013

# POLITECNICO DI MILANO

## ANALYSIS OF SEDIMENT PARTICLE MOTION ON A SMOOTH BED

A Master thesis submitted to Department of Civil and Environmental Engineering in partial fulfillment of the requirements for the degree of **Master of Science in Civil Engineering for Risk Mitigation**.


**Submitted by:**

**Md. Sazadul Hasan**
Student ID: 783122
Session: 2011-2012

**Supervised by:**

**Dr. Alessio Radice**

Assistant Professor
Dept. of Civil and Environmental Engineering
Politecnico di Milano
Piazza L. da Vinci, 32
I-20133 Milan

**Co-supervised by:**

**Dr. Jenny Campagnol**

Dept. of Civil and Environmental Engineering
Politecnico di Milano
Piazza L. da Vinci, 32
I-20133 Milan

ABSTRACT (English)

Recent researches on the dynamics of sediment transport have been focused on the particle motion characteristics at small spatial scale, down to the particle scale or even smaller. Quantitative imaging techniques have been successfully introduced into the area of sediment transport to ensure the level of detail requested by the above-mentioned research. The research documented in this Thesis has considered the characteristics of motion of bed-load particles on a smooth bed, identifying and tracking each moving grain. The data used in this work were obtained from laboratory experiment which had been previously carried out under an extensive project at the Politecnico di Milano.

The software package Streams was used for image processing to obtain the particle trajectories, from which characteristics of individual particle motion were extracted for quantitative analysis. In total, 55 movies were processed for three experimental discharges of 8 l/s, 11.1 l/s and 13 l/s. All the results from particle tracking have been manually validated superimposing the measured trajectories to ongoing movies of particle motion, for full reliability of the results. The measurement finally produced a data sample of 2219 long trajectories that were then used for a statistical analysis.

The statistical parameters mean ($\mu$), standard deviation ($\delta$), coefficient of variation ($C_v$), skewness ($S_k$) and kurtosis ($K_u$) have been analysed for the variables angle of deviation ($\alpha$), velocity along the flowing direction ($V_x$), velocity along the transverse direction of flow ($V_y$) and tortuosity ($T_{tor}$). All the mentioned properties were trajectory-averaged, leaving the analysis of instantaneous values for follow-up studies. During the analysis, the longitudinal velocity ($V_x$) was recognized as being the most significant property for the smooth bed configuration, since the particle motion was substantially straight and thus the angle of deviation, transverse velocity and tortuosity yielded somehow trivial results. The trajectory-averaged particle velocity over a smooth bed resulted to be an increasing function of the hydrodynamic properties of the flow (e.g., the shear velocity). The pdfs and cdfs of longitudinal velocity were also studied, finding that they became progressively more right skewed with increasing discharges.

The characteristics of particle motions over a smooth bed were finally compared with those over a rough bed configuration, finding significant differences in the two kinds of motion. These data can thus support analysis of the contribution of bed roughness on bed-load sediment motion.

**Keywords**: sediment transport; particle motion; bed configuration; smooth bed; particle tracking; image processing.

ABSTRACT (Italian)

La ricerca sulla dinamica del trasporto solido si è recentemente concentrate sulle caratteristiche del moto delle particelle a scale di dettaglio, uguali o anche inferiori alla dimensione dei singoli grani, con una raffinatezza resa possibile anche dall'introduzione di sofisticate tecniche di analisi di immagine. La ricerca documentata in questa Tesi si inquadra in questo filone, avendo riguardato le caratteristiche del moto di granelli su un fondo liscio e avendo analizzato il moto di ogni singola particella. Sono stati usati dati sperimentali prodotti durante una campagna di laboratorio precedentemente condotta presso il Politecnico di Milano.

Le traiettorie delle particelle sono state ottenute da filmati degli esperimenti tramite il software Streams; successivamente, le quantità di interesse sono state dedotte dalle traiettorie per l'analisi successiva. In totale sono stati processati 55 filmati per le tre portate di 8 l/s, 11.1 l/s e 13 l/s. Tutti i risultati relativi alla fase di tracciamento delle particelle sono stati manualmente validati sovrapponendo le immagini degli esperimenti alle traiettorie misurate, in modo da garantire l'affidabilità delle misure. Il campione ottenuto contiene i dati di 2219 traiettorie, che sono stati usati per un'analisi statistica.

Sono state considerate le seguenti quantità: angolo di deviazione ($\alpha$), velocità parallela al flusso idrico ($V_x$), velocità trasversale ($V_y$) e tortuosità ($T_{tor}$). Tutte queste proprietà sono state considerate con riferimento al valore mediato sulla traiettoria, mentre l'analisi dei valori istantanei dovrà essere oggetto degli studi successivi. Per tutte le quantità sono state considerate le statistiche di sintesi: media ($\mu$), deviazione standard ($\delta$), coefficiente di variazione ($C_v$), skewness ($S_k$) e kurtosi ($K_u$). l'analisi ha mostrato come la proprietà di maggiore interesse fosse la velocità parallela al flusso, in quanto il moto delle particelle era sostanzialmente allineato con la corrente quindi le statistiche delle altre proprietà non fornivano risultati particolarmente significativi. La velocità media della particelle è risultata essere una funzione crescente della sollecitazione idrodinamica (espressa per esempio tramite le velocità di attrito). Le distribuzioni (pdf, cdf) della $V_x$ sono risultate progressivamente più asimmetriche al crescere della portata.

Le caratteristiche del moto dei grani su fondo liscio sono state confrontate con le omologhe su fondo scabro, ottenendo significative differenze la cui analisi potrà essere di supporto all'analisi del contributo della scabrezza del fondo alle proprietà del trasporto solido.

**Parole chiave**: trasporto solido; moto delle particelle; configurazione del letto; fondo liscio; particle tracking; elaborazione di immagini.

# DEDICATION

This thesis is dedicated to my father, who taught me that the best kind of study is that which is studied for its own sake; to my mother, who taught me the importance of study in my life; to my younger uncle who have supported me all the way of my study life since beginning; to my brother who have supported me at every step in my life.

Finally, this thesis is dedicated to all those who believe in the richness of learning.

# ACKNOWLEDGEMENTS

At first thanks to almighty ALLAH, I wish to express my sincere gratitude to my supervisor, Dr. Alessio Radice, whose expertise, understanding and patience added considerably to my graduate experience and supported me throughout the work.

A very special thanks to my co-supervisor Dr. Jenny Campagnol, who in spite of his busy schedule always found time for helping me in my research and solved the problems related to it.

I am grateful to all members of the hydraulic research group specially Campagnol, Bulankina, Lescova and Bergami who performed experimental campaign what I used in this research, during their study at the Politecnico di Milano to support me accomplish the thesis successfully.

I am also very grateful to friends and colleagues, for the inspiration through my study. Who played such important roles along the journey, as we mutually engaged in making sense of the various challenges we faced and in providing encouragement to each other at those times when it seemed impossible to continue.

I am thankful to my all professors for the assistance they provided at all levels during my study. Thanks to Politecnico di Milano for educational funding. Thanks to my parents for encouraging me all the time for my studies and for the support they have provided me through my entire life.

# LIST OF TABLES

**Table 1.1**: Size classification of sediment.

**Table 2.1**: List of the number of measurements for SB runs.

**Table 2.2**: Shear velocities for all tested discharges.

**Table 2.3**: Summarized all values in calculation of Shear velocity by Moody diagram.

**Table 2.4:** Shear velocities for all tested discharges.

**Table 2.5:** Near bed velocities in smooth bed configuration.

**Table 3.1**: List of the number of measurements for SB runs.

**Table 4.1**: Moments ($\mu$, $\delta$, $C_v$, $S_k$ and $K_u$) of the variables $\alpha$ (degree), $V_x$ (mm/s), $V_y$ (mm/s) and $T_{tor}$ (mm/mm).

**Table 4.2**: Angle of deviation moments for experimental discharges.

**Table 4.3**: Longitudinal velocity moments for experimental discharges.

**Table 4.4**: Transverse velocity moments for experimental discharges.

**Table 4.5**: Tortuosity moments for experimental discharges.

**Table 4.6**: Moments in smooth bed and rough bed configuration.

**Table 4.7**: Bulk and shear velocities in both bed configuration.

**Table 4.8**: Bulk, shear and near bed velocities in both bed configurations.

# LIST OF FIGURES

**Figure 1.1**: Total sediment load.

**Figure 1.2**: Typical Bed load and Suspended movement in river or channel.

**Figure 1.3**: Sediment movement in river.

**Figure 1.4**: Velocity and Concentration distribution of sediment.

**Figure 1.5**: Concept of the angle of repose.

**Figure 1.6**: Examples of angle of repose.

**Figure 1.7**: Forces acting on sediment.

**Figure 1.8**: Forces acing on a grain resting on a ground.

**Figure 1.9**: Conceptual representation of a particle trajectory consisting of three different ranges of scales: local, intermediate and global (Nikora et al., 2002).

**Figure 2.1**: Channel configuration at the Hydraulics Laboratory.

**Figure 2.2**: Flow meter.

**Figure 2.3**: Camera position for movie recording, side view.

**Figure 2.4**: Probes position for taking velocity profiles of flow and Doppler 2000.

**Figure 2.5**: Position of echo-sounder probe downstream; Sketch and real view.

**Figure 2.6**: Mean velocity profile for smooth bed configuration. a) Streamwise component. b) Vertical component.

**Figure 2.7**: Comparison of Mean velocity profiles for smooth bed & rough bed configurations. a) Streamwise component. b) Vertical component.

**Figure 2.8**: For discharge 13.0 l/s, (a) Streamwise velocity profiles with depth (in logarithmic scale). (b) Linear part only.

**Figure 2.9**: The relation between Reynolds number and dimensionless velocity.

**Figure 2.10**: The relation between experimental discharges vs bulk velocity and near bed velocities.

**Figure 3.1**: (a) Original (resized) image and (b) Filtered image for same frame.

**Figure 3.2**: Identified particle for the same frame.

**Figure 3.3**: Particle tracking with few frames.

**Figure 3.4**: Interruption in moving particle track.

**Figure 3.5**: pdfs of length for discharge (a) 8 l/s, (b) 11.1 l/s and (c) 13.0 l/s.

**Figure 3.6**: Validation of long trajectories.

**Figure 3.7**: Validation of long trajectories.

**Figure 3.8**: The path length, $\mathcal{L}_p$, the straight length, $L_p$, and its longitudinal length Lpx and transversal length $L_{py}$.

**Figure 3.9**: (a) Distribution for left skewed and (b) Distribution for right skewed.

**Figure 4.1**: For all groups of data set; (a) Discharge vs mean angle of deviation and (b) Discharge vs standard deviation of angle of deviation.

**Figure 4.2**: For all groups of data set; Discharge vs (a) mean longitudinal velocity; (b) standard deviation of longitudinal velocity; (c) coefficient of variation of longitudinal velocity; (d) skewness of longitudinal velocity and (e) kurtosis of longitudinal velocity.

**Figure 4.3**: For all groups of data set; (a) Discharge vs mean transverse velocity; and (b) Discharge vs standard deviation of transverse velocity.

**Figure 4.4**: (a) Discharge vs mean tortuosity; and (b) Discharge vs standard deviation of tortuosity.

**Figure 4.5**: For smooth & rough bed configuration; Discharge vs (a) mean longitudinal velocity; (b) Standard deviation of longitudinal velocity; (c) Coefficient of variation of longitudinal velocity, (d) Skewness of longitudinal velocity and (e) Kurtosis of longitudinal velocity.

**Figure 4.6**: For smooth & rough bed configuration; Shear velocity vs (a) mean longitudinal velocity; (b) Standard deviation of longitudinal velocity; (c) Coefficient of variation of longitudinal velocity, (d) Skewness of longitudinal velocity and (e) Kurtosis of longitudinal velocity.

**Figure 4.7**: For smooth & rough bed configuration; Bulk velocity vs (a) mean longitudinal velocity; (b) Standard deviation of longitudinal velocity; (c) Coefficient of variation of longitudinal velocity, (d) Skewness of longitudinal velocity and (e) Kurtosis of longitudinal velocity.

**Figure 4.8**: For smooth & rough bed configuration; near bed velocity for full diameter distance vs (a) mean longitudinal velocity and (b) Standard deviation of longitudinal velocity.

**Figure 4.9**: For smooth & rough bed configuration; near bed velocity for half diameter distance vs (a) mean longitudinal velocity and (b) Standard deviation of longitudinal velocity.

**Figure 4.10**: For smooth & rough bed configuration; (a) Reynolds number vs dimensionless mean velocity; (b) Critical Reynolds number vs dimensionless mean velocity; (c) Reynolds number vs Standard deviation of dimensionless longitudinal velocity and (d) Critical Reynolds number vs Standard deviation of dimensionless longitudinal velocity.

**Figure 4.11**: For smooth & rough bed configuration; (a) Reynolds number vs dimensionless mean velocity; (b) Friction Reynolds number vs dimensionless mean velocity; (c) Reynolds number vs Standard deviation of dimensionless longitudinal velocity and (d) Friction Reynolds number vs Standard deviation of dimensionless longitudinal velocity.

**Figure 4.12**: For smooth & rough bed configuration; (a) Reynolds number vs dimensionless mean velocity; (b) Friction Reynolds number vs dimensionless mean velocity; (c) Reynolds number vs Standard deviation of dimensionless longitudinal velocity and (d) Friction Reynolds number vs Standard deviation of dimensionless longitudinal velocity.

**Figure 4.13**: For smooth & rough bed configuration; (a) Reynolds number vs dimensionless mean velocity; (b) Friction Reynolds number vs dimensionless mean velocity; (c) Reynolds number vs Standard deviation of dimensionless longitudinal velocity and (d) Friction Reynolds number vs Standard deviation of dimensionless longitudinal velocity.

**Figure 4.14**: Velocities for experimental discharges with corresponding bed configurations.

**Figure 4.15**: For discharge Q = 8 l/s; (a) Angle of deviation (degree) vs pdf; (b) Longitudinal velocity vs pdf; (c) Transverse velocity vs pdf and (d) Tortuosity vs pdf.

**Figure 4.16**: For discharge Q = 11.1 l/s_1st group; (a) Angle of deviation (degree) vs pdf; (b) Longitudinal velocity vs pdf; (c) Transverse velocity vs pdf and (d) Tortuosity vs pdf.

**Figure 4.17**: For discharge Q = 11.1 l/s_2nd group; (a) Angle of deviation (degree)

vs pdf; (b) Longitudinal velocity vs pdf; (c) Transverse velocity vs pdf and (d) Tortuosity vs pdf.

**Figure 4.18**: For discharge Q = 11.1 l/s_All (combined both group); (a) Angle of deviation (degree) vs pdf; (b) Longitudinal velocity vs pdf; (c) Transverse velocity vs pdf and (d) Tortuosity vs pdf.

**Figure 4.19**: Longitudinal velocity vs pdf of all groups for discharge Q = 11.1 l/s.

**Figure 4.20**: For discharge Q = 13.0 l/s_1st group; (a) Angle of deviation (degree) vs pdf; (b) Longitudinal velocity vs pdf; (c) Transverse velocity vs pdf and (d) Tortuosity vs pdf

**Figure 4.21**: For discharge Q = 13.0 l/s_2nd group; (a) Angle of deviation (degree) vs pdf; (b) Longitudinal velocity vs pdf; (c) Transverse velocity vs pdf and (d) Tortuosity vs pdf.

**Figure 4.22**: For discharge Q = 13.0 l/s_All (combined both group); (a) Angle of deviation (degree) vs pdf; (b) Longitudinal velocity vs pdf; (c) Transverse velocity vs pdf and (d) Tortuosity vs pdf.

**Figure 4.23**: Longitudinal velocity vs pdf of all groups for discharge Q = 13.0 l/s.

**Figure 4.24**: Longitudinal velocity vs pdf of all discharge Q = 8, 11.1 & 13.0 l/s.

**Figure 4.25**: (a) Dimensionless velocity (Vx/U) vs pdf and (b) Dimensionless velocity (Vx/U*) vs pdf for all discharge Q = 8, 11.1 & 13.0 l/s.

**Figure 4.26**: For discharge Q = 8.0 l/s; (a) Angle of deviation (degree) vs cdf; (b) Longitudinal velocity vs cdf; (c) Transverse velocity vs cdf and (d) Tortuosity vs cdf.

**Figure 4.27**: For discharge Q = 11.1 l/s_1st group; (a) Angle of deviation (degree) vs cdf; (b) Longitudinal velocity vs cdf; (c) Transverse velocity vs cdf and (d) Tortuosity vs cdf.

**Figure 4.28**: For discharge Q = 11.1 l/s_2nd group; (a) Angle of deviation (degree) vs cdf; (b) Longitudinal velocity vs cdf; (c) Transverse velocity vs cdf and (d) Tortuosity vs cdf.

**Figure 4.29**: For discharge Q = 11.1 l/s_All (combined both group; (a) Angle of deviation (degree) vs cdf; (b) Longitudinal velocity vs cdf; (c) Transverse velocity vs cdf and (d) Tortuosity vs cdf.

**Figure 4.30**: Longitudinal velocity vs cdf of all groups for discharge Q = 11.1 l/s.

**Figure 4.31**: For discharge Q = 13.0 l/s_1st group; (a) Angle of deviation (degree) vs cdf; (b) Longitudinal velocity vs cdf; (c) Transverse velocity vs cdf and (d) Tortuosity vs cdf.

**Figure 4.32**: For discharge Q = 13.0 l/s_2nd group; (a) Angle of deviation (degree) vs cdf; (b) Longitudinal velocity vs cdf; (c) Transverse velocity vs cdf and (d) Tortuosity vs cdf.

**Figure 4.33**: For discharge Q = 13.0 l/s_All (combined both group); (a) Angle of deviation (degree) vs cdf; (b) Longitudinal velocity vs cdf; (c) Transverse velocity vs cdf and (d) Tortuosity vs cdf.

**Figure 4.34**: Longitudinal velocity vs cdf of all groups for discharge Q = 13.0 l/s.

**Figure 4.35**: Longitudinal velocity vs cdf of all groups for all discharges.

**Figure 4.36**: (a) Dimensionless velocity ($V_x/U$) vs cdf and (b) Dimensionless velocity ($V_x/U^*$) vs cdf for all discharge Q = 8, 11.1 & 13.0 l/s.

# Table of Contents

ABSTRACT (English)……..……..……...i
ABSTRACT (Italian)……..……...ii
DEDICATION.……..iii
ACKNOWLEDGEMENTS..……..……..iv
LIST OF TABLES ……v
LIST OF FIGURES ……..vi

**INTRODUCTION**..... 4

**CHAPTER 1: THEORETICAL FOCUS & LITERATURE REVIEW ..... 9**

1.1 SEDIMENT TRANSPORT ..... 9
1.1.1 TOTAL LOAD OF SEDIMENT TRANSPORT..... 10
1.1.1.1 SUSPENDED LOAD ..... 11
1.1.1.2 BED LOAD ..... 11
1.1.1.3 DETERMINATION OF TOTAL LOAD ..... 12

1.2 CHARACTERISTICS OF AN OPEN CHANNEL ..... 14

1.3 PROPERTIES OF SEDIMENT..... 16
1.3.1 PHYSICAL PROPERTIES OF SEDIMENT..... 16
1.3.1.1 DIAMETER OF SEDIMENT ..... 16
1.3.1.2 SPECIFIC GRAVITY OR RELATIVE DENSITY ..... 17
1.3.1.3 POROSITY..... 17
1.3.1.4 ANGLE OF REPOSE (Ø) ..... 18
1.3.1.5 SETTLING VELOCITY..... 19
1.3.2 PROPERTIES OF THE FLOW..... 19
1.3.2.1 MEAN VELOCITY PROFILE..... 20
1.3.2.2 EDDY VISCOSITY PROFILE..... 20

1.4 SEDIMENT MOTION ..... 21
1.4.1 IMPORTANCE OF INCIPIENT MOTION OF THE PARTICLE..... 21
1.4.2 FORCES ACTING ON THE PARTICLE ..... 21
1.4.3 INCIPIENT OF SEDIMENT MOVEMENT ..... 22
1.4.4 ENTRAINMENT ..... 24
1.4.5 DISTRAINMENT..... 24

1.5 DIMENSIONLESS VARIABLES..... 25

1.6 RESEARCH BACKGROUND ..... 26

1.7 THE RESEARCH PROJECT IN WHICH THIS WORK TAKES PART ..... 29

1.8 OBJECTIVES..... 30

**CHAPTER 2: EXPERIMENTAL SETUP ..... 31**
2.1 INTRODUCTION ..... 31
2.2 EXPERIMENTAL SETUP ..... 32
2.2.1 CHANNEL AND SEDIMENT CHARACTERISTICS ..... 32
2.2.2 PROCEDURE OF EXPERIMENT ..... 33
2.2.3 MOVIE RECORDING ..... 34
2.2.4 VELOCITY MEASUREMENT ..... 35
2.3 CHARACTERISTICS OF FLOW ..... 38
2.3.1 VELOCITY PROFILE ..... 38
2.3.2 SHEAR VELOCITY AND BULK VELOCITY ..... 40
2.3.2.1 CALCULATION OF SHEAR VELOCITY BY MOODY DIAGRAM ..... 42
2.3.3 VELOCITIES NEAR BED ..... 44
**CHAPTER 3: IMAGE PROCESSING & VALIDATION ..... 46**
3.1 INTRODUCTION ..... 46
3.2 IMAGE PROCESSING ..... 46
3.2.1 FILTERING IMAGES ..... 47
3.2.2 IDENTIFICATION OF PARTICLES ..... 48
3.2.3 PARTICLE TRACKING ..... 49
3.2.4 OUTPUT OF PTV ..... 50
3.3 VALIDATION ..... 52
3.4 ANALYZED VARIABLES ..... 54
**CHAPTER 4: RESULTS & DISCUSSION ..... 57**
4.1 STATISTICAL ANALYSIS RESULTS ..... 57
4.1.1 COMPARISON OF MOMENTS ..... 58
4.1.1.1 ANGLE OF DEVIATION ..... 59
4.1.1.2 LONGITUDINAL VELOCITY ($V_X$) ..... 60
4.1.1.3 TRANSVERSE VELOCITY ($V_Y$) ..... 62
4.1.1.4 TORTUOSITY ($T_{TOR}$) ..... 63
4.1.2 COMPARISON OF MOMENTS WITH ROUGH BED ..... 65
4.1.2.1 MOMENTS WITH RESPECT TO DISCHARGE ..... 65
4.1.2.2 MOMENTS WITH RESPECT TO SHEAR VELOCITY (U*) ..... 67
4.1.2.3 MOMENTS WITH RESPECT TO BULK VELOCITY (U) ..... 69
4.1.2.4 MOMENTS WITH RESPECT TO NEAR BED VELOCITY ($U_D$) ..... 71
4.1.2.5 MOMENTS WITH RESPECT TO NEAR BED VELOCITY ($U_{D/2}$) ..... 71
4.1.2.6 MOMENTS WITH RESPECT TO DIMENSIONLESS VELOCITY ($V_X/U^*$) ..... 72
4.1.2.7 MOMENTS WITH RESPECT TO DIMENSIONLESS VELOCITY ($V_X/U$) ..... 74
4.1.2.8 MOMENTS WITH RESPECT TO DIMENSIONLESS VELOCITY ($V_X/U_D$) ..... 75

4.1.2.9 MOMENTS WITH RESPECT TO DIMENSIONLESS VELOCITY ($V_X/U_{D/2}$) ..... 76
4.1.3 COMPARISON OF VELOCITIES WITH ROUGH BED ..... 78

4.2 PROBABILITY DENSITY FUNCTIONS (PDFS) ..... 80
4.2.1 PDF FOR DISCHARGE Q = 8 L/S ..... 80
4.2.2 PDF FOR DISCHARGE Q = 11.1 L/S ..... 81
4.2.2.1 Q = 11.1 L/S _ 1ST GROUP ..... 81
4.2.2.2 Q = 11.1 L/S _ 2ND GROUP ..... 82
4.2.2.3 Q = 11.1 L/S _ ALL (COMBINED BOTH GROUP) ..... 83
4.2.2.4 COMPARISON OF ALL GROUPS OF DATA FOR Q = 11.1 L/S ..... 84
4.2.3 PDF FOR DISCHARGE Q = 13.0 L/S ..... 85
4.2.3.1 Q = 13.0 L/S _ 1ST GROUP ..... 85
4.2.3.2 Q = 13.0 L/S _ 2ND GROUP ..... 86
4.2.3.3 Q = 13.0 L/S _ ALL (COMBINED BOTH GROUP) ..... 87
4.2.3.4 COMPARISON OF ALL GROUPS OF DATA FOR Q = 13.0 L/S ..... 88
4.2.4 COMPARISON OF LONGITUDINAL VELOCITY ($V_X$) ..... 89
4.2.4.1 LONGITUDINAL VELOCITY PDF FOR ALL DISCHARGES ..... 89
4.2.4.2 PDF WITH DIMENSIONLESS VELOCITY FOR ALL DISCHARGES ..... 90

4.3 CUMULATIVE DENSITY FUNCTIONS (CDFS) ..... 91
4.3.1 CDF FOR DISCHARGE Q = 8 L/S ..... 91
4.3.2 CDF FOR DISCHARGE Q = 11.1 L/S ..... 92
4.3.2.1 Q = 11.1 L/S _ 1ST GROUP ..... 93
4.3.2.2 Q = 11.1 L/S _ 2ND GROUP ..... 93
4.3.2.3 Q = 11.1 L/S _ ALL (COMBINED BOTH GROUP) ..... 94
4.3.2.4 COMPARISON OF ALL GROUPS OF DATA FOR Q = 11.1 L/S ..... 95
4.3.3 CDF FOR DISCHARGE Q = 13.0 L/S ..... 96
4.3.3.1 Q = 13.0 L/S _ 1ST GROUP ..... 97
4.3.3.2 Q = 13.0 L/S _ 2ND GROUP ..... 97
4.3.3.3 Q = 13.0 L/S _ ALL (COMBINED BOTH GROUP) ..... 98
4.3.3.4 COMPARISON OF ALL GROUPS OF DATA FOR Q = 13.0 L/S ..... 99
4.3.4 COMPARISON OF LONGITUDINAL VELOCITY ($V_X$) ..... 100
4.3.4.1 LONGITUDINAL VELOCITY CDF FOR ALL DISCHARGES ..... 100
4.3.4.2 CDF WITH DIMENSIONLESS VELOCITY FOR ALL DISCHARGES ..... 101

CONCLUSIONS ..... 104
REFERENCES ..... 107

# INTRODUCTION

A clear understanding and assessment of sediment transport plays an important role in evolution of rivers, design of channels, estimation of sediment load transport, management process etc. On the other hand, present reliability of prediction formulae is still unsatisfactory despite strong research efforts have been made during the past decades. Inadequacy of theoretical relationships for quantifying the sediment transport rates have stimulated increasing attention onto the phenomenological aspects of the process resulting in extensive research on individual sediment particle mechanics. Such analysis of the sediment transport process is a challenging task as the path line of a particle in a flow is highly variable. A review of the most recent scientific developments regarding sediment transport shows that imaging techniques have been increasingly used as new methods to improve understanding of the fundamentals of sediment transport.

This work is the part of an extensive project carried out at the Politecnico di Milano, aimed at understanding the individual sediment particle motion and behaviour by using Lagrangian particle trajectory analysis. Since the particle motion is expected to result from the interaction of the moving sediments with (i) the flow turbulence, (ii) the bed roughness and (iii) other moving particles, the experimental campaign has been designed in order to try to separate the effects of these interactions. Particularly, different configurations of bed roughness have been used. The full experimental campaign thus comprises a fixed-rough-bed condition, a movable-rough-bed condition, a smooth-bed condition and a bed with artificial spherical obstacles, representing macro-roughness elements on the bed surface. The purpose of the research project is to analyze data for the different configurations separately, then to compare the obtained results.

In this context, the main objective of this work is to analyse the individual sediment particle motion for the smooth bed configuration. An image processing technique was implied to measure velocity, direction, tortuosity of trajectories. The statistic of these variables have been analyzed, put into relationship with the properties of the flow and finally compared to the corresponding results for the rough bed.

The laboratory experiments had been accomplished with white sediments on a black smooth bed configuration to simplify the tracking process. Image processing was performed by using the software package Streams, which was applied to the images taken from the

experiments to identify the moving sediment particles. Then, Particle Tracking Velocimetry (PTV) analysis was applied. All the obtained trajectories were manually validated for full reliability of the results. A wide statistical analysis in terms of moments of distributions, probability distribution functions and cumulative distribution functions was performed for the characteristics of the moving particle trajectories. The results from the statistical analysis were compared to the corresponding results for the rough bed configuration.

This advance analysing technique allows perceiving a very detailed phenomenon of the moving sediment particle. Introduced measurements and insights obtained with particle tracking velocimetry (PTV) analysis are an important image based tools for investigating the individual particle motion behaviour. Consequently, the PTV data allows extracting the velocity components by using the Lagrangian (high-speed system) approach.

When crumbled materials termed as sediments formed and transported by the natural action with flowing fluid or air is termed as sediment transport. Usually the significant part of the materials is transported as bed load and suspended load with flowing medium. Transported sediments fall mainly in cohesive and non-cohesive categories. Here non-cohesive sediments movement in open channel at small scale are the primary concern. Diameter, specific gravity, porosity, angle of repose, settling velocity etc. express the main properties of sediments where bulk velocity, shear stress, shear velocity, friction as the properties of a channel have an important role in sediment transport. Also the flow velocities, viscosities have an effect on sediment transport. Sediment movements in a liquid is variable, it can stop and change directions frequently. So sediment particle motion in flowing fluid is very significant to understand the characteristics. Sediment researches began very early in this century. The researchers have tried to unite the sediment transport at big scale. Einstein (1950) described the modes of sediment transport at different layers under turbulence. Bagnold (1966) developed his expression of a suspended load and bed load based on the energy conservation law. Meyer-Peter and. Muller (1948), Einstein (1950) and other scientists they developed the bed load transport formulas. Then, analysis moved to more detailed aspects of particle mechanics and particle tracking. Shinohara et al. (1958); West (1949); Kidson & Carr 1961); Dobbs (1958); Kidson et al. (1962); Longuet-Higgins & Parkin (1962), they used different particles to track the sediment movements. Paintal (1969) ; Rossinskiy & Lyubomirova (1969) ; Fernandez Luque & van Beek (1976) ; Nakagawa, Tsujimoto & Hosokawa (1980), they

introduced motion-picture photography or video recording techniques to study bedload transport which become leading and successful tool for sediment tracking. Drake et al. (1988) showed this technique is almost uniquely capable of detailed observation and quantitative information on both the modes of motion of individual bedload particles and the collective motions. Nikora et al. (2001) suggests model for longitudinal and transverse diffusion of moving bed particles under weak bed load transport that the particle motion is diffusive and comprises at least three ranges of temporal and spatial scales with different diffusion regimes; the local range (ballistic diffusion), the intermediate range (normal or anomalous diffusion) and the global range (sub diffusion). This conceptual mode have been used I this work. Very recent Lajeunesse et al. (2010) presented an experimental investigation on the bed load particle motion over a flat sediment bed of uniform grain size in turbulent flow at the grain scale. Also an extensive project is being undertaken at the Politecnico di Milano aimed to Lagrangian analysis of individual particle motion, accounting for trajectory-averaged and instantaneous particle velocities, properties of intermediate particle trajectories (intermediate in the sense of Nikora et al.'s model), diffusion of bed-load sediment particles and fractal properties of trajectories. Since the particle motion is expected to be influenced by turbulence, bed structure and other moving particle, the experimental campaign was designed to try to separate these effects, and thus experiments have been performed with different discharges, different bed configurations (smooth, fixed rough, movable rough, with macro-roughness elements). The objective of this work is to analyse of the experiments for smooth bed; processing of available images; validation of the tracking results; properties of particle motion in terms of velocity, direction, tortuosity of trajectories; statistical analysis in terms of moments of distributions and pdf, cdf; comparison with analogous results for the rough bed.

The laboratory experiments were performed before at the Hydraulics Laboratory of the Politecnico di Milano. It was carried out using 5.8 m long pressurized duct, with a cross section 40 cm wide and 11 cm high. White quasi-spherical PBT particles with an equivalent diameter 3 mm and density $\rho_s$ = 1.27 g/cm$^3$ were used. CCD camera with a frequency of 32 Hz was used. In total 55 movies were taken in five sequences. For flow discharge $Q_1$ = 8.0 l/s in total 19 movies in one sequence and discharges $Q_2$ = 11.1 l/s and $Q_3$ = 13.0 l/s in total 36 movies were taken in four sequences. Each video has duration of about 50 s. 11.1 l/s and 13.0 l/s were divided in two groups while taking images. The sediments were dropped into the duct

manually. Ultrasonic Doppler Velocity measuring technique was used to measure the velocity profiles for discharge 13.0 l/s then other shear velocities were calculated from linear approximation after analysing the relation by using Moody diagram. Also the near bed velocities were calculated by equation.

The software package Streams was used to make particle tracking by using the obtained images taken in the laboratory experiment. Streams allow removing image background to avoid uneven light or reflection. Particle was identified by the parameters of minimum, maximum diameter and image pixels. Particle tracking velocimetry was used to track the particles. The output of the PTV analysis was a matrix with values of position and velocity with time for each recognized particle. The pdfs of the length of particle movements showed for two groups for discharge in 11.1 l/s and 13.0 l/s. It showed group of data showed different characteristics. So it was analysed both separately and combined. Also to remove too short trajectories; less than 200 mm trajectories were discarded. Tracked particle path was validated by the superimposition of the images by MATLAB code. There were total 2219 validated long trajectories for three discharges 8, 11.1 and 13 l/s. After validation trajectory duration T, minimum distance or straight length $L_p$, travelled full path length $L_p$, the longitudinal distance of the trajectory $L_x$ and transverse direction $L_y$, the velocities of the particle motion also in longitudinal direction $V_x$, in transverse direction $V_y$, tortuosity $T_{tor}$ and the angle $\alpha$ for long trajectories were found as integral and instantaneous properties. But in post processing, the statistical parameters have been analyzed are mean ($\mu$), standard deviation ($\delta$), coefficient of variation ($C_v$), skewness ($S_k$) and kurtosis ($K_u$) for the variables angle of deviation ($\alpha$), velocity along the flowing direction ($V_x$), velocity along the transverse direction of flow ($V_y$) and tortuosity ($T_{tor}$) as integral properties. Also statistical distribution has been done for the analyzed variables mentioned above as probability distribution function and cumulative distribution function.

Results of statistical analysis of smooth bed showed that the angle of deviation increased with the increasing discharge but with very small negative value where the expected value was equal to zero. Here small negative values indicate that the camera was probably a bit skewed in comparison with the mean flow direction, but the angle is however not large. It deviated constantly from the mean. Longitudinal velocity increased with the increasing discharge but it deviated more from the mean velocity. The experimental data are more stable

for larger discharges. Longitudinal velocities turns from left skewed to right skewed with increasing discharges. Transverse velocity more deviated with the increasing discharge. The value of transverse velocity showed negative which was consistent with the values of angle of deviation. Tortuosity is decreased with the increasing discharge. Data were not varied much with respect to the mean value with increasing discharge and the experimental data are stable. The mean values of tortuosity were around 1 for all experimental discharges. Within the same discharges; combined set of data values have very small difference with 1st and 2nd groups of data and the values are within this two group values. So combined data was used as the data of corresponding discharge. Comparison of moments with respect to discharge, shear velocity, bulk velocity and near bed velocity for all experimental discharges has been considered. It showed the mean longitudinal velocity was increased in smooth bed configuration. Rough bed longitudinal velocities were deviated more from the mean value. Smooth bed velocities were more stable then rough bed data. Rough bed velocities more right skewed than smooth bed velocities. Dimensionless mean velocities with respect to bulk velocity, shear velocity, near bed velocities in smooth bed configuration were more and increased very rapidly compared to rough bed which was more or less constant. For rough bed shear velocity increased with increasing discharge and also it is higher compare to smooth bed configuration because the roughness was increased in rough bed. The velocity near bed for smooth bed configuration was slowly increased with increasing discharges. In pdf analysis, for discharge 11.1 and 13.0 l/s the pdfs of angle of deviation, longitudinal velocity, transverse velocity and tortuosity are similar. So in comparison, combined group data were used for discharge 11.1 and 13.0 l/s data. For very less tortuosity, the pdfs of tortuosity became very sharp peak near 1. For discharge 11.1 l/s, the pdfs of longitudinal velocities of different groups are same and weakly right skewed but for 13.0 l/s, longitudinal velocity pdfs were strongly right skewed as the tail in right was longer than left. All the pdfs of tortuosity showed same behaviour. The pdfs of dimensionless velocities ($V_x/U$) and ($V_x/U^*$) showed similar behaviour. The dimensionless velocities were increased with increasing discharges. It was also right skewed as right tail was longer than the left tail. The cdfs of longitudinal velocity for discharge 8.0 l/s were similar but for discharge 11.1 l/s and 13.0 l/s were asymmetric; in this case right tail is longer. It showed becoming asymmetric with increasing discharge. So the obtained experimental data are more consistent than low discharges.

# Chapter 1

# THEORETICAL FOCUS & LITERATURE REVIEW

## 1.1 Sediment transport

The Sediment is defined as fragmented material formed by physical and chemical weathering or erosion of rocks. When it transported by the force of gravity acting on the sediment particles due to the slope of resting surface or by the action of wind, water, or ice is termed as sediment transport.

Transport is driven by the gravity and drag forces between the sediment and surrounding fluid like air or water. Sediment transport is typically use in natural systems, where the particles are sand, gravel, boulders, mud, or clay in the fluid like air, water or ice.

Due to currents and tides in rivers, the oceans, lakes, seas and other bodies of water fluid become in motion. In open surfaces of loose materials it can occur under the influence of high wind. Sediment transport can happen only due to gravity on steep sloping area.

The wind draws its energy from atmospheric pressure gradients, and therefore depends on climatic conditions. For natural water bodies, it draws the energy from the elevation of the catchment area and causing it to run downward through the river system or the current, tides or storm etc.

Sediment transport describes the occurrence, magnitude and characteristics of

erosion and deposition that is important in hydraulic structures and civil engineering. So it has important role in the fields of geology, geomorphology and engineering.

Sediments will also fall into the cohesive or non-cohesive category. Cohesive sediments are dominated by inter-particle interactions while non-cohesive sediments are dominated by gravitational forces [4]. We will continue our discussion about non-cohesive sediments.

### 1.1.1 Total load of sediment transport

The transported material is called sediment load. It is transported in specific or combined ways. Based on mechanism of transport, sediment transport can be divided into three main load forms:

1. Suspended load
2. Bed load
3. Wash load

In geomorphology of channel the most important forms of transport are suspended load and bed load. In river, for having a mixture of non-uniform sediments, the suspended load usually consists of the finer grains and the bed load usually consists of the coarser particles transported by the flow in a layer close to the bed.

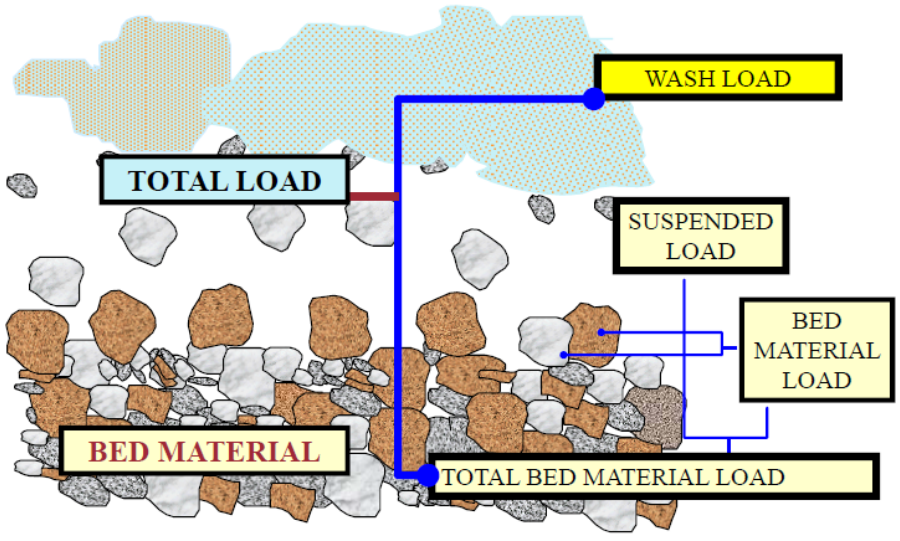


Figure 1.1: Total sediment load.

#### 1.1.1.1 Suspended load

Suspended load refers to that part of the total sediment transport which is maintained in suspension by turbulence in the flowing water for considerable periods of time without contact with the stream bed. It moves with practically the same velocity as that of the flowing water.

Turbulent flow suspends the eroded material like clay and silt from the boarder surface and channel bed itself in the stream. Those suspended materials that moves through the channel in the water column are termed as suspended load. These materials, mainly silt and sand are kept in suspension by the upward flux of turbulence generated at the bed of the channel.

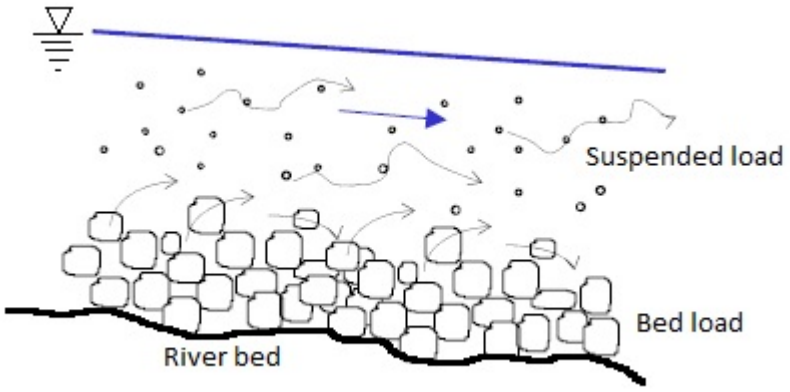


Figure 1.2: Typical Bed load and Suspended movement in river or channel.

#### 1.1.1.2 Bed load

Bed load is the material that moves through the channel fully supported by the channel bed itself. The bed load materials mainly consists of sand and gravel, which are kept in motion (rolling and sliding) by the shear stress acting at the boundary.

The bed load movement is usually occurred by the shear velocity at the bed and effective resistance of the sediment particle. Although it is difficult to make predictions, experiment and theory suggest that the rate of bed load transport ($q_B$) is proportional to the cube of the shear velocity ($u^*$). So very small changes in current speed or bed roughness can have significant effects on the rate of bed load transport.

### 1.1.1.3 Determination of total load

Bed load is the part of total load which has more or less continuous contact with the bed. Thus the bed load must be determined in relation to the effective shear stress which acts directly on the grain surface. Suspended load is the part of the total load which is moving without continuous contact with the bed as the result of the agitation of the fluid turbulence [3].

The reality is not so simple like this. Because there is no clear specification to differentiate this two states exactly.

Bed load transport, $q_B$ is often expressed in the form of dimensionless intensity of the solid discharge $q^*_B$ as bed-load is obtained,

$$q^*_B = \frac{q_B}{d\sqrt{(s-1)gd}} - - - - - - - - (1.1)$$

Where,

$q_B$ is the volumetric solid discharge per unit width

$d$ is the particle diameter

$s$ is specific or relative density

$g$ is the acceleration due to gravity

Meyer-Peter formula:

$$q^*_B = 8\,(\theta' - \theta_c)^{1.5} - - - - (1.2)$$

Where,

$\theta'$ is effective Shields parameter

$\theta_c$ is critical Shields parameter

Einstein-Brown formula:

$$q^*_B = 40\,K(\theta')^3 - - - - (1.3)$$

$$K = \sqrt{\frac{2}{3} + \frac{36v^2}{(s-1)gd_{50}^3}} - \sqrt{\frac{36v^2}{(s-1)gd_{50}^3}}$$

Where,

$v$ is kinematic viscosity of water = $10^{-6}$ $m^2$ $s^{-1}$

$d_{50}$is value of grain diameter for which 50% of the material weight is finer.

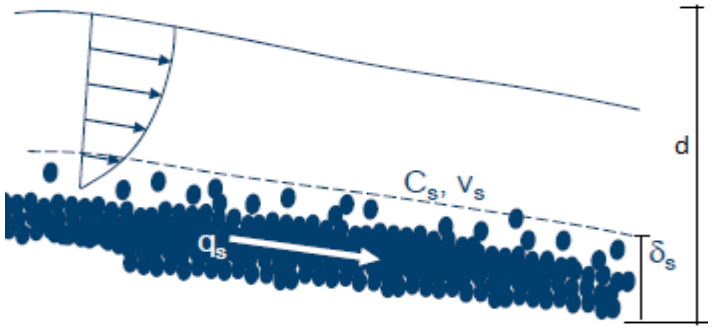


Figure 1.3: Sediment movement in river.

Also $q_B$ depends on the velocity profile and the sediment concentration,

$$q_B = C_s \delta_s V ----(1.4)$$

Where, $C_s$ is the concentration of sediment

$V$ is the velocity.

$\delta_s$ is the bed load layer thickness

Suspended sediment transport depends on the product of sediment concentration profiles (for each size class) and the velocity profile [9].

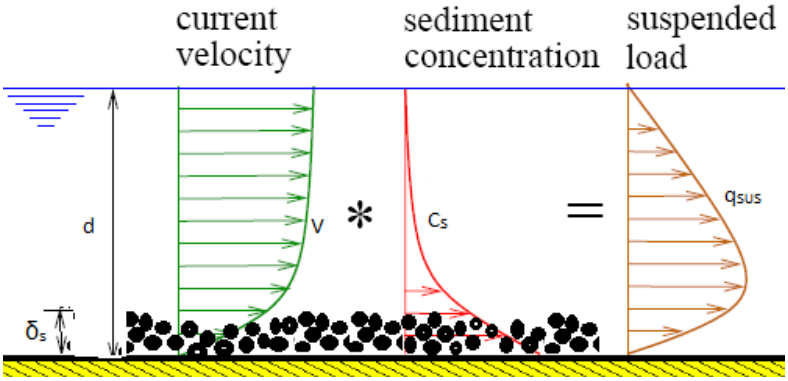


Figure 1.4: Velocity and Concentration distribution of sediment.

$$q_S = \int_{\delta_s}^{d} C_s V . dy ----(1.5)$$

Where, $d$ is the depth of water

Sediment transport rate include the bed load rate and suspended load rate. Mathematically, total sediment transport rate is the summation of bed load rate and suspended load rate.

$$q_T = q_B + q_S ---(1.6)$$

## 1.2 Characteristics of an open channel

Bulk velocity (U): Instead of determining exact velocities at different location in same cross section in a flow channel, bulk velocity allows to determine the average velocity at that section. For regular channel with same cross section:

Mathematically, $Bulk\ velocity = \frac{Flow\ discharge}{Cross\ section\ of\ the\ cahnnel}$

Shear stress (τ): Shear stress in flowing fluid is termed as the lateral force per unit area imposed by transversely-moving fluids that generate shear forces. It can be calculated in terms of density, hydraulic radius and friction slope by the equation:

$$\tau = \rho g R_H S_f ----(1.7)$$

Where, $\rho$ is the fluid density

$R_H$ is hydraulic raidus

$S_f$ is friction slope

Shear velocity ($u^*$): Shear velocity, also called friction velocity, is a form by which a shear stress expressed in terms of velocity. It can be calculated mathematically by:

$$Shear\ velocity\ (u^*) = \sqrt{\frac{Shear\ stress\ (\tau)}{Fluid\ density\ (\rho)}}$$

Friction factor (λ): It is a measure of the shear stress (or shear force per unit area) that the turbulent flow exerts on the wall of a pipe; it is expressed in dimensionless form as:

$$\lambda = 8\left(\frac{u^*}{U}\right)^2 = \frac{8\tau}{\rho U^2} - - - (1.8)$$

Where, τ is the shear stress, $\rho$ is the density of the liquid and $U$ the mean velocity of the flow.

For turbulent flow in a smooth pipe, friction factor can be calculated in terms of Reynolds number and shape factor by the following equation:

$$\frac{1}{\sqrt{\lambda}} = 2\log\left(\frac{F * Re * \sqrt{\lambda}}{2.51}\right) - - - (1.9)$$

Where, λ is the Friction factor

F is Shape factor

Re is Reynolds number

Friction slope ($S_f$): The energy loss per unit of length of open or closed conduit due to friction is termed as friction slope. It can be calculated in terms of bulk velocity, friction factor and hydraulic radius by the equation:

$$S_f = \frac{\lambda}{4R_H}\frac{U^2}{2g} - - - - - (1.10)$$

Where, λ is the Friction factor

$U$ is bulk velocity

$R_H$ is hydraulic raidus

Hydraulic radius ($R_H$): It is the ratio of the cross-sectional area to the wetted perimeter of a channel section. In a flowing fluid it can be calculated by:

$$Hydraulic\ radius = \frac{Total\ cross\ sectio}{Wetted\ perimeter\ of\ the\ cahnnel}$$

## 1.3 Properties of Sediment

Sediment transport depends on sediment properties, characteristics of the sediment bed, and properties of the fluid flow. In natural channels and bodies of water the bed is not fixed but is composed of mobile particles; e.g. gravel, sand, silt or mixed.

### 1.3.1 Physical properties of Sediment

Physical properties of sediments (e.g., mineralogy, texture, sorting) or bulk properties relating to arrangements in a deposit or landform (e.g., porosity, shear strength, imbrication, fabric, structures) can control the rate and type of geomorphic processes. The properties of individual sediment grains include sediment size, sediment density, shape, and chemical composition [8].

#### 1.3.1.1 Diameter of sediment

Diameter or size of sediment is the most important property in sediment transport. Since natural particles have very irregular shapes the concept of diameter is somewhat imprecise. Where there is a range of particle sizes the cumulative percentage is attached to the diameter; e.g. the median diameter $d_{50}$ is that sieve size which passes 50% (by weight) of particulate [8].

Different definition of sediment size:

The *sieve diameter* represents the diameter of the smallest circle that encompasses one dimension of the grain. It is the scale of the sieve mesh that would trap the sediment. It would be close to short and intermediate diameter.

The *nominal diameter* represents the diameter of the sphere that would take up the same volume as the sediment grain. It would be somewhere in between long and short diameter.

The *standard fall* diameter represents the diameter of the quartz sphere that would settle at the same speed as the sediment grain in still, distilled water at $24^{o}$/C. It arises from settling type measures of grain size. A typical size classification is showing in table 1.1.

Table 1.1: Size classification of sediment

| **Type** | **Diameter** |
|---|---|
| Boulders | >256 mm |
| Cobbles | 64 mm – 256 mm |
| Gravel | 2 mm – 64 mm |
| Sand | 0.06 mm – 2 mm |
| Silt | 0.002 mm – 0.06 mm |
| Clay | <0.002 mm (cohesive) |

### 1.3.1.2 Specific gravity or Relative density

The specific gravity (or relative density), $s$ is the ratio of the density of particles ($\rho_s$) to that of the fluid ($\rho$). Sediment density ($\rho_s$) depends on the mineralogy of the sediment [8].

$$s = \frac{\rho_s}{\rho} - - - -(1.11)$$

The density of quartz, $\rho_s$ = 2.65 g/cm$^3$ = 2650 kg/m$^3$, is often assumed for sediment density in transport formulas [6].

### 1.3.1.3 Porosity

The porosity P is the ratio of voids to total volume of material; i.e. in a volume $V$ of space there will actually be a volume $(1 - P)V$ of sediment. Porosity is important in, for example, modeling changes to bed morphology and the leaching of pollutants through the bed. For natural uncompact sediment P is typically about 0.4 [6].

### 1.3.1.4 Angle of repose (∅)

The angle of repose is that maximum angle (to the horizontal) which a pile of sediment may adopt before it begins to avalanche. It is easily measured in the laboratory.

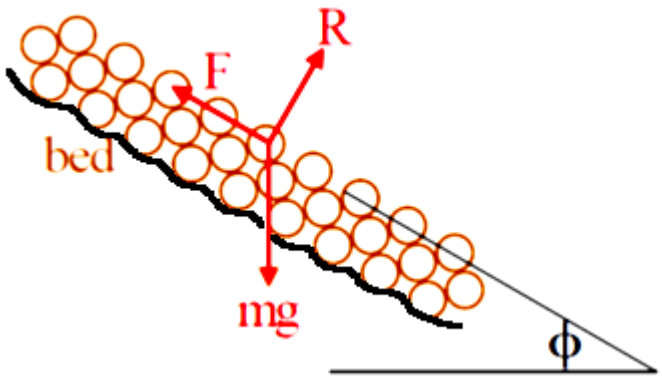


Figure 1.5: Concept of the angle of repose.

It gives some measure of resistance to incipient motion via an effective coefficient of friction ($\mu_f$).

Incipient motion occurs when the downslope component of weight equals the maximum friction force ($\mu_f$ × normal reaction).

Then, $mg * sin\emptyset = \mu_f\ (mg * cos\emptyset)$

so, $\mu_f = tan\emptyset ----(1.12)$

Although the mechanism for causing motion is not the same, $\mu_f$ can then be used to estimate the onset of motion on a flat bed when the motive force is that due to the fluid stress, not gravity [8].

The angle of repose equals the sweeping angle of the connected line between a particle center of mass and the contact point around which the particle rotates on the bed surface when the particle center of mass is vertically above the contact point, and thus the angle of repose depends on the shape of the particle, the size of the particle, and the particle orientation on the bed surface. For sediment particles, the angle of repose varies in range usually from 26° to 42°.

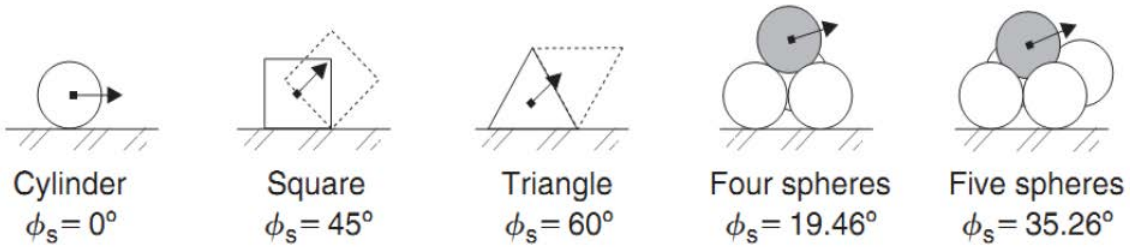


Figure 1.6: Examples of angle of repose.

#### 1.3.1.5 Settling velocity

Settling of a sediment particle depends on the weight of sediment, buoyant force, drag force, density of fluid and particles. So the settling velocity depends on:

- Particle Diameter
- Particle Density
- Particle Concentration
- Particle Shape
- Viscosity of Water (Temperature)
- Turbulence

Settling velocity, $v_s = \sqrt{\frac{(\rho_P - \rho) g V_P}{C_D A_P \rho}} - - - -(1.13)$

Where, $C_D$ is the drag coefficient

$\rho_P$ is the density of the particle

$\rho$ is the density of the medium (water)

$V_P$ is the volume of the particle

$A_P$ is the area of the particle

### 1.3.2 Properties of the flow

When the sediment moves in water then the movement depends on the flow characteristics too. Flow properties of medium generally effect on the velocities and viscosities of sediment.

### 1.3.2.1 Mean velocity profile

A fully-developed turbulent boundary layer adopts a logarithmic mean-velocity profile. There are lots of available laws for mean velocity profile. For a rough boundary this is of the form [8].

$$U(z) = \frac{u^*}{k} \ln\left(33\frac{z}{k_s}\right) - - - - - (1.14)$$

Where, $u^*$ is the the friction velocity

$k$ is von Kármán's constant ~ 0.41

$k_s$ is the roughness height (typically 1 – 2.5 times particle diameter)

$z$ is the distance from the bed

### 1.3.2.2 Eddy viscosity profile

It expresses internal friction at a larger scale. A classical model for the effective shear stress $\tau$ in a turbulent flow is to assume, by analogy with laminar flow, that it is proportional to the mean-velocity gradient. Shear stress for Fluid undergoing turbulence requires an extra term to account for Eddy-viscosity.

For Laminar flow, $\tau = \mu \frac{dU}{dy}$

For turbulent flow, $\tau = (\mu + v_t) \frac{dU}{dy}$

Here, $v_t$ is called a kinematic eddy viscosity. It is not a true viscosity, but a means of modeling the effect of turbulent motion on momentum transport. Such models are called eddy-viscosity models and they are widely used in fluid mechanics. In a fully turbulent flow $v_t$ is many times larger than the molecular kinematic viscosity $v$ [8].

## 1.4 Sediment Motion

The dynamic interaction between turbulent fluid forces and solid particles for flows over an erodible boundary constitutes a central problem in earth surface dynamics and engineering. The fundamental assumption in modeling sediment transport is involved in the mechanism of incipient motion of sediment transport on the bed surface. The stability of granular material in the river bed depends on the angle of repose at which the motion of particles occurs. The threshold conditions are satisfied when the hydrodynamic moments of forces acting on the single particle balance the resisting moments of force [2].

Shields (1936) determined the threshold condition by measuring the Shields parameter at least twice as large as the critical value and then plotted Shields curve marking the permanent trend between critical Shields parameter and the grain Reynolds number for applying other cases. The critical value was determined as 0.047 that has been widely used for a single size particle at high grain Reynolds number [2].

### 1.4.1 Importance of incipient motion of the particle

Incipient motion of sediment in gravel bed streams is a very important process because it represents the difference between bed stability and bed mobility. Incipient motion is a basis for the analysis and design of stable river beds. One use is for determining maximum flows at which a contaminated bed will remain stable and retain toxic substances that otherwise might contaminate the water and affect aquatic organisms and human health at downstream sections.

### 1.4.2 Forces acting on the particle

The hydrodynamic forces consist of the weight of the particle, buoyancy force, lift force, drag force, and resisting force as shown in figure 1.7.

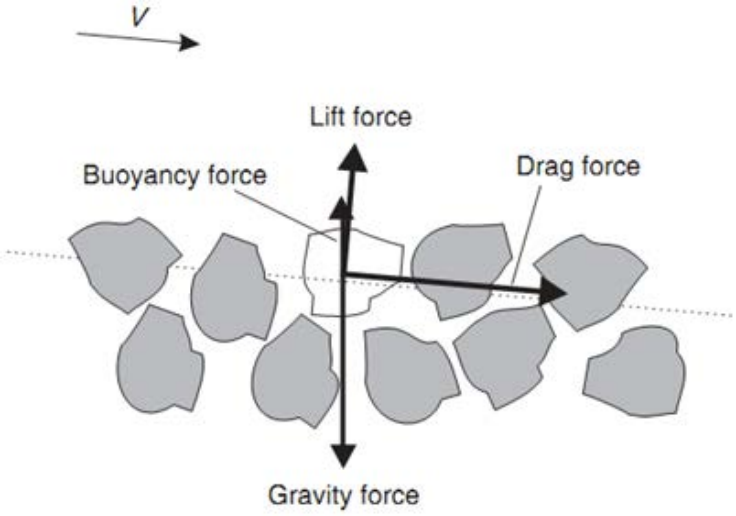


Figure 1.7: Forces acting on sediment.

Here the weight of the particle, as gravity force directly acts downward. Buoyancy force is acting upward. Lift force is acting perpendicular to the flow direction. Drag force is acting along the direction of flow. If the sediment particle is resting on the ground then resisting force will act at the bottom surface.

### 1.4.3 Incipient of sediment movement

Consider a steady flow over cohesion less grain composed bed. The acting forces are showing in figure 1.8.

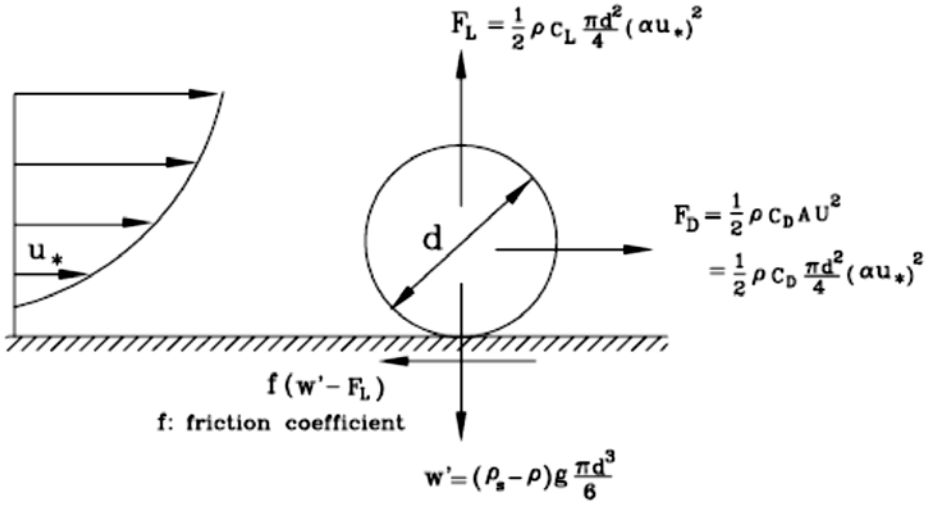


Figure 1.8: Forces acing on a grain resting on a ground.

Now,

$$\text{The driving drag force, } F_D = \frac{1}{2}\rho C_D \frac{\pi {d_s}^2}{4}(\alpha u^*)^2 - - - -(1.15)$$

$$\text{Lifting force, } F_L = \frac{1}{2}\rho C_L \frac{\pi {d_s}^2}{4}(\alpha u^*)^2 - - - -(1.16)$$

$$\text{Weight of the grain, } W = (\rho_s - \rho) g \frac{\pi {d_s}^3}{6} - - - - - - -(1.17)$$

$$\text{Friction Force, } F = f(W - F_L) - - - - - - - - (1.18)$$

Where,

$u^*$ is the friction velocity (velocity close to the bed)

$\alpha$ is a coefficient used to modify $u^*$

$d_s$ is the diameter of the particle

$\rho_s$ is the density of the sediment particles, kg/m$^3$

$g$ is the constant of gravity acceleration, m/s$^2$

$\rho$ is the density of water, kg/m$^3$

$C_D$ and $C_L$ are the drag and lift coefficients, respectively

Let, ${u^*}_c$ is the critical friction velocity. When the grain is about to move, then the drag force is equal to the friction force.

$$\frac{1}{2}\rho C_D \frac{\pi {d_s}^2}{4}(\alpha {u^*}_c)^2 = \text{f } [(\rho_s - \rho) g \frac{\pi {d_s}^3}{6} - \frac{1}{2}\rho C_L \frac{\pi {d_s}^2}{4}(\alpha {u^*}_c)^2 ] - - - -(1.19)$$

After rearranging,

$$\frac{{u^*}_c^2}{(s-1)gd} = \frac{f}{\alpha^2 C_D + f\alpha^2 C_L} \frac{4}{3\alpha^2} - - - - - (1.20)$$

Shields (1936) determined the threshold condition by measuring the Shields parameter defined as,

$$\theta = \frac{{u^*}_c^2}{(s-1)gd} - - - - - (1.21)$$

So, the sediment will start to move when,

$u^* > {u^*}_c$ , the critical friction velocity

or, $\tau_b > \tau_{bc}$ , the critical bottom shear stress = $\rho {u^*}_c$

or, $\theta > \theta_c$ , the critical shield parameter = $\frac{{u^*}_c^2}{(s-1)gd}$

### 1.4.4 Entrainment

The effects of turbulent flow on the initial entrainment of sediment were recognized as far back as 1939 by Lane and Kalinske. Drake et al. (1988) defined entrainment as "Because some particles in repose vibrated or jostled against their neighbors without going anywhere, we defined entrainment operationally as continuous movement a net horizontal distance of one particle diameter".

Consider, fluid flows over a bed consisting of loose (mobile) and cohesion less solid particles. When liquid starts flowing, the hydrodynamic forces are exerted on the sediments of the bed. Particle entrainment refers to the commencement of movement of bed particles due to forces exerted by flow. Entrainment of sediment particles is governed by flow and particle characteristics.

Entrainment occurred by rollover consisted of tipping and overturning of the particles, by liftoff and by impact ejection when struck on the bed hard enough to initiate their displacement [9].

### 1.4.5 Distrainment

Distrainment is the ending of sediment displacement. Drake et al. (1988) defined distrainment as "We defined distrainment as absence of net horizontal motion for 0.25 s or longer following displacement."

Saltating particles usually were abruptly stopped by head-on or nearly head-on impacts with larger bed particles. Rolling particles often decelerated gradually over distances of one or two particle diameters before distrainment [9].

The duration of the distrainment phase is very short with respect to the other phases of particle motion; indeed settlement of moving particles is usually nearly instantaneous (Roseberry et al., 2012).

## 1.5 Dimensionless variables

In recent research studies the kinematic properties of moving sediments is expressed as a function of these dimensionless parameters. Sediment motion depends on flow behavior and particle characteristics. Some of this parameters show the properties of sediment and some of them show the properties of flow as well. The variables usually we considered to characterize the flow field and sediment are the fluid density, viscosity, the flow depth, shear stress, diameter of particle, density of particles etc.

Explicit Particle Reynold's number (initiation of motion, settling velocity):

$$R_{ep} = \frac{d\sqrt{\frac{(\rho_s - \rho)}{\rho} gd}}{v} - - - (1.22)$$

Where,

d is particle diameter

$v$ is viscocity

$\rho_s$ $and$ $\rho$ are density of sediment and fluid respectively

Froude Number ($F_R$):

$$F_R = \frac{u}{\sqrt{gh}} - - - (1.23)$$

$F_R < 1$, Sub critical. Wave can travel upstream

(normal alluvial conditions, $F_R < 0.5$)

$F_R = 1$, Critical, Standing wave

$F_R > 1$, Super critical, Wave cannot travel upstream (steep slope)

Where, u is the velocity

Rouse Number (mode of sediment transport):

The Rouse number dictates the mode of sediment transport. It is the ratio of particle settling velocity to the shear velocity.

$$Rouse\ no. = \frac{v_s}{ku^*} - - - (1.24)$$

Rouse no. > 2.5, Bed load

2.5 > Rouse no. > 1.2, 50% suspended load

1.2 > Rouse no. > 0.8, 100% suspended load

0.8 > Rouse no., wash load

Where,

$v_s$ is the settling velocity

$u^*$ is shear velocity

K is Von Karman's constant = 0.40

Shield Number (sediment transport, initiation of motion):

Initiation of motion and sediment transport must depend on, at least: boundary shear stress, sediment and fluid density (buoyancy), and grain-size.[4]

$$\theta = \frac{u_*^2 \rho}{(\rho_s - \rho) dg} - - - (1.25)$$

## 1.6 Research Background

Research about sediment particle behavior and transport start very early in this century where formulae for the sediment transport rate were tuned. Einstein (1942) introduced the idea that the sediment particles move in steps or saltating proportional to their size and defined the bed load layer thickness as twice the particle's diameter. Also, he used the approach of probability analysis to formulate a relationship for sediment discharge on the bed surface [15]. Einstein (1950) defines a sub-layer thickness of two particle diameters as the motion region of sliding, rolling in which the sediment particles sometimes may jump only to a longitudinal length of several particle diameters. The bed load layer adjacent to the bed is so thin that the turbulent stress cannot influence the sediment particles, and thus the suspension of particles is impossible in this layer [16]. Bagnold (1966) developed his expression of a suspended load and bed load based on the energy conservation law. Bagnold assigned all of the unknown parameters by experiments. Since the energy loss due to bed load transport has been counted twice, Yang (1986) corrected his suspended load formula [2]. Bagnold (1973) defines the bed

load transport as that in which successive contacts of particles with the bed are strictly limited by the effect of gravity, while the suspended load transport is defined as that in which the excess weight of particles is supported wholly by a random succession of upward impulses imparted by turbulent eddies (Van Rijn 1985), wherein the motion of rolling, sliding and saltation for particles occurs in the bed load transport [2]. Van Rijn (1985) employ the approach of Bagnold in their research on the sediment transport, which means the rolling, sliding and saltation are included in the bed load layer in which the turbulence is of minor importance. The wavy flow condition in some marine environment results in the evolution of the river bed features, such as erosion, ripples, dunes, sorting and grading. The geographic features in nearly all cases result from interaction of a turbulent flow with the sediment particles on the erodible bed [7].

Then, analysis moved to more detailed aspects of particle mechanics. During the 1950s and early 1960s that serious development of the technique took place. Studies involved the use of tagged particles to determine transport; it was used with considerable success in many sand transport studies. Other historical attempts at tracking sediment have included the use of materials such as pulverised coal (Shinohara et al. 1958), broken bricks (West 1949; Kidson & Carr 1961), painted shingle (Dobbs 1958; Kidson et al. 1962; Longuet-Higgins & Parkin 1962) etc. A number of investigators have therefore used motion-picture photography or video recording techniques to study bedload transport (Paintal 1969 ; Rossinskiy & Lyubomirova 1969 ; Grass 1970; Francis 1973 ; Fernandez Luque & van Beek 1976 ; Abbot & Francis 1977; Nakagawa, Tsujimoto & Hosokawa 1980; Hammond, Heathcrshaw & Langhorne 1984; Hubbell et al. 1986) [9]. This technique gradually became the predominant and most successful of particle tracking methods. Drake et al. (1988) show motion-picture photography is almost uniquely capable of detailed observation and quantitative information on both the modes of motion of individual bedload particles and the collective motions. It can be used to show the entrainment and distrainment of particles, their concentrations, speeds, and modes of motion during displacement, and their interactions with the water, the bed, and each other. Moreover, it can supply not only the average values but also the statistical distributions. It can provide nearly all

the qualitative information and quantitative data needed to develop and test theories of bedload transport [9]. This stimulated a number of phenomenological studies, measurement of velocities of individual and development of a physically based model explaining anomalous particle diffusion. Nikora et al. (2001) introduced a new conceptual model for longitudinal and transverse diffusion of moving bed particles under weak bed load transport. For both rolling/sliding and saltating modes the model suggests that the particle motion is diffusive and comprises at least three ranges of temporal and spatial scales with different diffusion regimes; the local range (ballistic diffusion), the intermediate range (normal or anomalous diffusion) and the global range (sub diffusion).

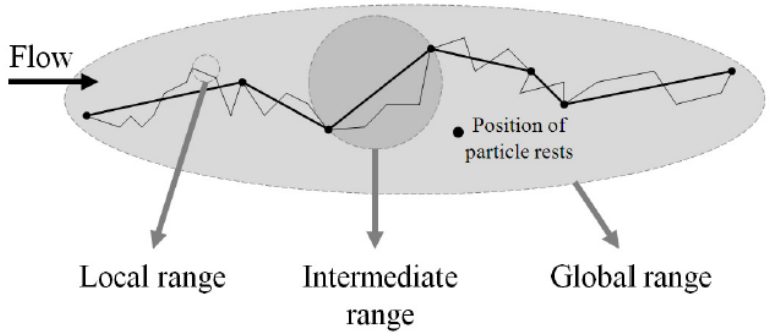


Figure 1.9: Conceptual representation of a particle trajectory consisting of three different ranges of scales: local, intermediate and global (Nikora et al., 2002).

The local range corresponds to ballistic particle trajectories between two successive collisions with the static bed particles. The intermediate range corresponds to particle trajectories between two successive periods of rest. These trajectories consist of many local trajectories and may include tens or hundreds of collisions with the bed. The global range of scales corresponds to particle trajectories consisting of many intermediate trajectories, just as intermediate trajectories consist of many local trajectories [12].

Very recent studies on the dynamics of sediment transport over a plane bed have demonstrated a growing interest for the link between the near-bed turbulent structure

and the resulting particle motion. Lajeunesse et al. (2010) presented an experimental investigation on the bed load particle motion over a flat sediment bed of uniform grain size in turbulent flow at the grain scale. They showed that the particles entrained by the flow exhibit an intermittent behavior composed of a succession of periods of motion with a highly fluctuating velocity, called 'flights', and periods of rests. During one flight, a particle may successively through a phases of rolling and sliding. Also they showed quantitative analysis about threshold, density of moving particles, particle velocity distributions, mean particle velocity, flight duration and length [22]. Radice et al. (2010) presented a tentative application of Particle Tracking Velocimetry to bed-load particles, as a step towards obtaining Lagrangian measurements of particle motion to support the development of probabilistic models for bed load. They showed that Lagrangian analysis is very effective in particle motion analysis [13]. Campagnol et al. (2012) presented a statistical analysis of the kinematic variables of the intermediate trajectories for mobile and fixed beds and two flow discharges. They showed the travel time, the covered distance and the velocity in stream-wise direction seem to be higher for a grain moving over a fixed bed than over a mobile bed. Also for the same experimental conditions, the bed configuration can affect the kinematics of moving grains [11]. Radice et al. (2013) are performed experiments with simultaneous measurement of areal bed-load sediment concentration and water velocity (horizontal and vertical components) made at 1.5 particle diameters above the mean bed. The same spatial and temporal scales were employed to measure the kinematic properties of flowing water and sediments. They obtained the results are integrated into a conceptual picture attempting to bridge previous depictions of the bed-load transport mechanics [14].

## 1.7 The research project in which this work takes part

An extensive project is being undertaken at the Politecnico di Milano. The project scope is Lagrangian analysis of individual particle motion, accounting for trajectory-averaged and instantaneous particle velocities, properties of intermediate particle trajectories (intermediate in the sense of Nikora et al.'s model), diffusion of bed-load

sediment particles and fractal properties of trajectories. Since the particle motion is expected to be influenced by turbulence, bed structure and other moving particle, the experimental campaign was designed to try to separate these effects, and thus experiments have been performed with different discharges, different bed configurations (smooth, fixed rough, movable rough, with macro-roughness elements). The project activities are related with PhD thesis of Campagnol, M.Sc theses of Bulankina and Lescova, B.Sc thesis of Bergami.

## 1.8 Objectives

This experimental work performed by using a Lagrangian framework (e.g., Niño and Garcìa, 1998; Lajeunesse et al., 2010; Furbish et al., 2012), considering the particle scale. The objectives of this research work to process the database of the laboratory experiments for smooth bed configuration that had been already performed by of Bulankina and Lescova in their M.Sc theses. The specific objectives of this research work are:

- Analysis of the experiment results for smooth bed configuration for different flow discharges;
- Processing of available images and tracking the moving particle over smooth bed;
- validation of the tracking results obtained from image processing;
- Analysis of the properties of particle motion in terms of velocity, direction, tortuosity of trajectories;
- Statistical analysis in terms of moments of distributions and probability distribution function (pdf), Cumulative distribution function;
- Comparison of the smooth bed analysis results with the corresponding results for the rough bed configuration.

# Chapter 2

# EXPERIMENTAL SETUP

## 2.1 Introduction

A wide experimental campaign was performed at the Hydraulics Laboratory of the Politecnico di Milano under an extensive project of Lagrangian analysis of individual bedload particle at grain scale. Even though the experimentation was performed before the beginning of this work, some description of the laboratory setup is however given for better understanding of the experimental set up, particle details, experimental procedure and conditions. . In the final part of the chapter, some characterization of the flow properties in the experiments assigned is performed.

For getting the individual particle trajectories by experiment, we need sufficient number of moving particles. Experimental constraints have frequently limited the amount of data obtainable, with possible implications for the statistical significance of the results. Also in laboratory experiment for getting more flexibility in result, we use manual process which needs much more time. More recent efforts have thus seen the search for automatic measurements (e.g., Papanicolaou et al., 1999; Frey et al., 2003).

For this laboratory work, the conceptual model proposed by Nikora et al. (2001, 2002) were used. Aim of this experiment is to examine sediment kinematics under smooth bed condition and hydrodynamic conditions.

## 2.2 Experimental setup

The experimental part of this work was performed by Campagnol, Bulankina, Lescova and Bergami in their theses at the Hydraulics Laboratory of the Politecnico di Milano, Italy. Bed load particle motion depends on two main phenomena: bed-particle and fluid-particle interactions. To understand the effect of each mechanism on particle motion five flow rates and seven bed configurations (Mobile bed, Fixed Rough and smooth bed) configuration for different roughness were tested.

For this research work only the fixed smooth bed configuration part was analyzed. So in this chapter describes only fixed smooth bed configuration experiment.

### 2.2.1 Channel and Sediment characteristics

It has been carried out using a pressure duct with transparent wall and lid in a 5.8 m long pressurized duct, with a cross section 40 cm wide and 11 cm high shown in figure 2.1. Smooth plates were laid on the duct bottom.

Sediments used in the experiments were uniform, quasi-spherical PBT particles with an equivalent dimension d = 3 mm and density $\rho_s$ = 1.27 g/cm$^3$. White sediments were used those tracked for analysis of particle motion.

During tests, the sediment motion was filmed from above using a digital motion camera shown in figure 2.1 with a resolution of 970 × 700 pixel and a rate of 32 fps. The focus area was A = 49.80 × 36.5 cm$^2$, elongated in the flow direction. Series of movies were repeatedly acquired (See Table 2.1). Each video has duration of about 50 s.


Figure 2.1: Channel configuration at the Hydraulics Laboratory.

### 2.2.2 Procedure of experiment

Flow discharges used during smooth bed (SB) experiments were Q = 8.00 l/s, Q = 11.1 l/s and Q = 13.0 l/s. Therefore first series of experiments was carried out for Q = 8.0 l/s. The higher flow discharges are in agreement with the ones used for rough bed (RB) runs such as particle motion for different bed configurations can be compared ceteris paribus. The particles were manually dropped from feeder.


Figure 2.2: Flow meter.

The sediments were dropped into the duct manually to make movies. As a consequence interaction between moving sediments is less for smooth bed tests. Prior to execution of experiments the plates were placed into the duct and the discharge was increased to test value. Sediments were feed close to the inlet and they were filmed when they passed through the working section. For each tested flow discharge the mean velocity profile in the middle of the working section was measured.

In laboratory experiment, total five groups of data set have been taken for different discharges. More specifically for discharge 8 l/s one group of data set with 19 movies, for discharge 11.1 l/s two groups of data set with 11 and 7 movies respectively and for discharge 13.0 l/s two groups of data set with 11 and 7 movies respectively. For discharges 11.1 l/s and 13.0 l/s, two groups of data were taken at the same condition but in different days.

At the same time the velocity profiles were controlled (longitudinal and vertical components of velocity, $V_x$ and $V_y$ respectively), with further analysis of their characteristics. This estimation was done, taking into consideration the parameters of system, like the discharge Q and condition of bed.

Table 2.1: List of the number of measurements for SB runs.

| **Discharge Q (l/s)** | **8.00** | **11.1** | | **13.0** | |
|---|---|---|---|---|---|
| Group of data | 1st | 1st | 2nd | 1st | 2nd |
| Movie | 19 | 11 | 7 | 11 | 7 |
| Velocity profile | 1 | 1 | 1 | 1 | 1 |

### 2.2.3 Movie recording

The motion of the sediments was filmed with CCD camera with a frequency of 32 Hz (one image each 0.03125 seconds), positioning the camera above the controlled flow field and observing the process through the transparent lid of the duct (see Figure 2.1 & 2.3) The focus area of used camera was equal to A = 49.80 x 36.5 cm = 1817.7 $cm^2$, what refers to resolution of the image 960 x 700 px (the conversion rate in this case is mm: px = 0.529).

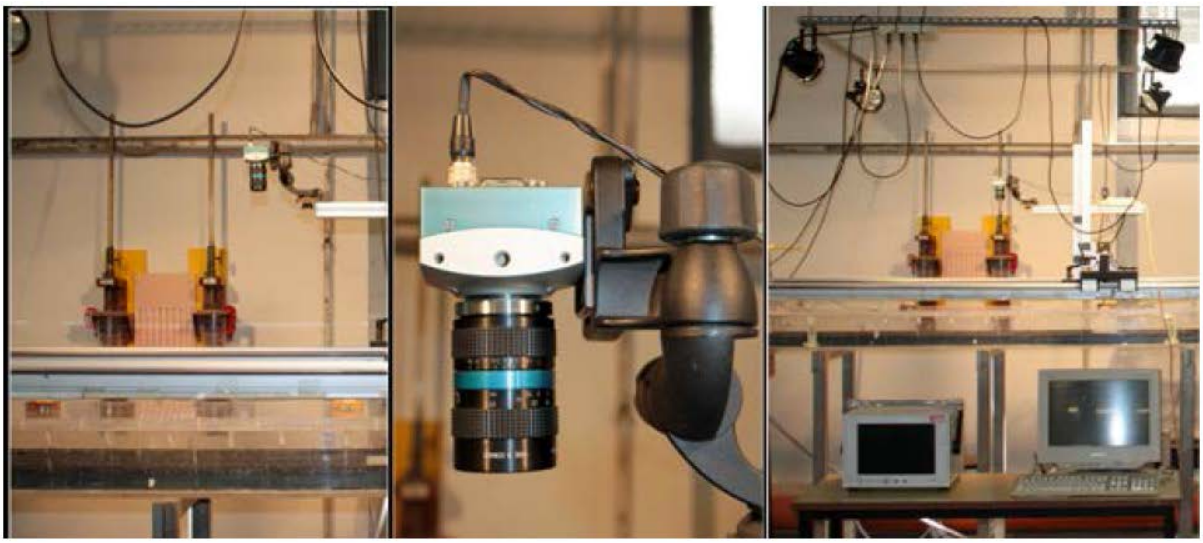

Figure 2.3: Camera position for movie recording, side view.

The controlled area was elongated in the stream-wise direction as appropriate for given particles trajectory characteristics. For three discharges; $Q_1$ = 8.0 l/s, $Q_2$ = 11.1 l/s and $Q_3$ = 13.0 l/s in total 55 movies were taken in five sequences. For lowest discharge $Q_1$ = 8.0 l/s in total 19 movies in one sequence and highest discharges $Q_2$ = 11.1 l/s and $Q_3$ = 13.0 l/s in total 36 movies were taken in four sequences. The duration of each single movie is t = 49.84 seconds, and the number of pictures n = 1595. Consequently, total duration of 55 movies is T = 45.69 minutes.

### 2.2.4 Velocity measurement

Ultrasonic Doppler Velocity measuring technique was used. DOP2000 (shown in figure 2.4) ultrasonic echo technique allows to measure instantaneously velocity profiles, Doppler energy profiles, echo profiles, spectral density (FFT) and histogram. It computes and displays in real time these data profiles based on the analysis of a user's specified number of gates placed along the ultrasonic beam. The digital ultrasonic synthesizer included can generate any emitting frequencies between 0.45 MHz and 10.5 MHz.

Figure 2.4: Probes position for taking velocity profiles of flow and Doppler 2000.

DOP2000 provides a sequence of measurements along the beam which is subdivided into small volumes the mean instantaneous velocity is computed within each volume or

gate. The computed velocity of each gate is associated to the coordinate of its center along the axis of the beam, $z_{DOP}$. Sampling volumes have a circular section and their width is imposed by diffusion of the ultrasonic beam with the distance from the emission source.

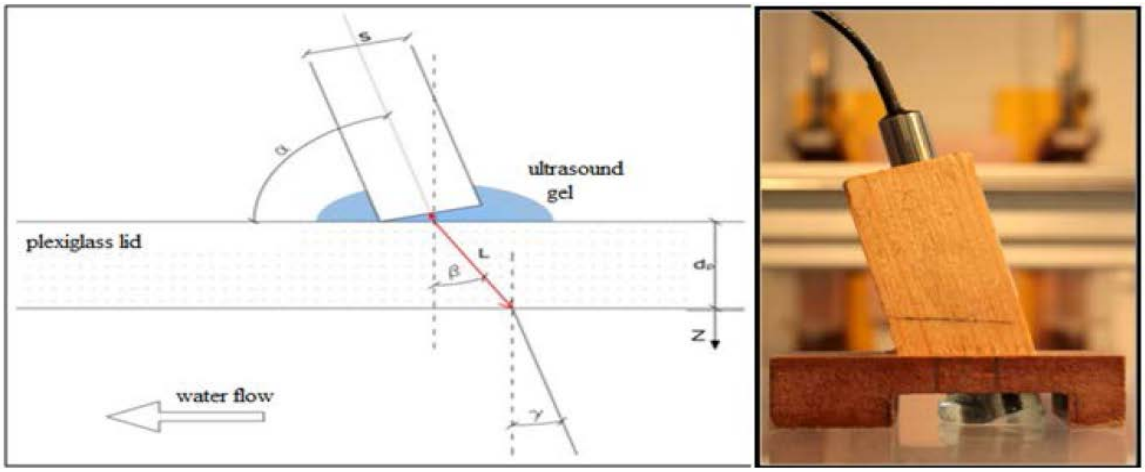


Figure 2.5: Position of echo-sounder probe downstream; Sketch and real view.

In this particular configuration, to convert the coordinate provided by the instrument into z-coordinates with respect to the coordinate system above defined, the following equation has been used:

$$z = \left( z_{DOP} - \frac{s}{2tg\alpha}\frac{c_w}{c_g} - \frac{d}{\cos\beta}\frac{c_w}{c_p} \right) \sin\alpha \quad ----(2.1)$$

Where, s is diameter of the probe = 0.012 m;

d is the thickness of plexiglass lid = 0.01 m;

α is the angle between the axis of the probe and the horizontal direction = 75º;

β is the angle between vertical direction and the inclination of beam through the plexiglass = 28.74 º (By the Snell law, Laws of refraction);

$c_w$ is the sound speed through water = 1480 m/s;

$c_g$ is the sound speed through ultrasound gel = 1480 m/s;

$c_p$ is the sound speed through plexiglass = 2750 m/s;

$z_{DOP}$ is the depth of the gate of maximum echo, mm.

Two probes A & B can be used in different orientations (shown in figure 2.4). The probe A was oriented from downstream to upstream while probe B was oriented from upstream to downstream. Assume, for the flow depth the flow velocity measured by probe A is d and the flow velocity measured by probe B is u. Then the longitudinal velocity ($V_x$) and vertical velocity ($V_z$) components of water velocity within the duct height has been computed by:

$$V_x = \frac{1}{2\cos\alpha}(u - d) \quad ----(2.2)$$

$$V_z = -\frac{1}{2\sin\alpha}(u + d) \quad ----(2.3)$$

Where,

d is the flow velocity (mm/s) obtained by the probe oriented from downstream to upstream direction;

u is the flow velocity (mm/s) obtained by the probe oriented from upstream to downstream direction;

α is the angle between the axis of the probe and the horizontal direction = 75$^o$;

While measuring the instantaneous stream-wise, $v_x$, and vertical, $v_z$, components of water velocity within the duct height. UVP-probes were placed in the centerline of the duct, in the middle of the working section. Measurements of instantaneous particle velocity were then used to obtain the time-averaged velocity profiles which are shown in chapter 1.

The data for profile was taken after the general test run, so the profiles show velocity values for stabilized flow of the water, not just after the changing the value of flow rate Q, what lets us assume them to be correct and acceptable according to all range of three discharges during the procedure. From output files of Doppler echo-sounder we can see values of the velocity (in chapter 1) and echo for each gate (with resolution of 2.06 mm). The position of the bed is defined by the gate location of lowest velocity value and highest echo reading. Such a determination for each discharge and bed configuration was done during elaborating Doppler output files.

## 2.3 Characteristics of flow

To analyze the characteristics of flow for all 8 l/s, 11.1 l/s and 13.0 l/s discharges the velocity profiles are described in the following.

### 2.3.1 Velocity profile

Measurements of the instantaneous particle velocity have been used to obtain the time-averaged velocity profiles. For plotting the results we need to transform obtained data taking into consideration other geometrical positioning parameters and properties of materials, therefore for longitudinal and vertical velocity components of each gate by the conversion principles discussed above.

The obtained time-averaged velocity profiles are shown in the Figure 2.6. The particle velocity identified more or less zero at both the top and the bottom of the duct. But streamwise mean velocity profile is not so similar to the theoretical one for plane channel flow.

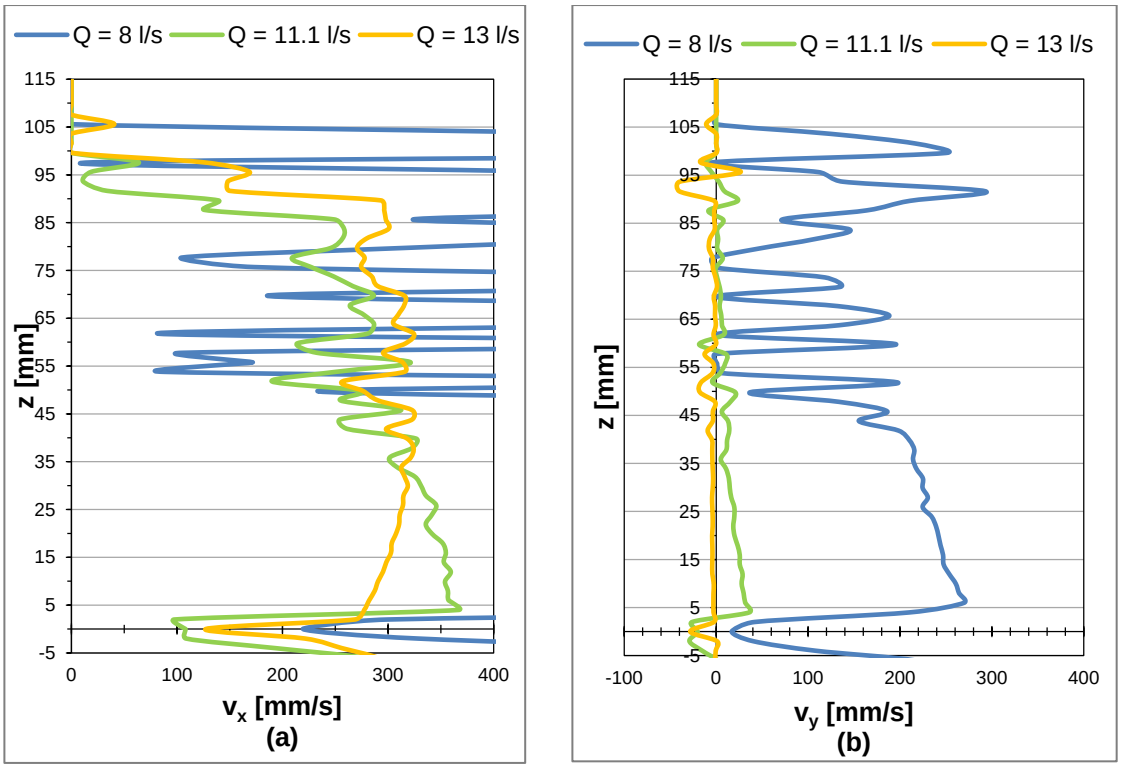


Figure 2.6: Mean velocity profile for smooth bed configuration. a) Streamwise component. b) Vertical component.

By observation it can be said that, the mean velocity profile streamwise and vertical component for discharge 13.0 l/s is qualitatively similar to the theoretical one but for discharges 8 l/s and 11.1 l/s are not similar to the theoretical one. This result is more probably due to presence of small air bubbles below the channel lid or malfunctioning of the probes which no longer have a 75° orientation with respect to the horizontal direction.

So the comparison of this smooth bed velocity profiles with rough bed configuration from the previous research are shown only for discharge 13.0 l/s in the figure 2.7.

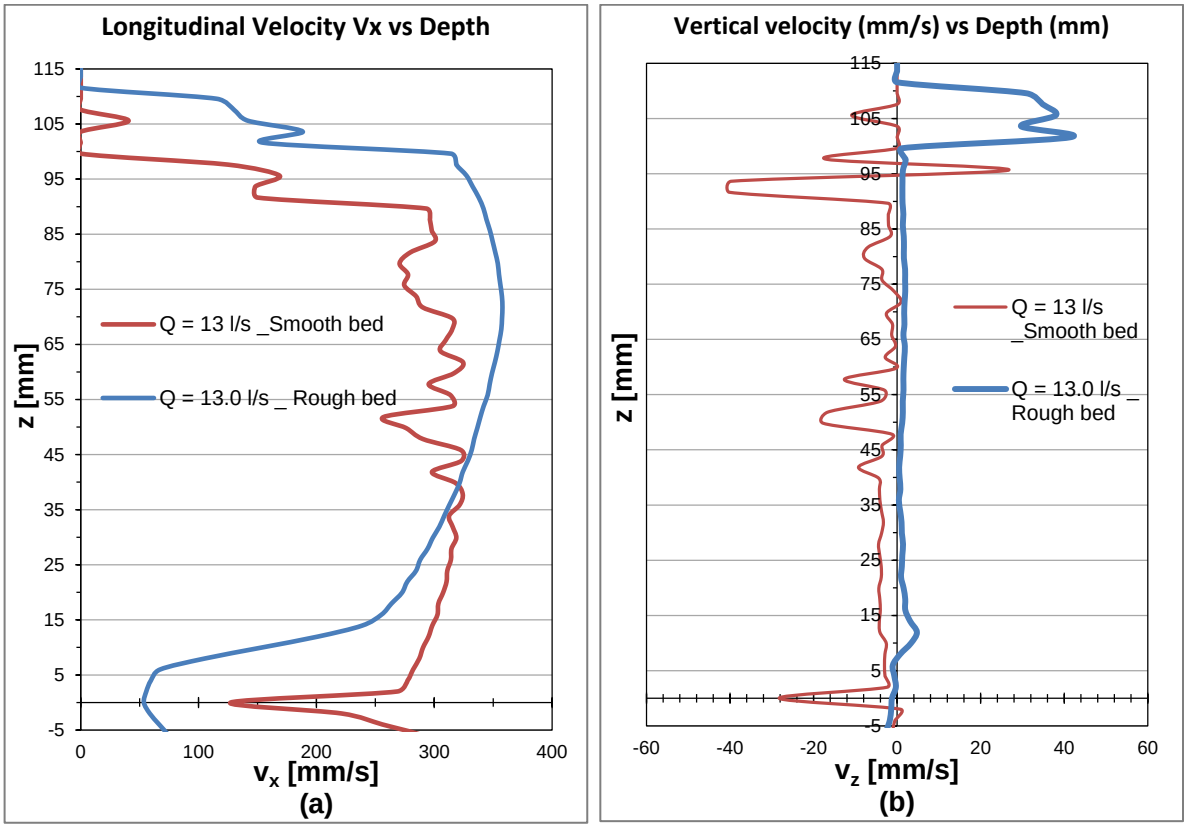


Figure 2.7: Comparison of Mean velocity profiles for smooth bed & rough bed configurations. a) Streamwise component. b) Vertical component.

By comparison it can be concluded that, for the same discharge 13.0 l/s, the mean velocity in streamwise direction decreased at bottom in rough bed configuration because of roughness as expected. Also in vertical component for discharge 13.0 l/s velocity more or less decreased in smooth bed configuration.

### 2.3.2 Shear velocity and Bulk velocity

To estimate shear velocity within the tested range of hydrodynamic conditions we have only one correct velocity profiles on smooth bed configuration for discharge 13.0 l/s.

The estimation of shear velocity (u*) was obtained by fitting the logarithmic equation of the velocity profile in the log-region as shown in figure 2.8. The velocity profiles in inner and outer layers are governed by different laws. The inner and outer layer solutions are matched together in logarithmic layer. So the equation of the velocity profile in this layer:

$$\frac{V(z)}{U^*} = \frac{1}{k} ln \frac{zU^*}{v} + B ----(2.4)$$

Where, $U^*$ is the shear velocity and

$k$ is the Von Karman constant

B = 5 (Kundu and choen, 1990; ASCE manual, 2005)

B is constant

We can write the equation:

$$V(z) = \frac{U^*}{k} ln \frac{zU^*}{v} + BU^* ---------- (2.5)$$

$$V(z) = \frac{U^*}{k} lnz + \left(\frac{U^*}{k} ln \frac{U^*}{v} + BU^*\right) = \frac{U^*}{k} lnz + D --- (2.6)$$

Where, D is constant

So by plotting lnz vs $V_x(z)$, we can calculate shear velocity from the equation 2.6.

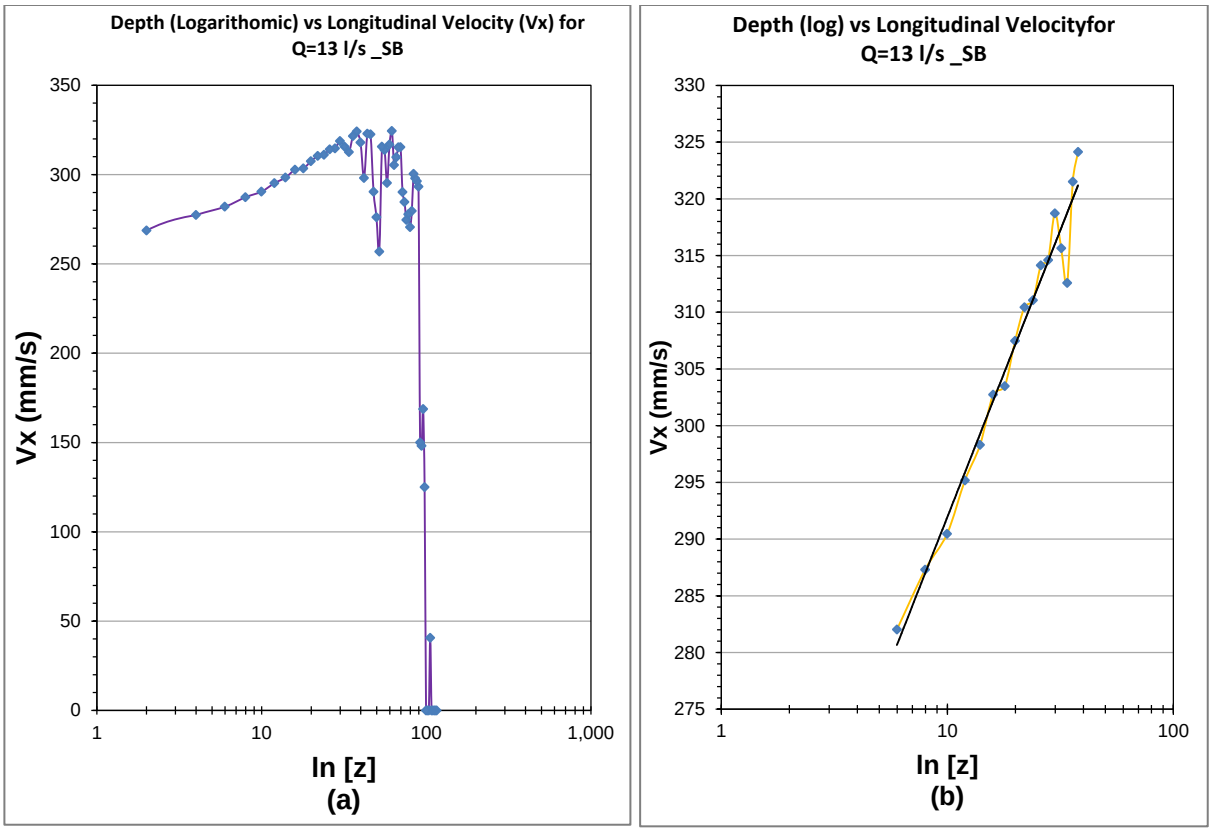


Figure 2.8: For discharge 13.0 l/s, (a) Streamwise velocity profiles with depth using logarithmic axis. (b) Linear part only.

By calculation, shear velocity was found only for discharge 13.0 l/s. By assuming as a first approximation the linear relation between discharge and shear velocity, shear velocity for other discharges have been calculated. Later it was checked with the Moody diagram.

Bulk velocities were simply calculated from the discharge and channel cross sections. Shear velocities from linear approximation and bulk velocities are shown in table 2.2.

Table 2.2: Shear velocities and Bulk velocities for all tested discharges.

| Discharge (l/s) | Bulk Velocity (U) (mm/s) | Shear Velocity (U*) (mm/s) |
|---|---|---|
| 8 | 181.8182 | 6.06508 |
| 11.1 | 250.0000 | 7.9643 |
| 13 | 295.4545 | 9.3275 |

### 2.3.2.1 Calculation of Shear velocity by Moody diagram

To estimate shear velocity within the tested range of hydrodynamic conditions, only for discharge 13.0 l/s has been found correctly. Shear velocity for other discharges were assumed by linear relation.

So, the relation between discharge and velocity for a range of discharge about 1 to 100 l/s in our hydraulic condition has been checked.

We know:

$$\frac{1}{\sqrt{\lambda}} = 2\log\left(\frac{FR_e\sqrt{\lambda}}{2.51}\right) - - - (2.7)$$

Where, λ is the Friction factor

F is Shape factor = 0.88

$R_e$ is Reynold's number

Table 2.3: Summarized all values in calculation of Shear velocity by Moody diagram.

| Discharge | Bulk vel. | Renld. No | Friction factor | Friction slope | Stress | Shear velocity | Dimensionless velocity | Nonlinear approximation |
|---|---|---|---|---|---|---|---|---|
| Q (l/s) | U (m/s) | Re | λ | Sf | τ0 | U* (m/s) | U*/U*(Q=13) | U* (mm/s) |
| 1 | 0.0227 | 6451.61 | 0.0361 | 0.0000 | 0.0023 | 0.0015 | 0.1055 | 0.9837 |
| 3 | 0.0682 | 19354.84 | 0.0269 | 0.0000 | 0.0157 | 0.0040 | 0.2734 | 2.5504 |
| 5 | 0.1136 | 32258.06 | 0.0238 | 0.0001 | 0.0384 | 0.0062 | 0.4283 | 3.9950 |
| 8 | 0.1818 | 51612.90 | 0.0213 | 0.0001 | 0.0882 | 0.0094 | 0.6491 | 6.0548 |
| 11.1 | 0.2523 | 71612.90 | 0.0199 | 0.0002 | 0.1579 | 0.0126 | 0.8686 | 8.1016 |
| 13 | 0.2955 | 83870.97 | 0.0192 | 0.0003 | 0.2093 | 0.0145 | 1.0000 | 9.3275 |
| 15 | 0.3409 | 96774.19 | 0.0186 | 0.0004 | 0.2703 | 0.0164 | 1.1364 | 10.5995 |
| 20 | 0.4545 | 129032.26 | 0.0175 | 0.0006 | 0.4525 | 0.0213 | 1.4703 | 13.7140 |
| 25 | 0.5682 | 161290.32 | 0.0167 | 0.0010 | 0.6756 | 0.0260 | 1.7965 | 16.7565 |
| 30 | 0.6818 | 193548.39 | 0.0161 | 0.0013 | 0.9379 | 0.0306 | 2.1167 | 19.7438 |
| 40 | 0.9091 | 258064.52 | 0.0153 | 0.0023 | 1.5759 | 0.0397 | 2.7438 | 25.5923 |
| 50 | 1.1364 | 322580.65 | 0.0146 | 0.0034 | 2.3591 | 0.0486 | 3.3570 | 31.3128 |
| 60 | 1.3636 | 387096.77 | 0.0141 | 0.0047 | 3.2824 | 0.0573 | 3.9598 | 36.9349 |
| 70 | 1.5909 | 451612.90 | 0.0137 | 0.0062 | 4.3414 | 0.0659 | 4.5540 | 42.4777 |
| 80 | 1.8182 | 516129.03 | 0.0134 | 0.0079 | 5.5331 | 0.0744 | 5.1412 | 47.9542 |
| 90 | 2.0455 | 580645.16 | 0.0131 | 0.0098 | 6.8544 | 0.0828 | 5.7222 | 53.3740 |
| 100 | 2.2727 | 645161.29 | 0.0129 | 0.0119 | 8.3032 | 0.0911 | 6.2980 | 58.7445 |

By considering (All values are in Kg, m, s, N),

Density of water, $\rho_w$ = 1000

Viscosity of water, $\mu_w$ = 0.001

Hydraulic radius, $R_h$ = 0.07

Width of the channel = 0.40

Depth of the channel = 0.11

Shape factor = 0.88

Gravity acceleration = 9.81

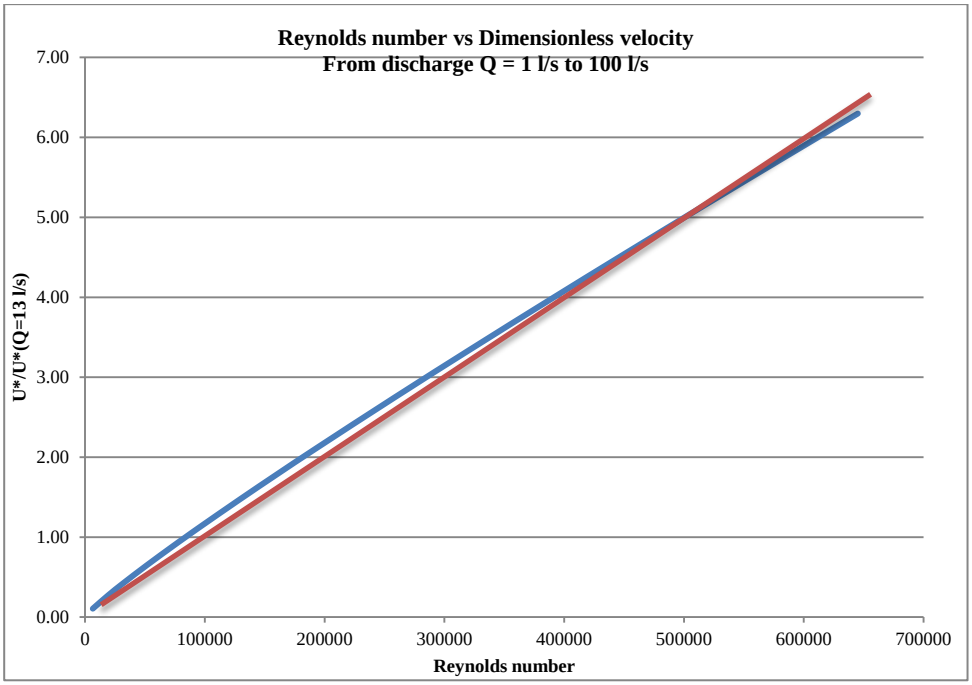


Figure 2.9: The relation between Reynolds number and dimensionless velocity.

From the figure, the dimensionless velocity varies with Reynolds number. The variation is not completely linear (shown in figure 2.9). So new nonlinear approximation for shear velocities were considered by dimensionless velocity with respect to shear velocity at Q = 13 l/s (in nonlinear relation) and compared with the linear approximation as shown in table 2.4.

Table 2.4: Shear velocities for all tested discharges.

| Discharge Q (l/s) | Shear velocity U* (mm/s) | | |
|---|---|---|---|
| | 1st_Linear approximation | 2nd_Non Linear approximation | Difference (%) |
| 8.00 | 6.06508 | 6.05477 | -0.17 |
| 11.10 | 7.96425 | 8.10159 | 1.72 |
| 13.00 | 9.32750 | 9.32750 | 0.00 |

It was observed the shear velocities calculated by nonlinear approximation was varied maximum around 1.72% from linear approximation. So, linear approximation of shear velocity was considered as shear velocity in smooth bed for further analysis.

### 2.3.3 Velocities near bed

Radice et al. (2009) described a conceptual picture according to which the dynamics of the bed-load sediment concentration is triggered by nearbed turbulent events which migrate along the flow, with the correlation of the concentration dynamics reasonably reflecting that of the flow field dynamics. [20] The velocity near bed was calculated with respect to the particle diameter. For full diameter 3 mm and also for half diameter 1.5 m velocity has been calculated by the equation 2.8.

The equation of velocity after simplifying:

$$V(z) = \frac{U^*}{k} lnz + D --- (2.8)$$

Where, $U^*$ is the shear velocity and

$k$ is the Von Karman constant = 0.41

$D$ is constant

Approximated nonlinear shear velocities were considered for calculating the near bed velocities. The constant D was considered by approximating the linear part of velocity profile. The velocities near bed are shown in table 2.5.

Table 2.5: Near bed velocities in smooth bed configuration.

| Discharge (l/s) | Near bed velocity (full dia.)_SB (mm/s) | Near bed velocity (half dia.)_SB (mm/s) |
|---|---|---|
| 8 | 157.2663 | 147.0126 |
| 11.1 | 162.3552 | 148.8908 |
| 13 | 166.0081 | 150.2390 |

The relation among discharges, bulk velocity and near bed velocities are shown in figure 2.10.

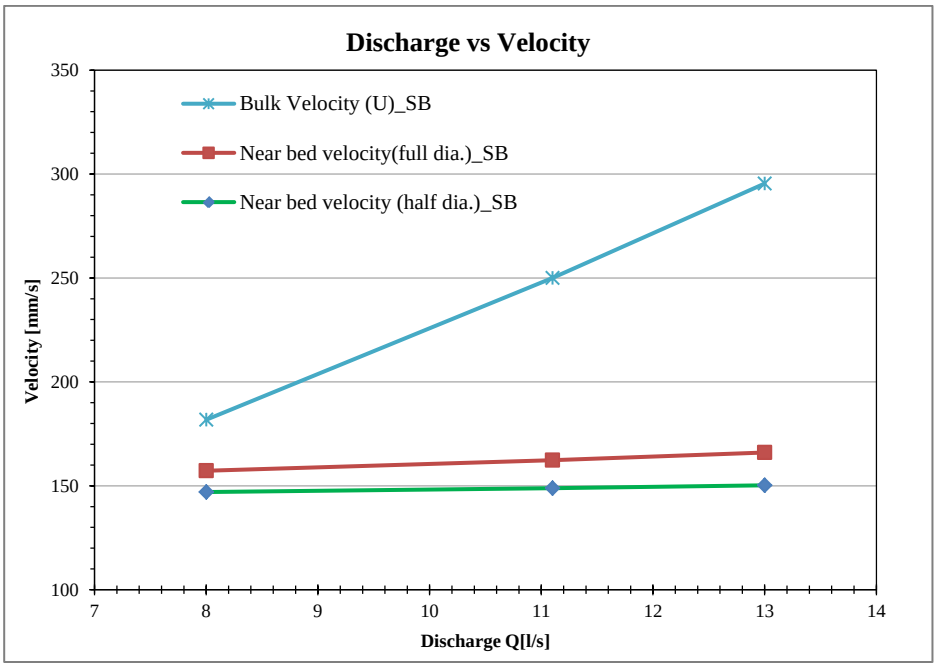


Figure 2.10: The relation between experimental discharges vs bulk velocity and near bed velocities.

Here, the near bed velocities for full diameter distance were higher than half diameter distance. Bulk velocity increased very fast and was higher than near bed velocity.

# Chapter 3

# IMAGE PROCESSING & VALIDATION

## 3.1 Introduction

Experimental fluid dynamics has always used flow visualization as a way of understanding and interpreting fluid flows [17]. Image processing or image analysis allows for quick processing of long sequences of photographs. The outputs show the phenomenon and characteristics of sediment over periods of time. These processes allow investigating a number of features of sediment transport. Specific information, such as particle velocity, can be analyzed to give statistics on the properties of a bed (Li et al. 1997).

The images have been taken during the experiment by using commercial high definition camera. The images were processed in sequences by the software Streams which extracts the particle tracking video from the sequenced images. MATLAB has been used for preprocessing the images with image properties for validation and further process.

## 3.2 Image processing

The images from the laboratory experiment were preprocessed to get the clear view of the channel portion have to be observed. The images resized from (960 x 700 px) to

(960x630 px) and record the conversion rate (mm/ px).

Streams software designed and implemented by the University of Canterbury (Nokes, 2012) has been used to identify and tracking of the white particles in the movies. This software allows processing the images and particle tracking. It has been developed, and has been successfully used, for application of PTV (particle velocimetry) to fluid flows. This technique is based on the principle of capturing video images of a specially illuminated particle seeded fluid flow, and from that video record extracting quantitative information about the flow field [17].

### 3.2.1 Filtering images

Filters provide Streams' image processing capabilities. A filter is defined to be an algorithm that can be applied to the color intensities (pixel) of a digital image in order to produce another digital image [17].

The particles which are in bright regions on a dark background or due to lighting non-uniformity the background intensity may vary across the image. The remove background filter is filtered by intensity of pixels within a fixed region of the image is used to obtain the average background intensity; this estimate is then subtracted to the pixels. Filtered pixel intensity that is less than zero is set to the minimum value zero [17].

(a)

(b)

Figure 3.1: (a) Original (resized) image and (b) Filtered image for same frame.

Effects of using removing background filter are shown in figure 3.1. Comparing the images, it was observed that after filtering procedure the each particle is more clearly defined.

### 3.2.2 Identification of particles

A particle identifier is defined as an algorithm that processes a digital image by locating particles within the image. Common to all particle identifiers is the assumption that particles are identified as regions within an image where the intensities of the pixels contrast with those in the rest of the image. [17]

Particle identification is based on an intensity threshold criterion. In processing, pixels with intensity 15 have been used as threshold. Higher than the threshold are labeled as “particle’s pixels” and once a pixel is found whose intensity exceeded the threshold, all “particle’s pixels” connected to that one are treated as part of the same particle. The output is a binary image where the background is black and particles are white. Minimum diameter has been used 1.5 mm that is the half diameter of sediment we used. Figure 3.2 shows result of particle identification. Red blobs represent the identified particles.

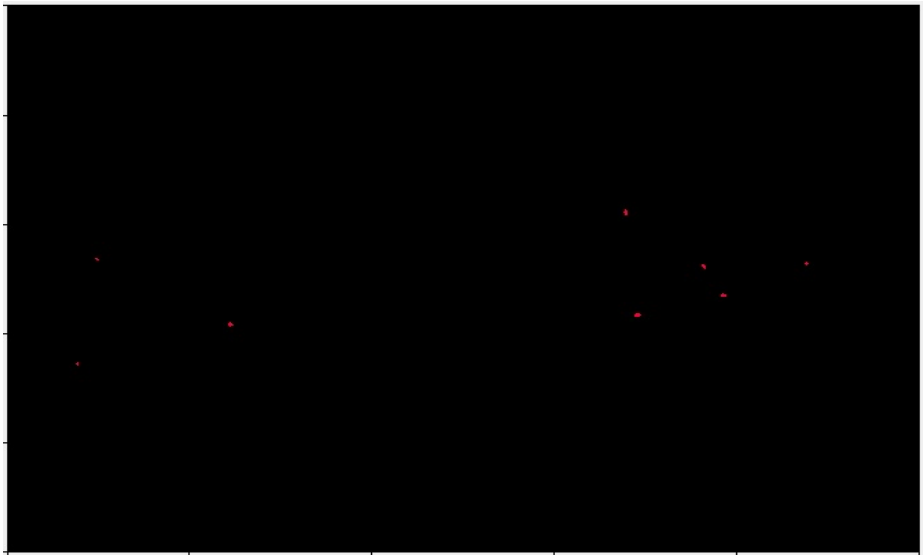

Figure 3.2: Identified particle for the same frame.

### 3.2.3 Particle tracking

The core phase of PTV is particle tracking which is based on the minimum distance separating the two images of the same particle in successive frames. This minimum distance criterion was suitable for this experiment because very low density white particle was used. The position of any particle is predicted as the original position by default and in next frame when particle changes the position that will be the closest one to the original position. The y distance weight was considered as 3. For optimization an appropriate research window was defined.

Typical results of particle tracking are shown in figure 3.3 where moving particles appear as red continuous or dotted curves and the matching portions of global trajectories as light blue lines.

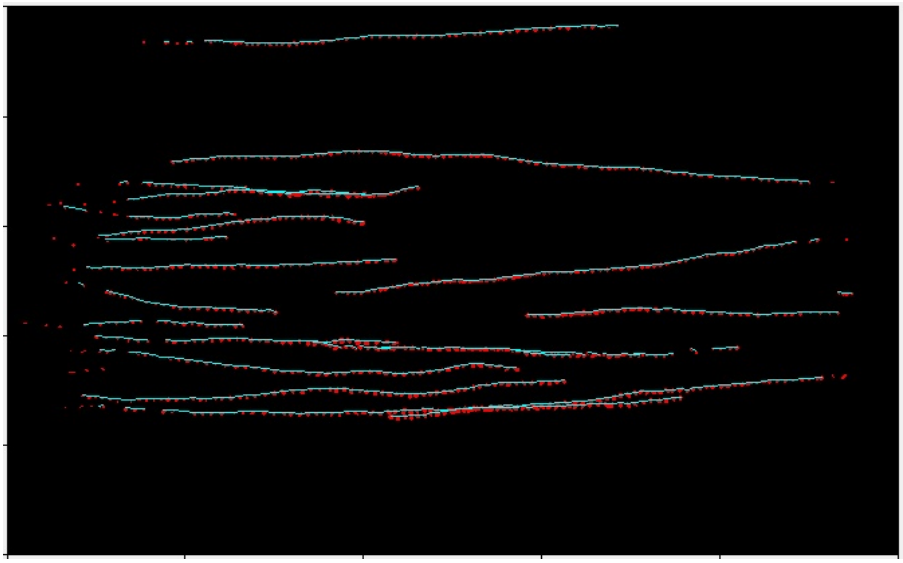

Figure 3.3: Particle tracking with few frames.

### 3.2.4 Output of PTV

The output of the PTV analysis was a matrix with values of position and velocity with time for each recognized particle which was very wide database. While analyzing in software Streams; it was found there were some interruption in particle moving trajectories and some short trajectories as shown in figure 3.4.

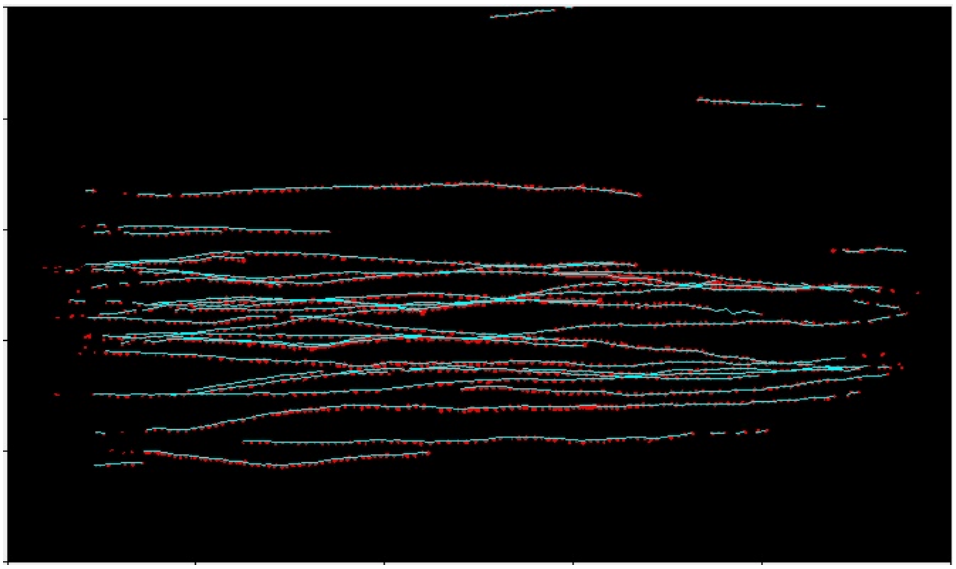

Figure 3.4: Interruption in moving particle track.

As we discussed in chapter 2 that one data set for discharge 8 and two data sets for 11.1 and 13.0 l/s were taken. From output of PTV; velocities and lengths of the particles for instant time were found. For removing too short trajectories; pdfs of length were calculated and compared as shown in figure 3.5.

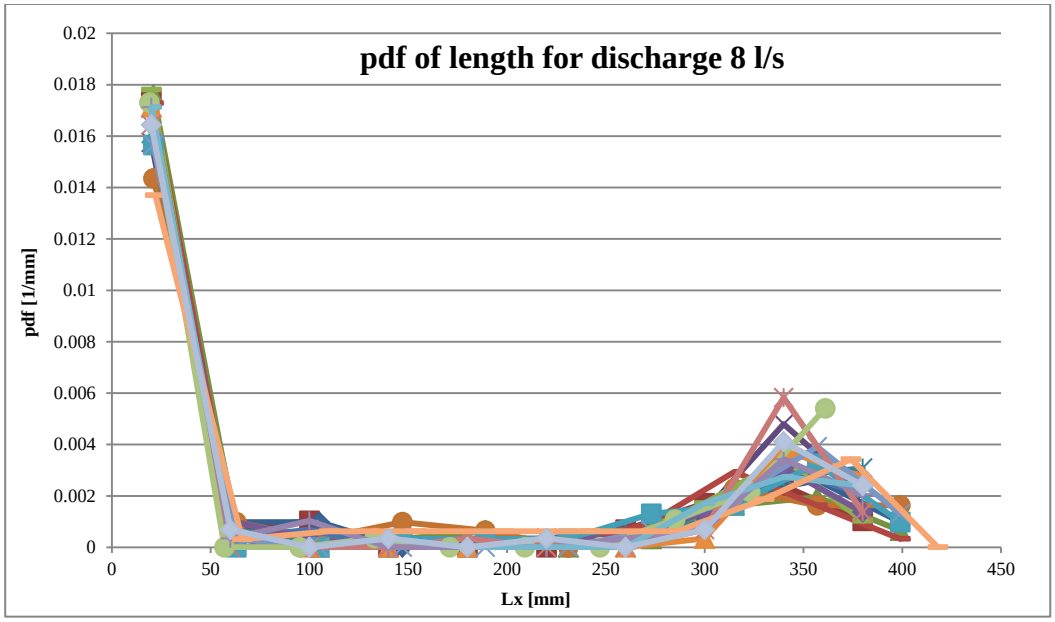


(a)

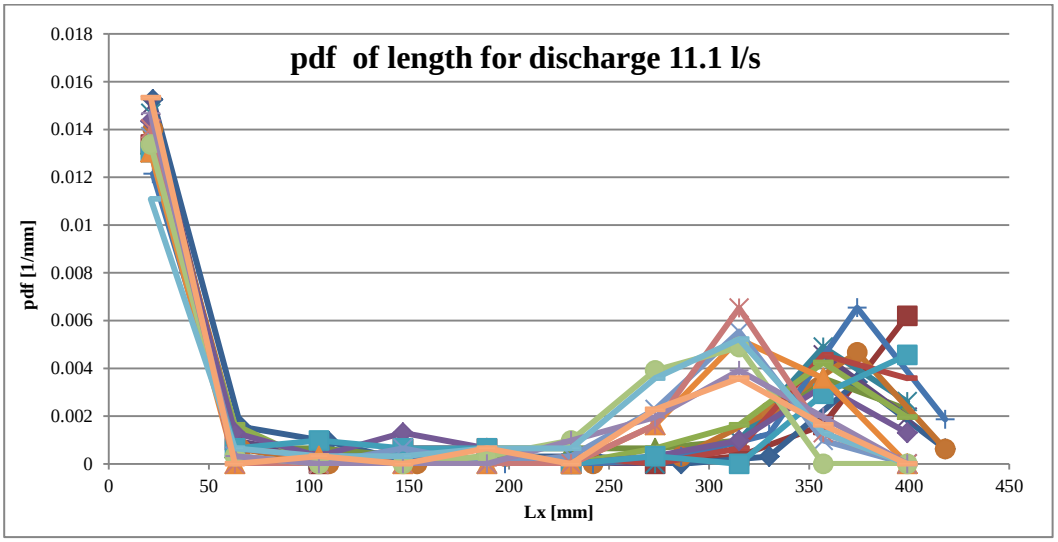


(b)

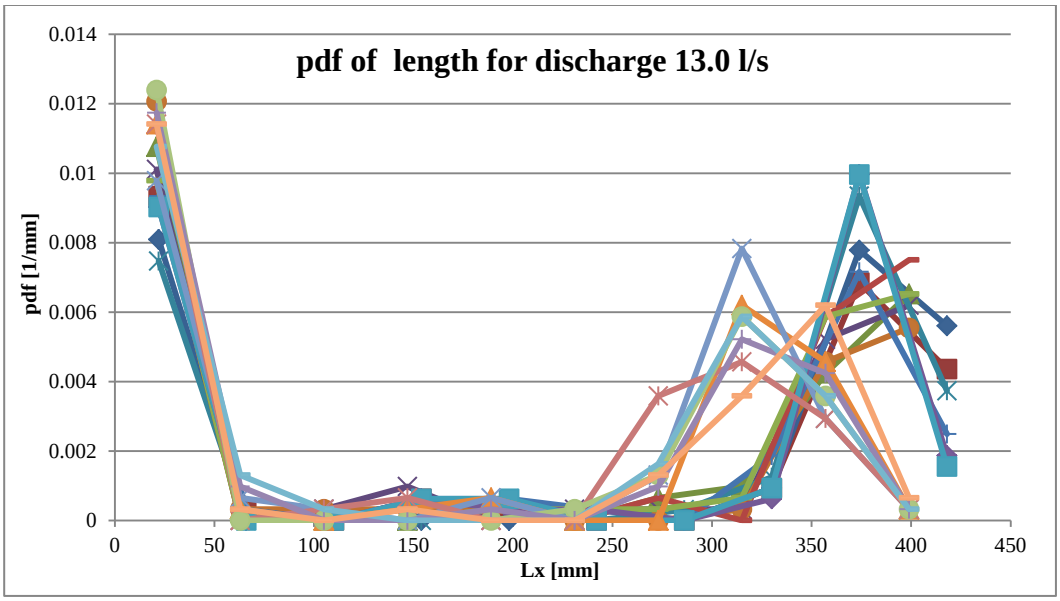


(c)

Figure 3.5: pdfs of length for discharge (a) 8 l/s, (b) 11.1 l/s and (c) 13.0 l/s.

It can be observed from the figure above; pdfs of length for discharge 8 l/s showed one general peak but for discharge 11.1 and 13.0 l/s showed two general peaks. The properties might be different for two groups. So those groups of data were considered separately and also combined for further analysis. Also to remove too short trajectories; the obtained lengths of trajectories were filtered by the threshold 200 mm means shorter than 200 mm trajectories were discarded.

## 3.3 Validation

Validation has been done for the trajectories longer than the threshold value 200 mm. The short trajectories could be wrong because of the two particles going together or following the same path. Validation has been done by MATLAB code based on the principle of superimposing trajectories and images of particles in the movie. After creating the trajectories properties from the output of image processing; too short trajectories were removed. By using the proper image conversion (mm/px); all the long trajectories (more than 200 mm) were validated. Typical MATLAB code based validation interface are shown in figure 3.6.

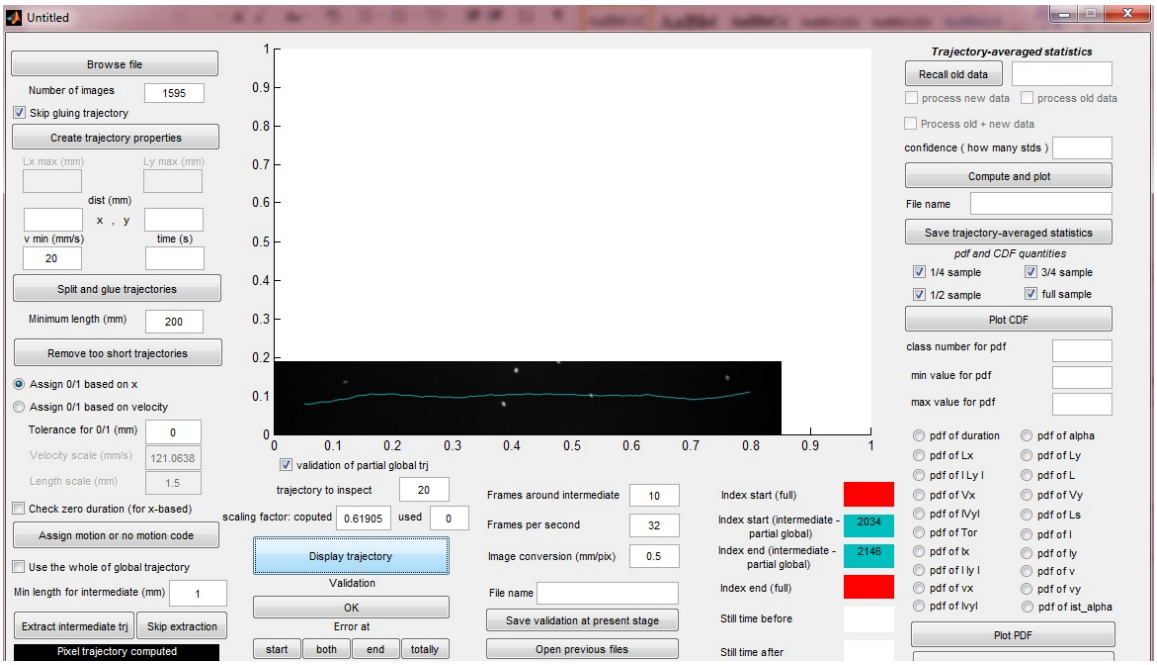


Figure 3.6: Validation of long trajectories.

Each of long trajectories in the database was checked that the moving particle follow the same path in superimposed trajectories and images of particle in movie then validated. A typical trajectory validation is shown in figure 3.7.

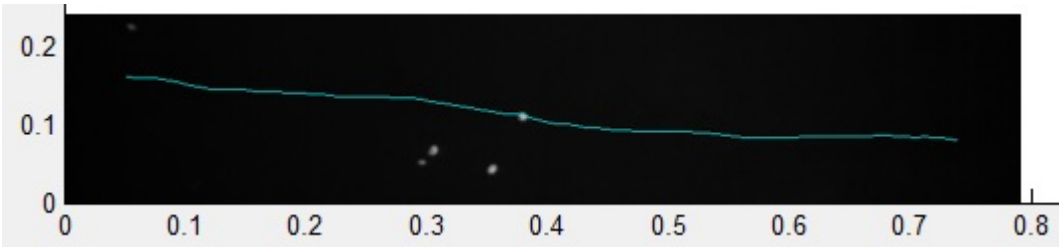


Figure 3.7: Validation of long trajectories.

There were total 2219 validated long trajectories for three discharges 8, 11.1 and 13 l/s. All the trajectories were found correct and validated as shown in table 3.1.

Table 3.1: List of the number of measurements for SB runs.

| For smooth bed configuration | Discharge (l/s) | | | | |
|---|---|---|---|---|---|
| | **8** | **11.1** | | **13** | |
| | | 1st Group | 2nd Group | 1st Group | 2nd Group |
| Number of checked movies | 19 | 11 | 7 | 11 | 7 |
| Number of intermediate trajectories found | 449 | 753 | 273 | 419 | 325 |
| Number of validated trajectories | 449 | 753 | 273 | 419 | 325 |
| Total number of validated trajectories | **449** | **1026** | | **744** | |

## 3.4 Analyzed variables

After removing short trajectories and validation, the average statistics of the following variables i.e: trajectory duration T, minimum distance or straight length $L_p$, traveled full path length $\mathcal{L}_p$, the longitudinal distance of the trajectory $L_x$ and transverse direction $L_y$, the velocities of the particle motion also in longitudinal direction $V_x$, in transverse direction $V_y$, tortuosity $T_{tor}$ and the angle α for long trajectories were found as integral and instantaneous properties.

The variables are shown graphically in figure 3.8.

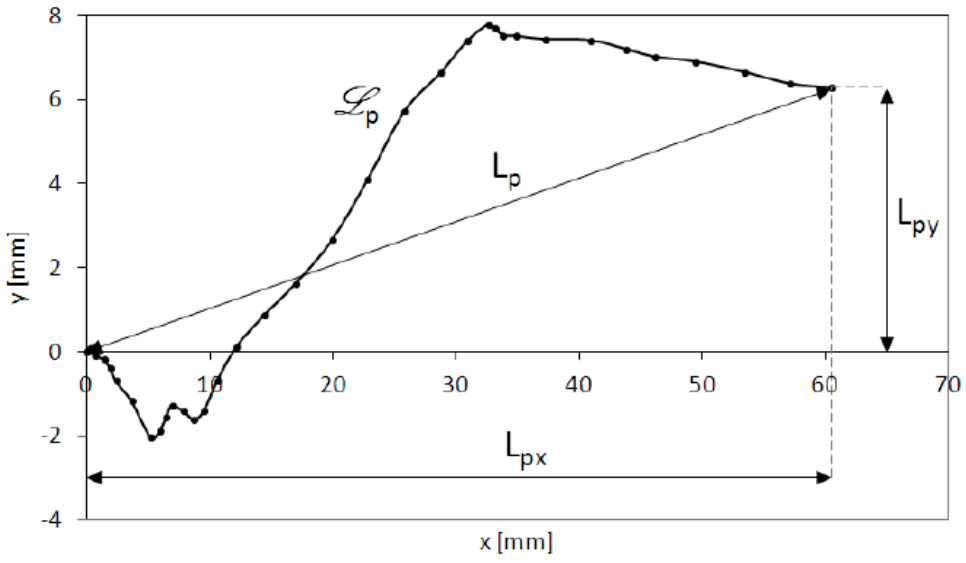


Figure 3.8: The path length, $\mathcal{L}p$, the straight length, $L_p$, and its longitudinal length $L_{px}$

and transversal length $L_{py}$.

$$\text{Then, angle, } \alpha = \arctan\frac{L_{py}}{L_{px}}$$

The following statistical parameters for velocity in longitudinal direction $V_x$, in transverse direction $V_y$, tortuosity $T_{tor}$ and the angle α as integral properties were analyzed:

*Mean ($\mu$)* is the arithmetic average of a set data. It can be calculated by mathematical averaging of a set of data. The mean approximation is very important in analyzing data.

*Standard deviation ($\delta$)* is a measure of the dispersion of a set of data from its mean. It gives an approximate picture of the average amount each number in a set varies from the center value. It can be calculated by the square root of the Variance.

$$Standard\ deviation\ (\delta) = \sqrt{\frac{\sum[x - mean(\mu)]^2}{Total\ number\ of\ sample}}$$

*Coefficient of variation ($C_V$)* is the normalized measure of dispersion of a probability distribution. It is expressed as the ratio of standard deviation and mean. Coefficient of variation is the measure of variability of the data. When the value of coefficient of variation is higher, it means that the data has high variability and less stability and vice versa when coefficient of variation is lower. It can be calculated by:

$$Coefficient\ of\ variation\ (C_V) = \frac{Standard\ deviation\ (\delta)}{Mean\ (\mu)}$$

*Skewness ($S_k$)* is the measure about symmetry around the sample mean. The skewness for a normal distribution or any symmetrical data is zero. Usually negative

values for the skewness indicate data that are skewed left means that the left tail is long relative to the right tail and positive values for the skewness indicate data that are skewed right means that the right tail is long relative to the left tail shown in figure 3.9.

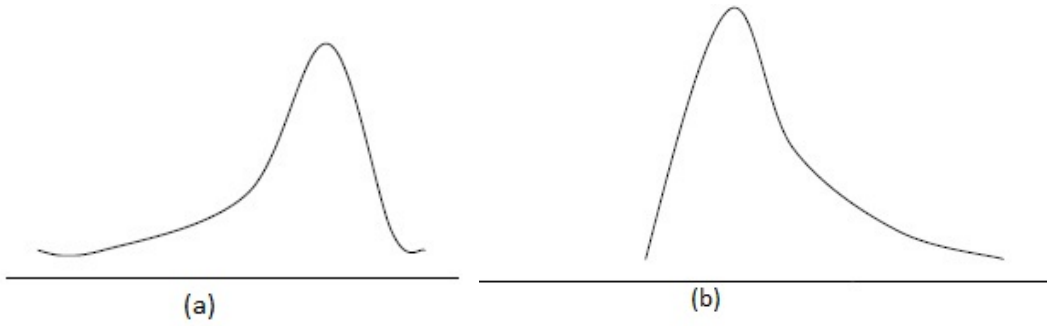


Figure 3.9: (a) Distribution for left skewed and (b) Distribution for right skewed.

*Kurtosis* ($K_u$) is defined as a normalized form of the fourth central moment. It is a distribution of statistical measure used to describe the distribution of observed data around the mean.

Also statistical distribution has been done for the analyzed variables mentioned above as probability distribution function and cumulative distribution function.

The results and the characteristics are shown in chapter 4.

# Chapter 4

# RESULTS & DISCUSSION

## 4.1 Statistical analysis results

In laboratory experiment, total five groups of data set have been taken for different discharges. For discharge 8 l/s, one group of data; discharges 11.1 l/s and 13.0 l/s, two groups of data were taken. In post processing for discharge 11.1 l/s and 13.0 l/s, the groups of data set have been analyzed in each group separately and also by combining both groups of data set. In post processing, the statistical parameters have been analyzed are mean ($\mu$), standard deviation ($\delta$), coefficient of variation ($C_v$), skewness ($S_k$) and kurtosis ($K_u$) for the variables angle of deviation ($\alpha$), velocity along the flowing direction ($V_x$), velocity along the transverse direction of flow ($V_y$) and tortuosity ($T_{tor}$) as integral properties. The results are shown in table 4.1.

Table 4.1: Moments (μ, δ, $C_v$, $S_k$ and $K_u$ ) of the variables α (degree), $V_x$ (mm/s), $V_y$ (mm/s) and $T_{tor}$ (mm/mm).

| Discharge (l/s) | Set of Data | Variable | Mean (μ) | Stand. Dev. (δ) | Coeff. of Var. (Cv) | Skewness (Sk) | Kurtosis (Ku) |
|---|---|---|---|---|---|---|---|
| 8 | All | α | -0.5419 | 1.9231 | -3.5490 | -0.1727 | 3.1547 |
| | | Vx | 69.9625 | 13.2052 | 0.1887 | -0.6400 | 5.3915 |
| | | Vy | -0.6681 | 2.3588 | -3.5308 | -0.1651 | 3.2597 |
| | | T_tor | 1.0096 | 0.0053 | 0.0052 | 3.7214 | 30.2642 |
| 11.1 | 1 st Group | α | -0.5760 | 2.2010 | -3.8215 | -0.0790 | 2.9716 |
| | | Vx | 119.7387 | 14.2279 | 0.1188 | 0.4806 | 3.5531 |
| | | Vy | -1.2254 | 4.6596 | -3.8024 | -0.1887 | 3.4414 |
| | | T_tor | 1.0050 | 0.0022 | 0.0022 | 1.5605 | 7.4384 |
| | 2 nd Group | α | -0.4235 | 2.1767 | -5.1400 | 0.0712 | 2.9194 |
| | | Vx | 120.5276 | 14.4667 | 0.1200 | 0.2693 | 2.8578 |
| | | Vy | -0.9042 | 4.5435 | -5.0249 | 0.1018 | 3.0915 |
| | | T_tor | 1.0047 | 0.0020 | 0.0020 | 1.3787 | 6.0119 |
| | All (combined both groups) | α | -0.5354 | 2.1945 | -4.0990 | -0.0410 | 2.9667 |
| | | Vx | 119.9486 | 14.2890 | 0.1191 | 0.4231 | 3.3514 |
| | | Vy | -1.1400 | 4.6290 | -4.0606 | -0.1178 | 3.3720 |
| | | T_tor | 1.0049 | 0.0022 | 0.0022 | 1.5318 | 7.2387 |
| 13 | 1 st Group | α | -0.1136 | 2.0308 | -17.8821 | 0.0937 | 2.9093 |
| | | Vx | 151.4252 | 17.0973 | 0.1129 | 0.9448 | 5.3720 |
| | | Vy | -0.3006 | 5.3900 | -17.9325 | 0.1190 | 3.0013 |
| | | T_tor | 1.0041 | 0.0017 | 0.0017 | 0.9872 | 4.0167 |
| | 2 nd Group | α | -0.4150 | 2.2341 | -5.3835 | -0.0066 | 2.9428 |
| | | Vx | 155.9346 | 17.3992 | 0.1116 | 0.6950 | 3.4194 |
| | | Vy | -1.2281 | 6.1458 | -5.0043 | -0.0358 | 2.9062 |
| | | T_tor | 1.0037 | 0.0018 | 0.0018 | 1.3057 | 5.3286 |
| | All (combined both groups) | α | -0.2452 | 2.1258 | -8.6684 | 0.0225 | 2.9672 |
| | | Vx | 153.3950 | 17.3631 | 0.1132 | 0.8190 | 4.3862 |
| | | Vy | -0.7057 | 5.7469 | -8.1431 | 0.0046 | 3.0219 |
| | | T_tor | 1.0039 | 0.0018 | 0.0018 | 1.1006 | 4.4897 |

### 4.1.1 Comparison of moments

The moments have been compared with the considered variables for all experimental discharges (8 l/s, 11.1 l/s and 13.0 l/s) and also for the group of data set ($1^{st}$ group, $2^{nd}$ group and combined) for the discharges 11.1 l/s and 13.0 l/s to analyze the behavior among different groups of data set and within the discharges too.

### 4.1.1.1 Angle of deviation (α)

The moments of angle of deviation for discharges are shown in table 4.2.

Table 4.2: Angle of deviation moments for experimental discharges.

| Data | Discharge (l/s) | Mean (μ) | Stand. Dev. (δ) | Coeff. of Var. (Cv) | Skewness (Sk) | Kurtosis (Ku) |
|---|---|---|---|---|---|---|
| Q=8 l/s_All | 8 | -0.5419 | 1.9231 | -3.5490 | -0.1727 | 3.1547 |
| Q=11.1 l/s_1st Gr. | 11.1 | -0.5760 | 2.2010 | -3.8215 | -0.0790 | 2.9716 |
| Q=11.1 l/s_2nd Gr. | 11.1 | -0.4235 | 2.1767 | -5.1400 | 0.0712 | 2.9194 |
| Q=11.1 l/s_All | 11.1 | -0.5354 | 2.1945 | -4.0990 | -0.0410 | 2.9667 |
| Q=13 l/s_1st Gr. | 13 | -0.1136 | 2.0308 | -17.8821 | 0.0937 | 2.9093 |
| Q=13 l/s_2nd Gr. | 13 | -0.4150 | 2.2341 | -5.3835 | -0.0066 | 2.9428 |
| Q=13 l/s_All | 13 | -0.2452 | 2.1258 | -8.6684 | 0.0225 | 2.9672 |

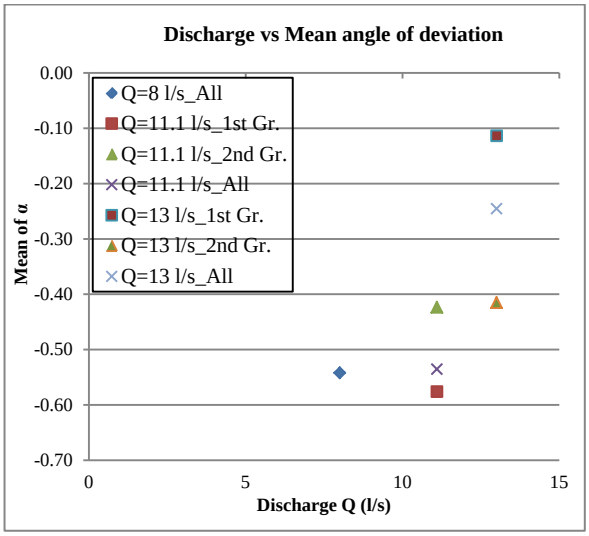


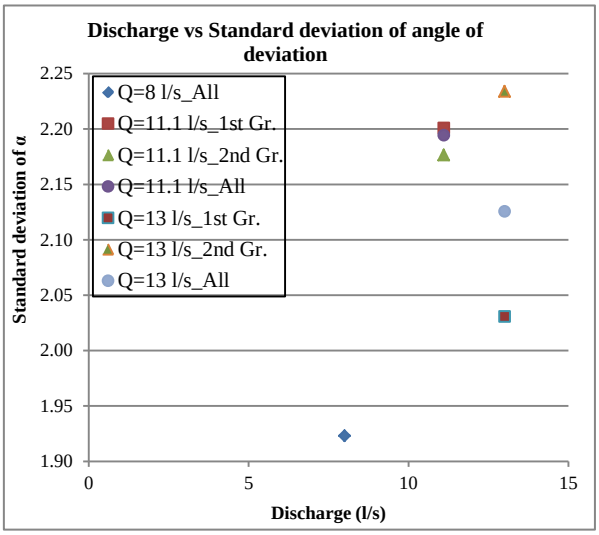


(a) (b)

Figure 4.1: For all groups of data set; (a) Discharge vs mean angle of deviation and (b) Discharge vs standard deviation of angle of deviation.

It was observed that; angle of deviation increased with the increasing discharge. Expected mean value of alpha was equal to zero. Here small negative values indicate that the camera was probably a bit skewed in comparison with the mean flow direction,

but the angle is however not large. Within the same discharges; combined set of data values have very small difference with 1st and 2nd groups of data and the values are within this two group values.

### 4.1.1.2 Longitudinal velocity ($V_x$)

The moments of longitudinal velocity ($V_x$) for all experimental discharges are shown in table 4.3.

Table 4.3: Longitudinal velocity moments for experimental discharges.

| Data | Discharge (l/s) | Mean (μ) | Stand. Dev. (δ) | Coeff. of Var. (Cv) | Skewness (Sk) | Kurtosis (Ku) |
|---|---|---|---|---|---|---|
| Q=8 l/s_All | 8 | 69.9625 | 13.2052 | 0.1887 | -0.6400 | 5.3915 |
| Q=11 l/s_1st Gr. | 11.1 | 119.7387 | 14.2279 | 0.1188 | 0.4806 | 3.5531 |
| Q=11 l/s_2nd Gr. | 11.1 | 120.5276 | 14.4667 | 0.1200 | 0.2693 | 2.8578 |
| Q=11 l/s_All | 11.1 | 119.9486 | 14.2890 | 0.1191 | 0.4231 | 3.3514 |
| Q=13 l/s_1st Gr. | 13 | 151.4252 | 17.0973 | 0.1129 | 0.9448 | 5.3720 |
| Q=13 l/s_2nd Gr. | 13 | 155.9346 | 17.3992 | 0.1116 | 0.6950 | 3.4194 |
| Q=13 l/s_All | 13 | 153.3950 | 17.3631 | 0.1132 | 0.8190 | 4.3862 |

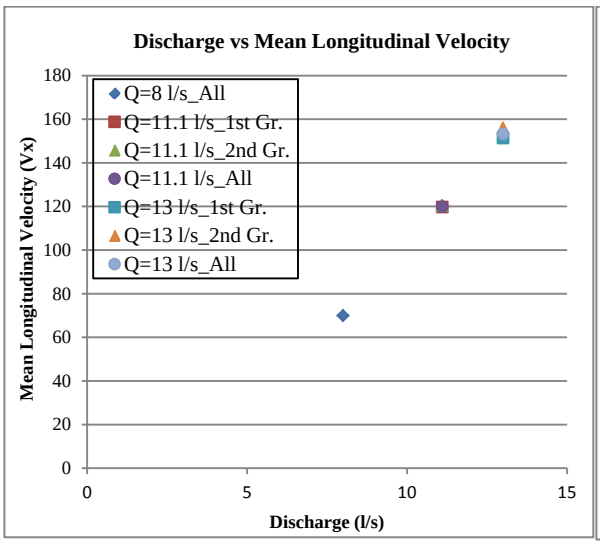


(a)

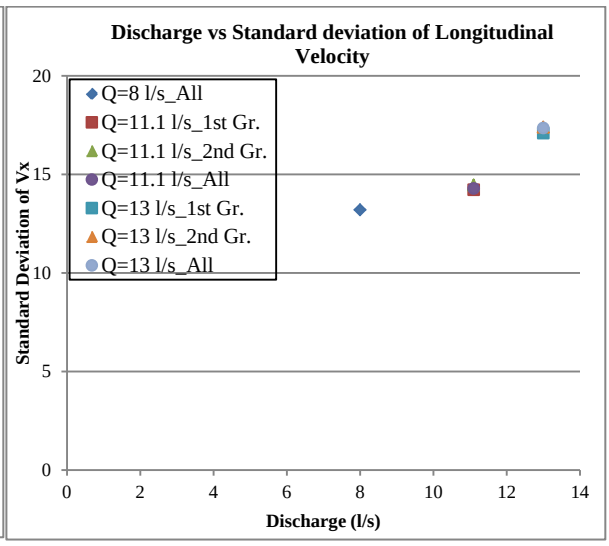


(b)

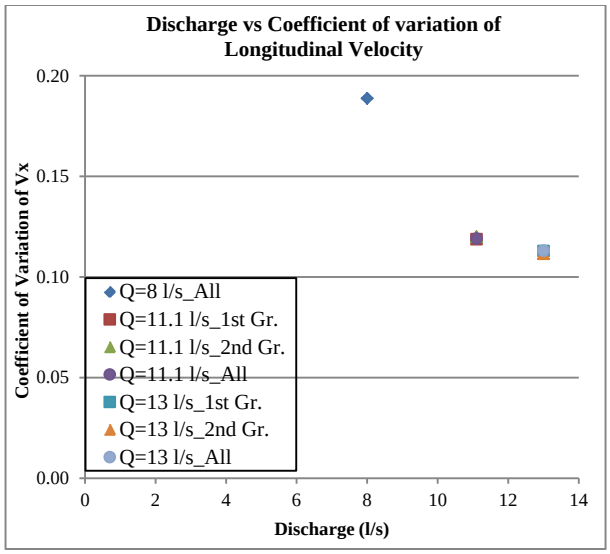


(c)

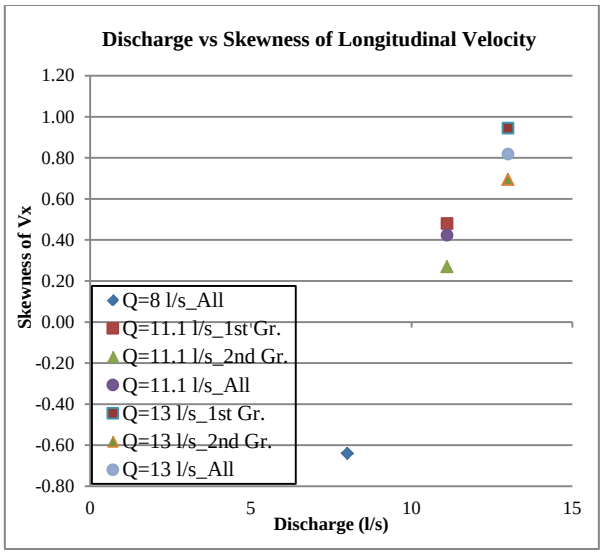


(d)

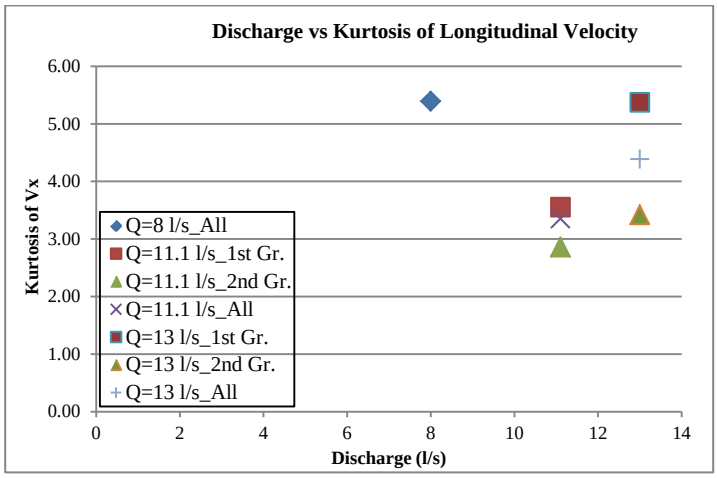


(e)

Figure 4.2: For all groups of data set; Discharge vs (a) mean longitudinal velocity; (b) standard deviation of longitudinal velocity; (c) coefficient of variation of longitudinal velocity; (d) skewness of longitudinal velocity and (e) kurtosis of longitudinal velocity.

It was observed that; longitudinal velocity increased with the increasing discharge. With increasing discharge longitudinal velocity became more deviated from the mean velocity. Within the same discharges; combined set of data values have very small difference with 1st and 2nd groups of data and the values are within this two group values. Coefficient of variation decreased with increasing discharge so it can be concluded the experimental data are more stable for larger discharges. Longitudinal

velocities turns from left skewed to right skewed with increasing discharges. As very small difference or less variability, the combined data were used in further analysis. The kurtosis values of all discharges were around 3 to 5; so the distributions of velocities are similar for all considered experimental discharges.

#### 4.1.1.3 Transverse velocity ($V_y$)

The moments of transverse velocities have been compared with the considered variables for all experimental discharges (8 l/s, 11.1 l/s and 13.0 l/s) and also for the group of data set ($1^{st}$ group, $2^{nd}$ group and combined) for the discharges 11.1 l/s and 13.0 l/s to analyze the behavior. The moments of transverse velocity for discharges are shown in table 4.4.

Table 4.4: Transverse velocity moments for experimental discharges.

| Data | Discharge (l/s) | Mean (μ) | Stand. Dev. (δ) | Coeff. of Var. (Cv) | Skewness (Sk) | Kurtosis (Ku) |
|---|---|---|---|---|---|---|
| Q=8 l/s_All | 8 | -0.6681 | 2.3588 | -3.5308 | -0.1651 | 3.2597 |
| Q=11.1 l/s_1st Gr. | 11.1 | -1.2254 | 4.6596 | -3.8024 | -0.1887 | 3.4414 |
| Q=11.1 l/s_2nd Gr. | 11.1 | -0.9042 | 4.5435 | -5.0249 | 0.1018 | 3.0915 |
| Q=11.1 l/s_All | 11.1 | -1.1400 | 4.6290 | -4.0606 | -0.1178 | 3.3720 |
| Q=13 l/s_1st Gr. | 13 | -0.3006 | 5.3900 | -17.9325 | 0.1190 | 3.0013 |
| Q=13 l/s_2nd Gr. | 13 | -1.2281 | 6.1458 | -5.0043 | -0.0358 | 2.9062 |
| Q=13 l/s_All | 13 | -0.7057 | 5.7469 | -8.1431 | 0.0046 | 3.0219 |

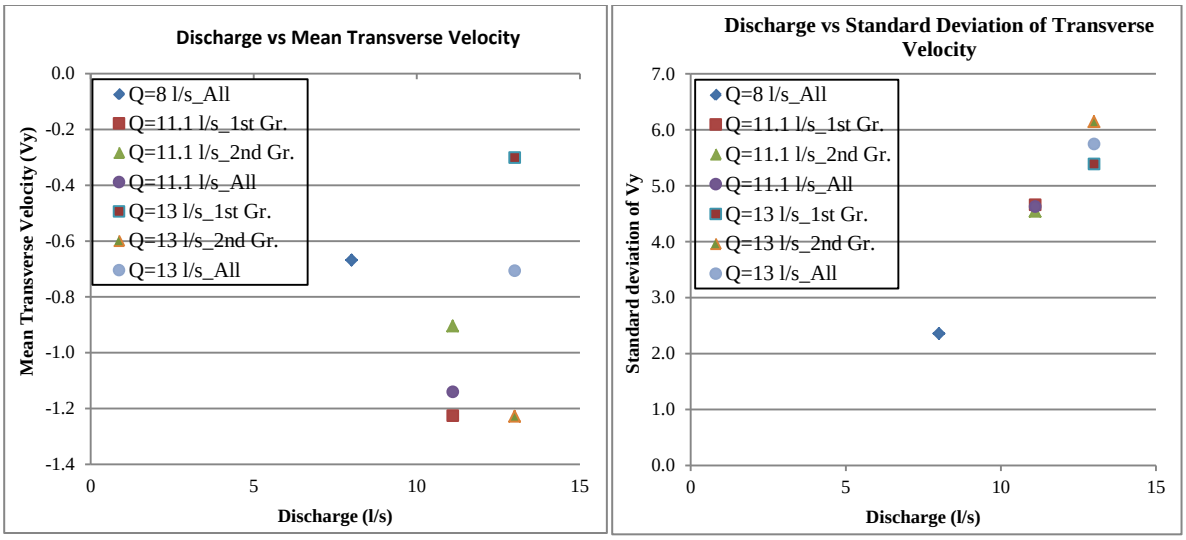


(a) (b)

Figure 4.3: For all groups of data set; (a) Discharge vs mean transverse velocity; and (b) Discharge vs standard deviation of transverse velocity.

It was observed that; transverse velocity more deviated with the increasing discharge which was as expected. Within the same discharges; combined set of data values have very small difference with 1st and 2nd groups of data and the values are within this two group values. For discharge 13.0 l/s transverse velocities deviated more for 2nd group data. Variation of transverse velocity for discharge 13.0 l/s_1st group is less stable. The value of transverse velocity showed negative which was consistent with the values of angle of deviation.

### 4.1.1.4 Tortuosity ($T_{tor}$)

The moments of tortuosity for all experimental discharges are shown in table 4.5.

Table 4.5: Tortuosity moments for experimental discharges.

| Data | Discharge (l/s) | Mean (μ) | Stand. Dev. (δ) | Coeff. of Var. (Cv) | Skewness (Sk) | Kurtosis (Ku) |
|---|---|---|---|---|---|---|
| Q=8 l/s | 8 | 1.0096 | 0.0053 | 0.0052 | 3.7214 | 30.2642 |
| Q=11.1 l/s_1st Gr. | 11.1 | 1.0050 | 0.0022 | 0.0022 | 1.5605 | 7.4384 |
| Q=11.1 l/s_2nd Gr. | 11.1 | 1.0047 | 0.0020 | 0.0020 | 1.3787 | 6.0119 |
| Q=11.1 l/s_All | 11.1 | 1.0049 | 0.0022 | 0.0022 | 1.5318 | 7.2387 |
| Q=13 l/s_DS-1 | 13 | 1.0041 | 0.0017 | 0.0017 | 0.9872 | 4.0167 |
| Q=13 l/s_DS-2 | 13 | 1.0037 | 0.0018 | 0.0018 | 1.3057 | 5.3286 |
| Q=13 l/s_DS-3 | 13 | 1.0039 | 0.0018 | 0.0018 | 1.1006 | 4.4897 |

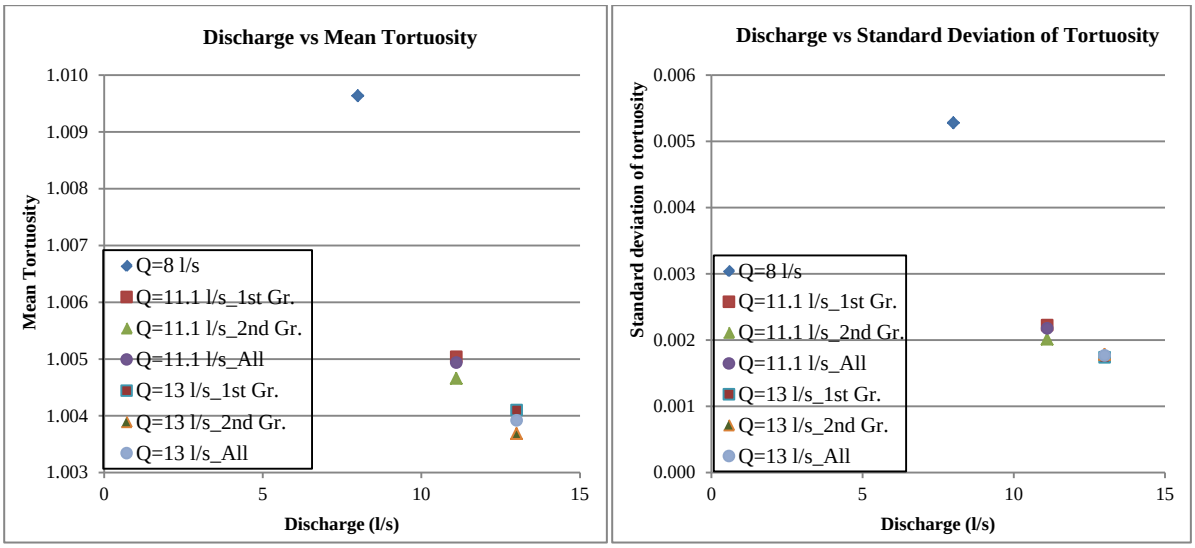


(a) (b)

Figure 4.4: (a) Discharge vs mean tortuosity; and (b) Discharge vs standard deviation of tortuosity.

It was observed that; tortuosity is decreased with the increasing discharge which was as expected because it was in smooth bed configuration so the particles move more straight with increasing discharge. Within the same discharges; combined set of data values have very small difference with 1st and 2nd groups of data and the values are within this two group values. Data were not varied much with respect to the mean value with increasing discharge and the experimental data are stable. The mean values of tortuosity were around 1 for all experimental discharges.

All the data from image processing and validation were analyzed correctly. Extensive analyses of the all properties of moving sediment were done precisely as possible. Finally it can be concluded that; the moving sediment properties angle of deviation ($\alpha$) and transverse velocity ($V_y$) were found with zero mean and another property tortuosity ($T_{tor}$) with a mean value of 1. Results for these properties are either scattered or somehow trivial. As expectable, the most significant property for this configuration of the bed is longitudinal velocity ($V_x$).

### 4.1.2 Comparison of moments with rough bed

The moments of longitudinal velocity for smooth bed configuration have been compared with respect to discharge, shear velocity, bulk velocity and dimensionless velocity to corresponding rough bed configuration data which was taken from the previous research experiment.

#### 4.1.2.1 Moments with respect to discharge

The considered variables (*Mean (μ), Standard Deviation (δ), Coefficient of Variation ($C_v$), Skewness ($S_k$) & Kurtosis ($K_u$)*) in smooth bed configuration for experimental discharges (8 l/s, 11.1 l/s and 13.0 l/s) and for rough bed configuration (11.1 l/s, 12.2 l/s & 13.0 l/s) are shown in table 4.6 and the comparisons are shown in figure 4.5.

Table 4.6: Moments in smooth bed and rough bed configuration.

| Discharge (l/s) | For longitudinal velocity $V_x$ (mm/s) | | | | |
|---|---|---|---|---|---|
| | SMOOTH BED | | | | |
| | Mean (μ) | Stand. Dev. (δ) | Coeff. of Var. (Cv) | Skewness (Sk) | Kurtosis (Ku) |
| 8.0 | 69.96 | 13.21 | 0.19 | -0.64 | 5.39 |
| 11.1 | 119.95 | 14.29 | 0.12 | 0.42 | 3.35 |
| 13.0 | 153.40 | 17.36 | 0.11 | 0.82 | 4.39 |

| Discharge (l/s) | ROUGH BED | | | | |
|---|---|---|---|---|---|
| | Mean (μ) | Stand. Dev. (δ) | Coeff. of Var. (Cv) | Skewness (Sk) | Kurtosis (Ku) |
| 11.1 | 29.38 | 16.60 | 0.56 | 0.82 | 0.38 |
| 12.2 | 28.73 | 19.61 | 0.68 | 1.08 | 0.82 |
| 13.0 | 32.61 | 20.54 | 0.63 | 1.07 | 1.13 |

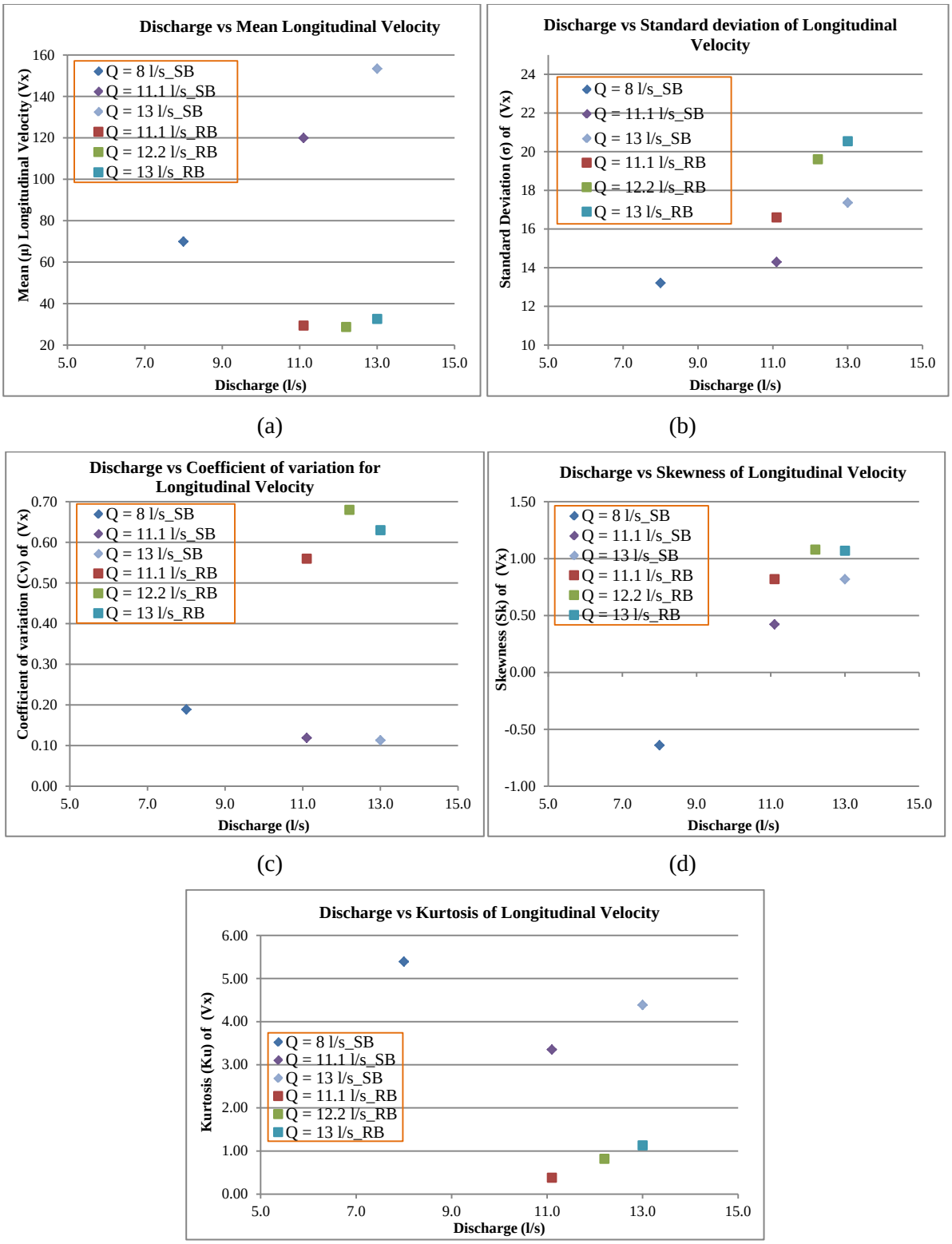


Figure 4.5: For smooth & rough bed configuration; Discharge vs (a) mean longitudinal velocity; (b) Standard deviation of longitudinal velocity; (c) Coefficient of variation of longitudinal

velocity, (d) Skewness of longitudinal velocity and (e) Kurtosis of longitudinal velocity.

In this analysis, for same discharges combined group data have been used in comparison as discussed above. It was observed that; mean longitudinal velocity is more in smooth bed configuration than rough bed. Within the same discharges mean velocity increased 300%. For individual experimental data, smooth bed velocities are less deviated. Smooth bed velocity data are more stable than rough bed configuration because it showed low coefficient of variation. Smooth bed velocities are right skewed where rough bed velocities are more right skewed in comparison. Longitudinal velocity distribution with smooth bed configuration have a distinct peak near to mean value where rough bed velocity distribution have a flat peak near mean value compare to smooth bed velocity distribution.

#### 4.1.2.2 Moments with respect to shear velocity (U*)

The shear velocities and bulk velocities in smooth bed configuration for experimental discharges (8 l/s, 11.1 l/s and 13.0 l/s) and for rough bed configuration (11.1 l/s, 12.2 l/s & 13.0 l/s) are shown in table 4.7 and the comparison of the moments with respect to shear velocity is shown in figure 4.6.

Table 4.7: Bulk and shear velocities in both bed configuration.

| | Smooth bed configuration | |
|---|---|---|
| Discharge (l/s) | Bulk velocity (U) (mm/s) | Shear velocity (U*) (mm/s) |
| 8.0 | 181.82 | 6.07 |
| 11.1 | 250.00 | 7.89 |
| 13.0 | 295.45 | 9.33 |

| | Rough bed configuration | |
|---|---|---|
| Discharge (l/s) | Bulk velocity (U) (mm/s) | Shear velocity (U*) (mm/s) |
| 11.1 | 250 | 16 |
| 12.2 | 280 | 18 |
| 13.0 | 300 | 23 |

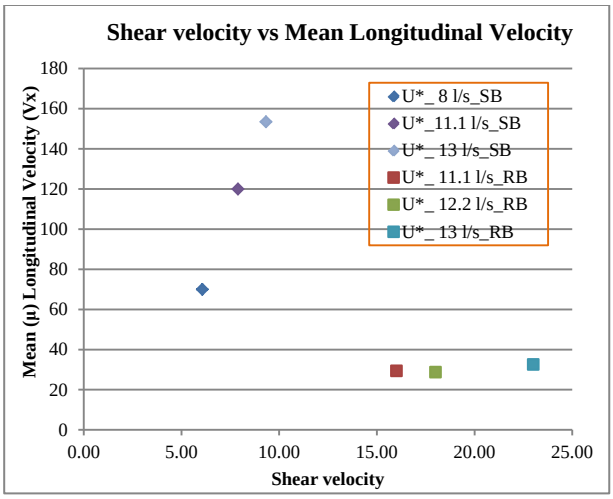
Shear velocity vs Mean Longitudinal Velocity
Mean (μ) Longitudinal Velocity (Vx)
Shear velocity
U*_ 8 l/s_SB
U*_11.1 l/s_SB
U*_ 13 l/s_SB
U*_ 11.1 l/s_RB
U*_ 12.2 l/s_RB
U*_ 13 l/s_RB

(a)

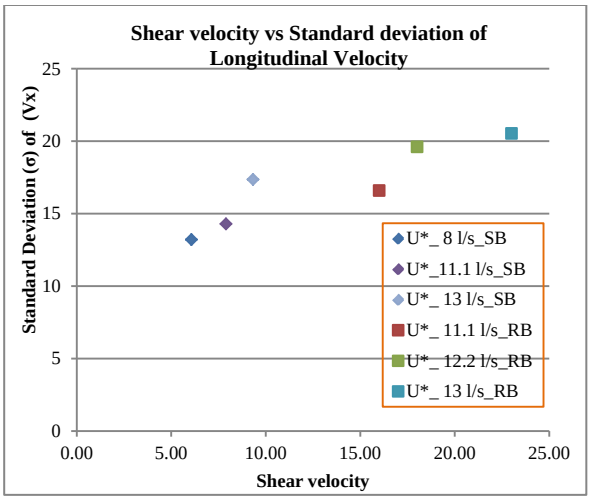
Shear velocity vs Standard deviation of Longitudinal Velocity
Standard Deviation (σ) of (Vx)
Shear velocity
U*_ 8 l/s_SB
U*_11.1 l/s_SB
U*_ 13 l/s_SB
U*_ 11.1 l/s_RB
U*_ 12.2 l/s_RB
U*_ 13 l/s_RB

(b)

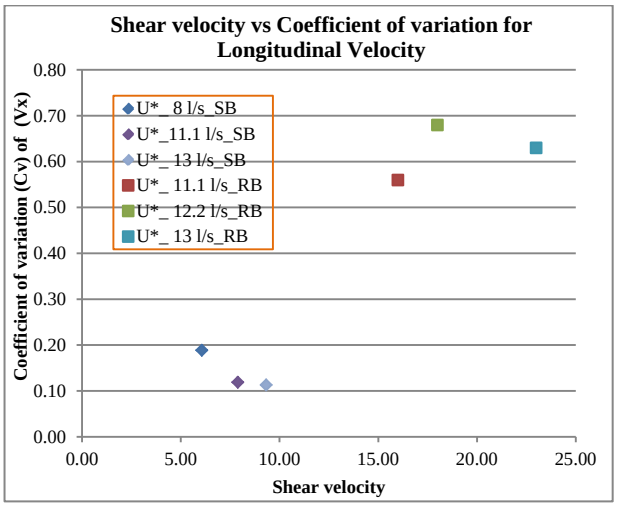
Shear velocity vs Coefficient of variation for Longitudinal Velocity
Coefficient of variation (Cv) of (Vx)
Shear velocity
U*_ 8 l/s_SB
U*_11.1 l/s_SB
U*_ 13 l/s_SB
U*_ 11.1 l/s_RB
U*_ 12.2 l/s_RB
U*_ 13 l/s_RB

(c)

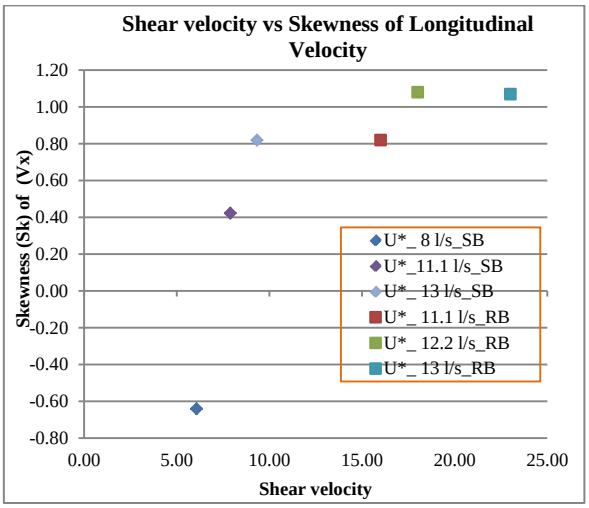
Shear velocity vs Skewness of Longitudinal Velocity
Skewness (Sk) of (Vx)
Shear velocity
U*_ 8 l/s_SB
U*_11.1 l/s_SB
U*_ 13 l/s_SB
U*_ 11.1 l/s_RB
U*_ 12.2 l/s_RB
U*_ 13 l/s_RB

(d)

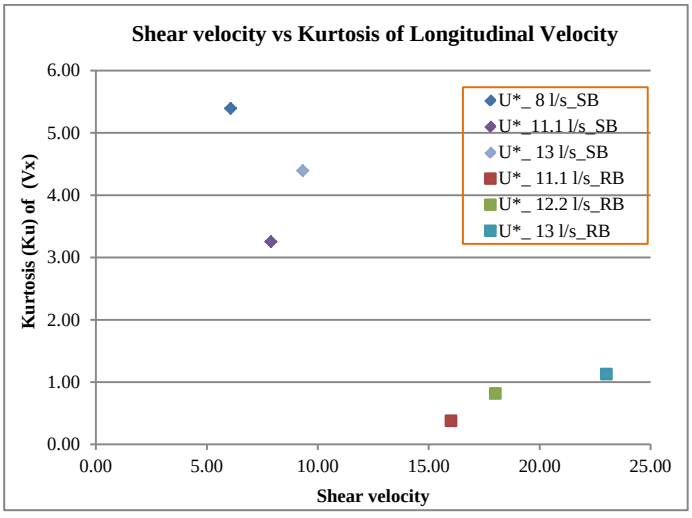
Shear velocity vs Kurtosis of Longitudinal Velocity
Kurtosis (Ku) of (Vx)
Shear velocity
U*_ 8 l/s_SB
U*_11.1 l/s_SB
U*_ 13 l/s_SB
U*_ 11.1 l/s_RB
U*_ 12.2 l/s_RB
U*_ 13 l/s_RB

(e)

Figure 4.6: For smooth & rough bed configuration; Shear velocity vs (a) mean longitudinal velocity; (b) Standard deviation of longitudinal velocity; (c) Coefficient of variation of longitudinal velocity, (d) Skewness of longitudinal velocity and (e) Kurtosis of longitudinal velocity.

In this analysis, for same discharges combined group data have been used in comparison as discussed above. It was observed that; with increasing shear velocity, mean longitudinal velocity is increased more rapidly than shear velocity in smooth bed configuration. But in rough bed, shear velocity increased more rapidly with more or less same mean velocity with increasing velocity. Rough bed velocities are more deviated with high shear velocity than smooth bed configuration. Rough bed velocity data are less stable than smooth bed configuration. Rough bed velocities are more right skewed in comparison to smooth bed. Longitudinal velocity distribution with smooth bed configuration have a distinct peak near to mean value and rough bed velocity distribution have a flat peak near mean value compare to smooth bed velocity distribution.

### 4.1.2.3 Moments with respect to bulk velocity (U)

The comparison of the moments with respect to bulk velocity is shown in figure 4.7.

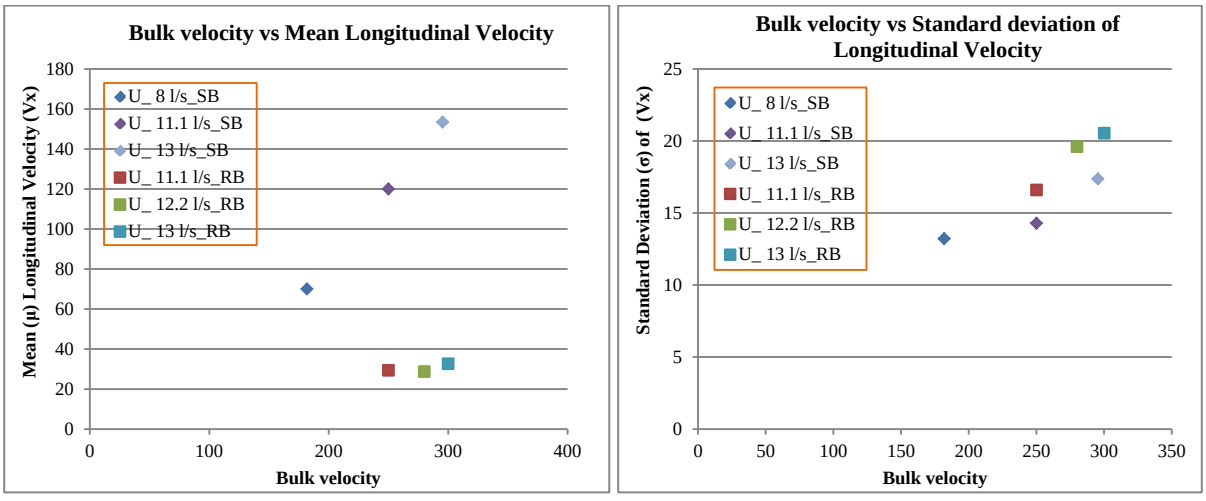


(a) (b)

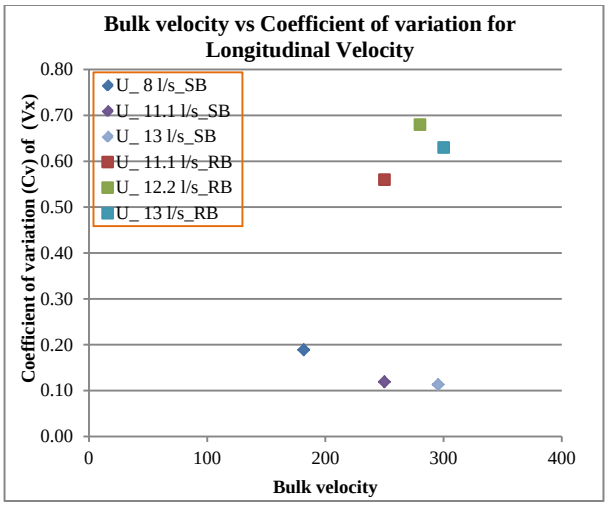


(c)

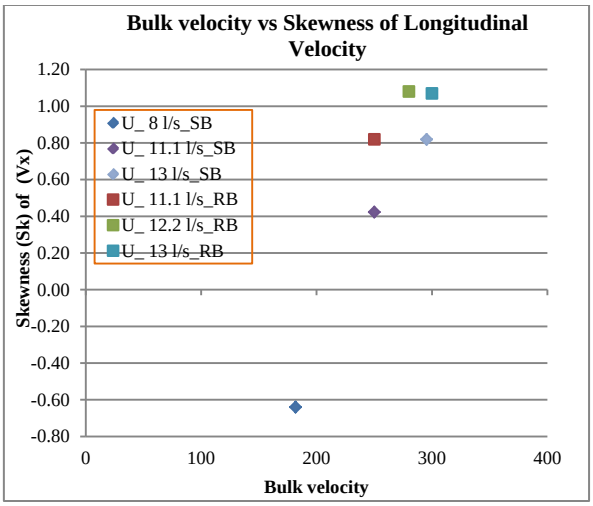


(d)

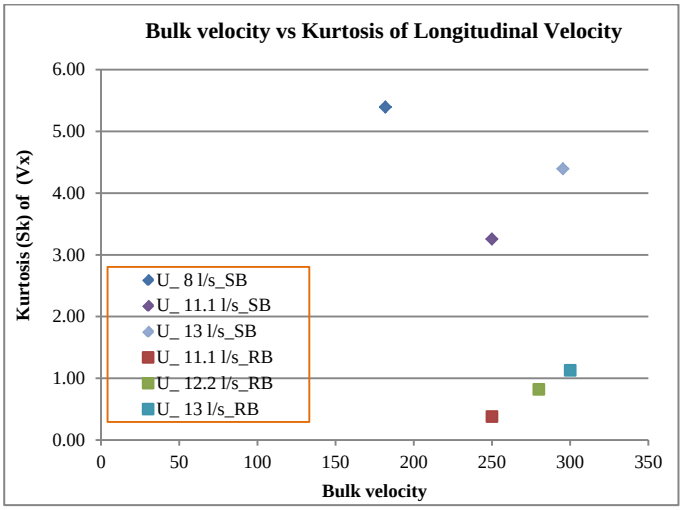


(e)

Figure 4.7: For smooth & rough bed configuration; Bulk velocity vs (a) mean longitudinal velocity; (b) Standard deviation of longitudinal velocity; (c) Coefficient of variation of longitudinal velocity, (d) Skewness of longitudinal velocity and (e) Kurtosis of longitudinal velocity.

It was observed that; it showed the same behavior as before comparison with respect to shear velocity. Mean longitudinal velocity is increased more rapidly in smooth bed configuration with increasing bulk velocity. But in rough bed, mean longitudinal velocity increased very slowly with increasing bulk velocity. Also smooth bed velocities are less than rough bed configuration. Rough bed velocity data are less stable than smooth bed configuration. Rough bed velocities are more right skewed in comparison to

smooth bed. Longitudinal velocity distributions show the same behavior as with respect to shear velocity.

### 4.1.2.4 Moments with respect to near bed velocity ($U_d$)

The comparison of the moments with respect to bulk velocity is shown in figure 4.8.

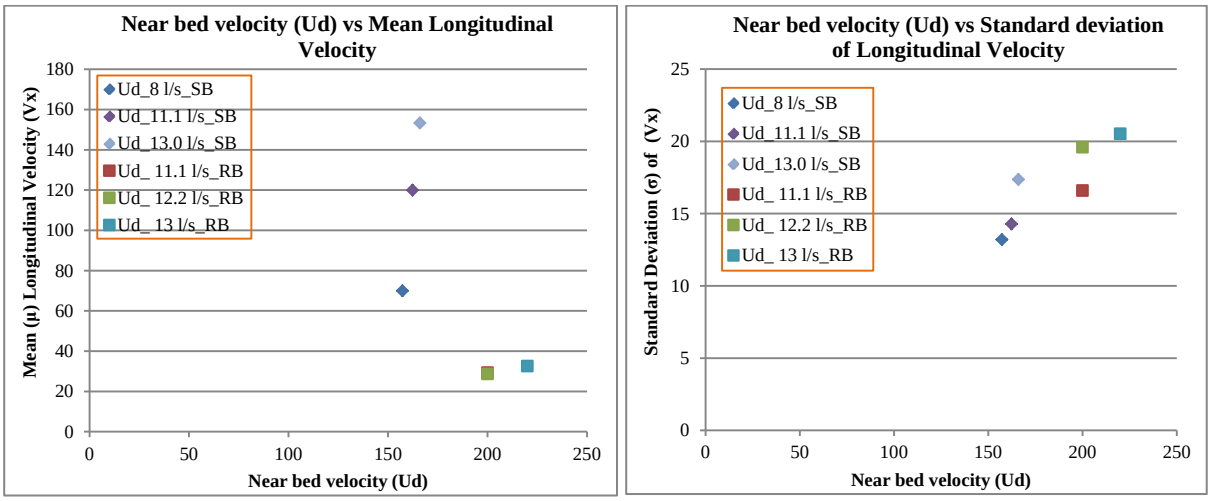


(a) (b)

Figure 4.8: For smooth & rough bed configuration; near bed velocity for full diameter distance vs (a) mean longitudinal velocity and (b) Standard deviation of longitudinal velocity.

It was observed that; for increasing discharge in smooth bed configuration, mean velocity increased very rapidly but near bed velocity more or less same. In rough bed, mean longitudinal velocity increased very slowly but near bed velocity increased with increasing discharge. Rough bed velocities were deviated more form mean velocities.

### 4.1.2.5 Moments with respect to near bed velocity ($U_{d/2}$)

The comparison of the moments with respect to bulk velocity is shown in figure 4.7.

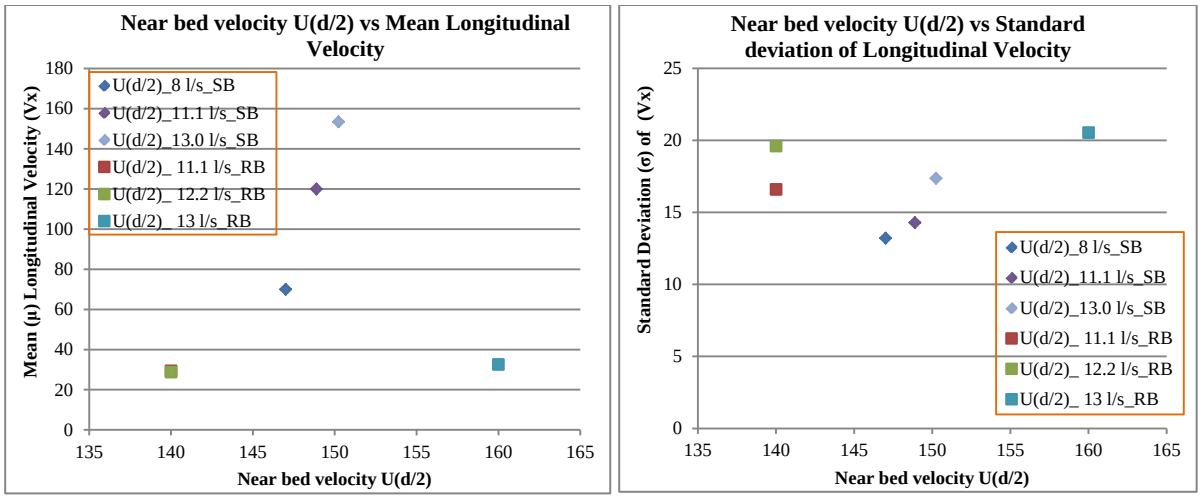


(a) (b)

Figure 4.9: For smooth & rough bed configuration; near bed velocity for half diameter distance vs (a) mean longitudinal velocity and (b) Standard deviation of longitudinal velocity.

It was observed that; for near bed velocity (half diameter) with increasing discharge was decreased in rough bed configuration with compare to near bed velocity (full diameter). In smooth bed configuration, mean velocity increased very rapidly but near bed velocity more or less same. In rough bed, mean longitudinal was same. Although near bed velocity (half diameter) in rough bed configuration was decreased comparatively but it was more deviated from the mean value.

After discussing above comparison of moments with respect to discharge, shear velocity, bulk velocity and near bed velocity for all experimental discharges; it can be concluded, the mean longitudinal velocity was increased in smooth bed configuration. Rough bed longitudinal velocities were deviated more from the mean value. Smooth bed velocities were more stable then rough bed data. Rough bed velocities more right skewed than smooth bed velocities. Longitudinal velocity distribution in smooth bed configuration have a distinct peak near to mean value compare to rough bed velocity distribution which have a flat peak near to mean value.

### 4.1.2.6 Moments with respect to dimensionless velocity ($V_x/U^*$)

For better understanding; statistical moments were compared with respect to

dimensionless velocities. The moments of longitudinal velocities normalized by shear velocity ($U^*$) as dimensionless velocity ($V_x/U^*$) and compared with Reynolds numbers (Re and $Re^*$). The comparison is shown in figure 4.10.

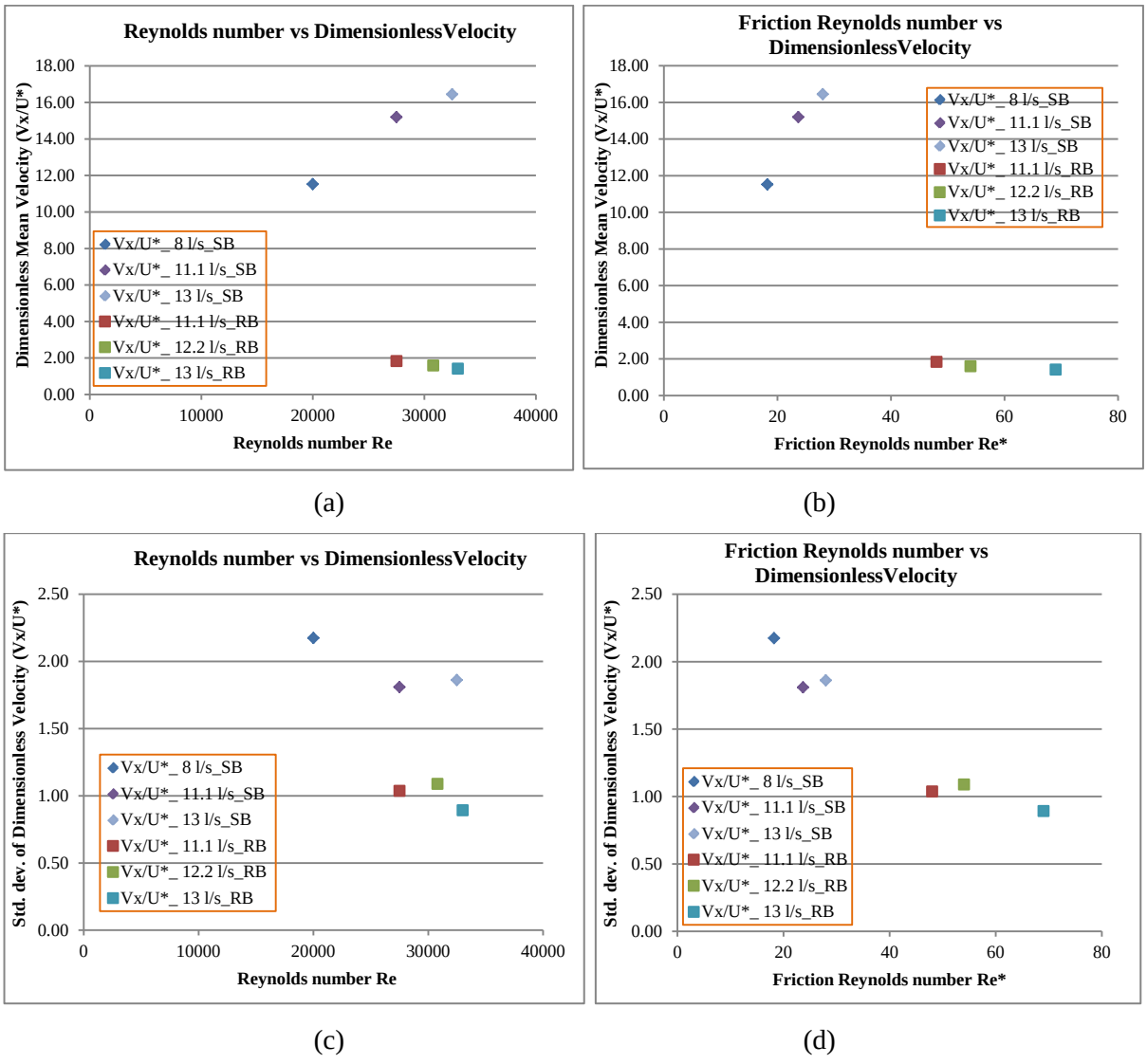


Figure 4.10: For smooth & rough bed configuration; (a) Reynolds number vs dimensionless mean velocity; (b) Critical Reynolds number vs dimensionless mean velocity; (c) Reynolds number vs Standard deviation of dimensionless longitudinal velocity and (d) Critical Reynolds number vs Standard deviation of dimensionless longitudinal velocity.

It can be concluded that; for smooth bed configuration dimensionless mean velocity increased but for rough bed configuration it showed more or less same value with

respect to Reynolds number (Re) and Friction Reynolds number ($Re^*$). In dimensionless velocity form, smooth bed configuration dimensionless velocities were more deviated than rough bed configuration. Noted that, in dimensionless form velocity normalized by shear velocity which had comparatively higher value for rough bed configuration.

### 4.1.2.7 Moments with respect to dimensionless velocity ($V_x/U$)

The moments of longitudinal velocities normalized by bulk velocity (U) as dimensionless velocity ($V_x/U$) and compared with Reynolds numbers (Re and $Re^*$). The comparison is shown in figure 4.11.

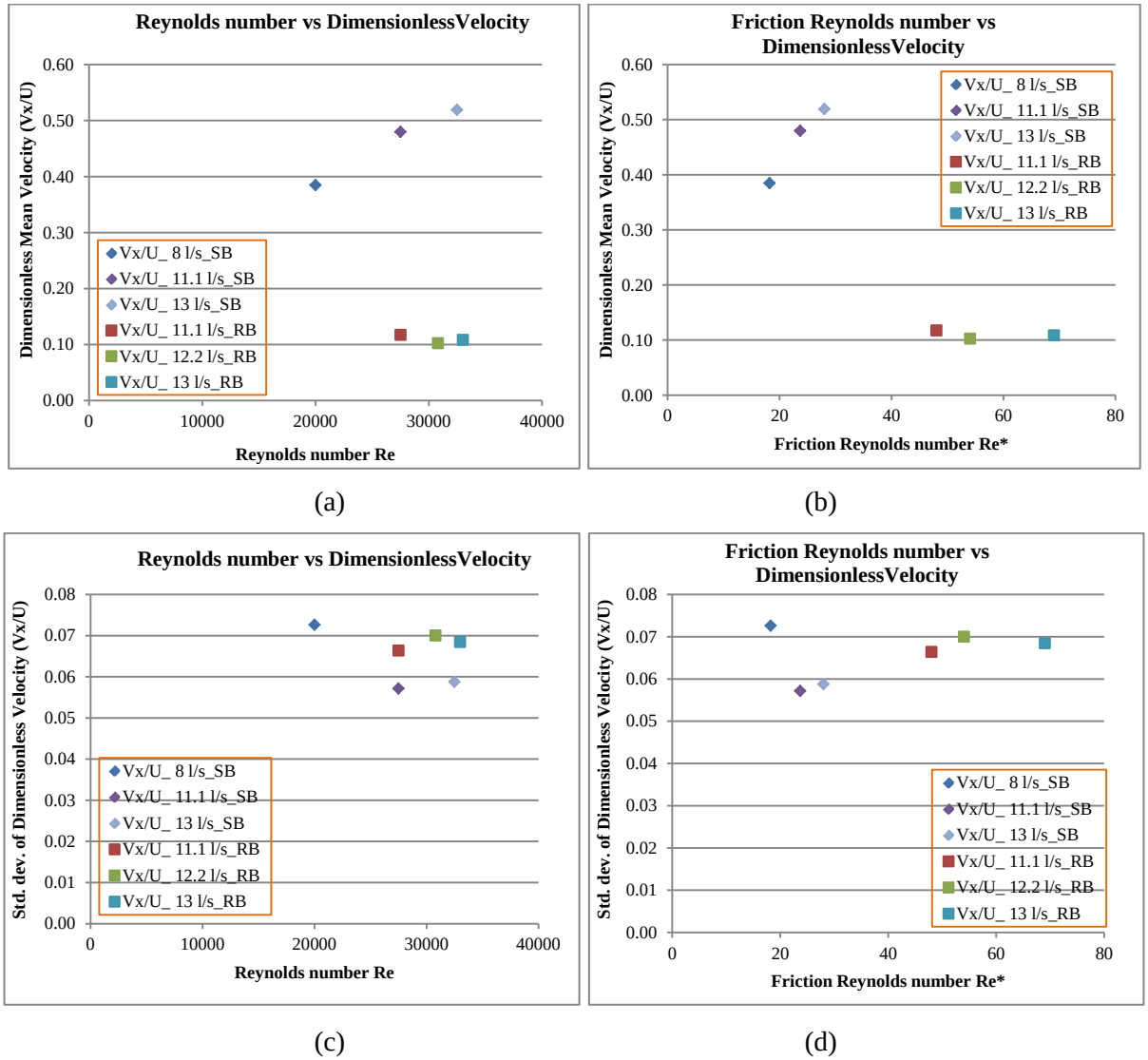

Figure 4.11: For smooth & rough bed configuration; (a) Reynolds number vs dimensionless mean velocity; (b) Friction Reynolds number vs dimensionless mean velocity; (c) Reynolds number vs Standard deviation of dimensionless longitudinal velocity and (d) Friction Reynolds number vs Standard deviation of dimensionless longitudinal velocity.

It was observed that; for dimensionless mean velocities showed the same behavior like normalized by shear velocity. Comparison showed, in rough bed configuration dimensionless velocities were more deviated than smooth bed configuration except the lowest discharge 8 l/s.

### 4.1.2.8 Moments with respect to dimensionless velocity ($V_x/U_d$)

The moments of longitudinal velocities normalized by near bed velocity ($U_{d/2}$) as dimensionless velocity ($V_x/U_{d/2}$) and compared with Reynolds numbers (Re and $Re^*$). The comparison is shown in figure 4.12.

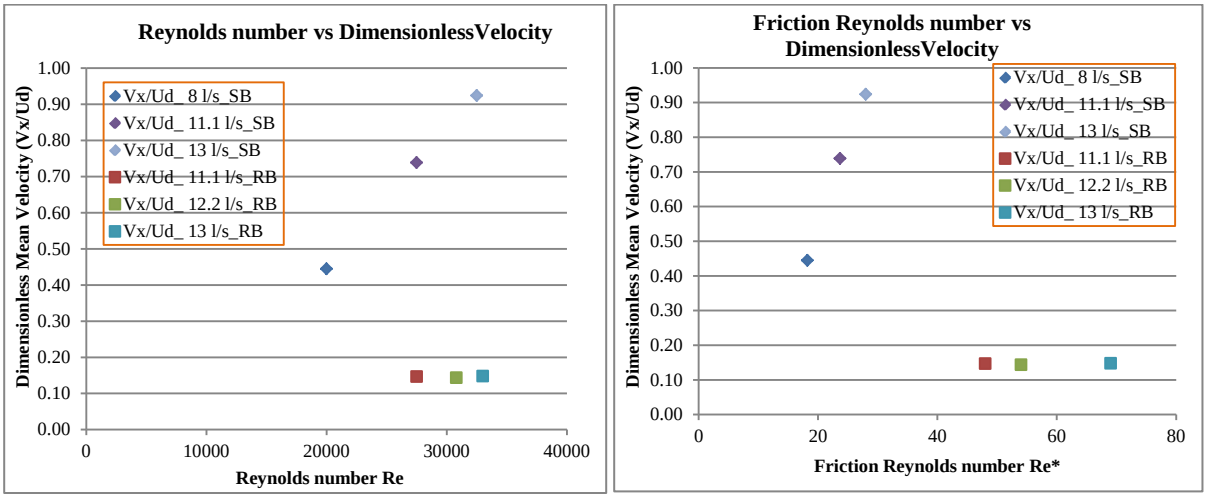


(a) (b)

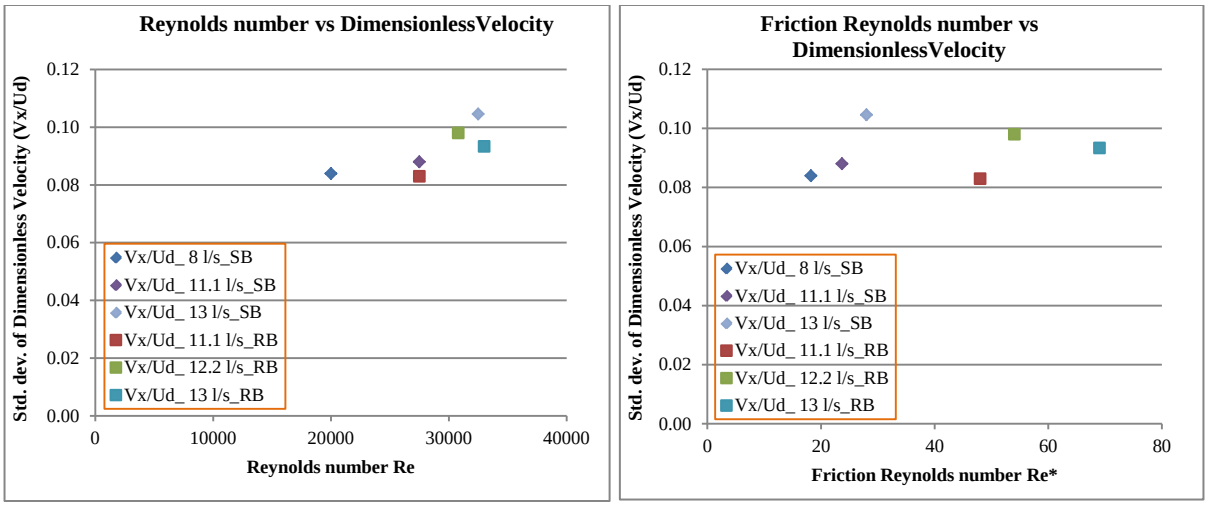


(c) (d)

Figure 4.12: For smooth & rough bed configuration; (a) Reynolds number vs dimensionless mean velocity; (b) Friction Reynolds number vs dimensionless mean velocity; (c) Reynolds number vs Standard deviation of dimensionless longitudinal velocity and (d) Friction Reynolds number vs Standard deviation of dimensionless longitudinal velocity.

It was observed that; for dimensionless mean velocities showed the same behavior like normalized by shear velocity and bulk velocity. Comparison showed deviation from the mean value in both bed configurations dimensionless velocities were same.

### 4.1.2.9 Moments with respect to dimensionless velocity ($V_x/U_{d/2}$)

The moments of longitudinal velocities normalized by bulk velocity (U) as dimensionless velocity ($V_x/U$) and compared with Reynolds numbers (Re and $Re^*$). The comparison is shown in figure 4.13.

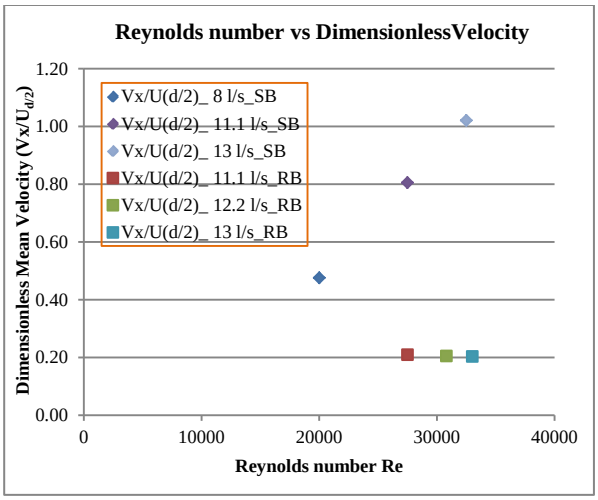


(a)

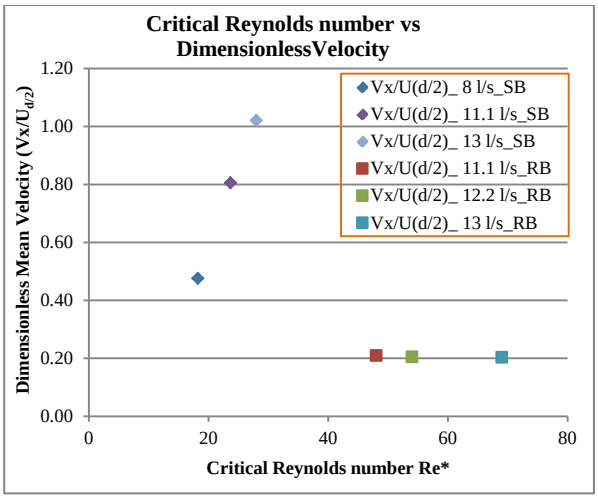


(b)

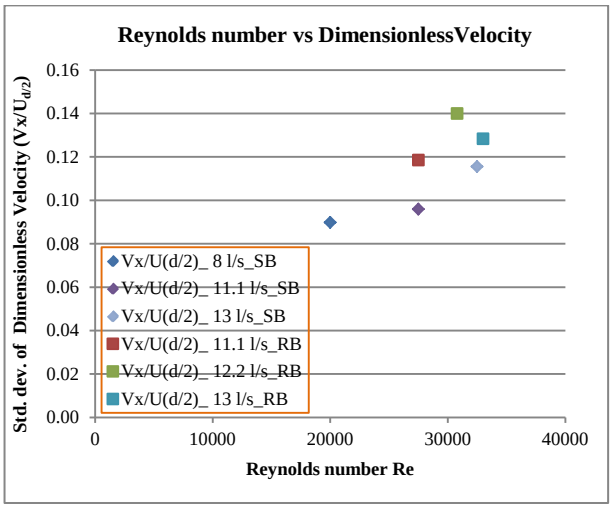


(c)

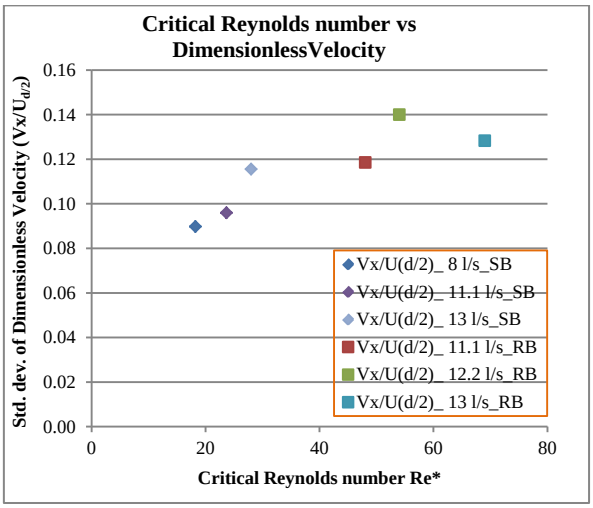


(d)

Figure 4.13: For smooth & rough bed configuration; (a) Reynolds number vs dimensionless mean velocity; (b) Friction Reynolds number vs dimensionless mean velocity; (c) Reynolds number vs Standard deviation of dimensionless longitudinal velocity and (d) Friction Reynolds number vs Standard deviation of dimensionless longitudinal velocity.

It was observed that; for dimensionless mean velocities showed the same behavior like normalized by other mentioned velocities. Comparison showed, in rough bed configuration dimensionless velocities were more deviated than smooth bed configuration.

From above discussion it can be concluded that; dimensionless mean velocities in smooth bed configuration was more and increased very rapidly compared to rough bed

configuration. In other hand the dimensionless mean velocity was more or less constant. Deviation from mean value for rough bed configuration was more expect comparison with dimensionless velocity normalized by shear velocity because in rough bed shear velocity was higher than smooth bed.

### 4.1.3 Comparison of velocities with rough bed

Bulk velocity, shear velocity, velocity near bed for half diameter, velocity near bed for full diameter and the mean velocities for smooth bed configuration have been compared to the corresponding velocities for rough bed configuration.

The bulk velocity, shear velocity and velocities near bed for smooth bed configuration were calculated as mentioned in chapter 2; for rough bed configuration were taken from the previous research experiment. The velocities for different discharges with both bed configurations summarize again for comparison which are shown in table 4.8.

Table 4.8: Bulk, shear and near bed velocities in both bed configurations.

| | Smooth bed configuration | | | |
|---|---|---|---|---|
| Discharge (l/s) | Bulk velocity (U) (mm/s) | Shear velocity (U*) (mm/s) | Near bed velocity (full dia.) (mm/s) | Near bed velocity (half dia.) (mm/s) |
| 8.0 | 181.82 | 6.06508 | 157.2662878 | 147.0126419 |
| 11.1 | 250.00 | 7.96425 | 162.3551865 | 148.890803 |
| 13.0 | 295.45 | 9.32750 | 166.0080722 | 150.2389745 |

| | Rough bed configuration | | | |
|---|---|---|---|---|
| Discharge (l/s) | Bulk velocity (U) (mm/s) | Shear velocity (U*) (mm/s) | Near bed velocity (full dia.) (mm/s) | Near bed velocity (half dia.) (mm/s) |
| 11.1 | 250 | 16 | 200 | 140 |
| 12.2 | 280 | 18 | 200 | 140 |
| 13.0 | 300 | 23 | 220 | 160 |

Comparison of all the velocities for smooth bed configuration to the corresponding velocities for rough bed configuration are shown in figure 4.14.

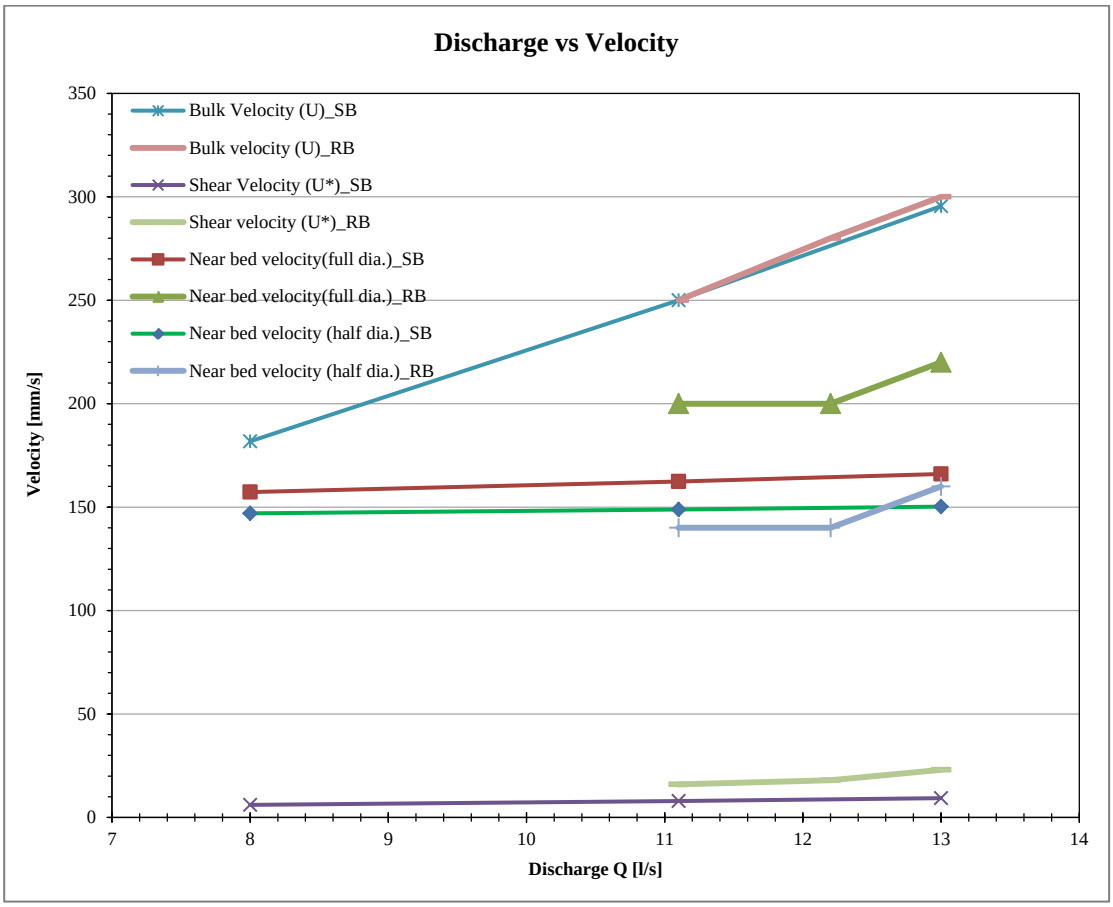


Figure 4.14: Velocities for experimental discharges with corresponding bed configurations.

It was observed that; the Bulk velocity for both bed configurations increased very fast with increasing discharges. Bulk velocity depends on discharge and channel cross sections only so there were no significant difference for bed configurations. Shear velocity is lower than the other velocities. For rough bed it configuration increased with increasing discharge and also it is higher compare to smooth bed configuration. The velocity near bed for smooth bed configuration was slowly increased with increasing discharges. Full diameter distance velocity is always higher than half diameter distance velocities. For rough bed condition; difference of full diameter distance velocity and half diameter distance velocity is significantly more than the corresponding difference in smooth bed configuration.

## 4.2 Probability density functions (pdfs)

The probability density function (pdf) of a continuous distribution is defined as the derivative of the cumulative distribution function. The results of probability density functions for all experimental discharges are shown below. For calculating pdf's of longitudinal velocity, same classes were used for better comparison.

### 4.2.1 pdf for discharge Q = 8 l/s

The probability distribution functions of the considered variables for experimental discharge 8 l/s are shown in figure 4.15.

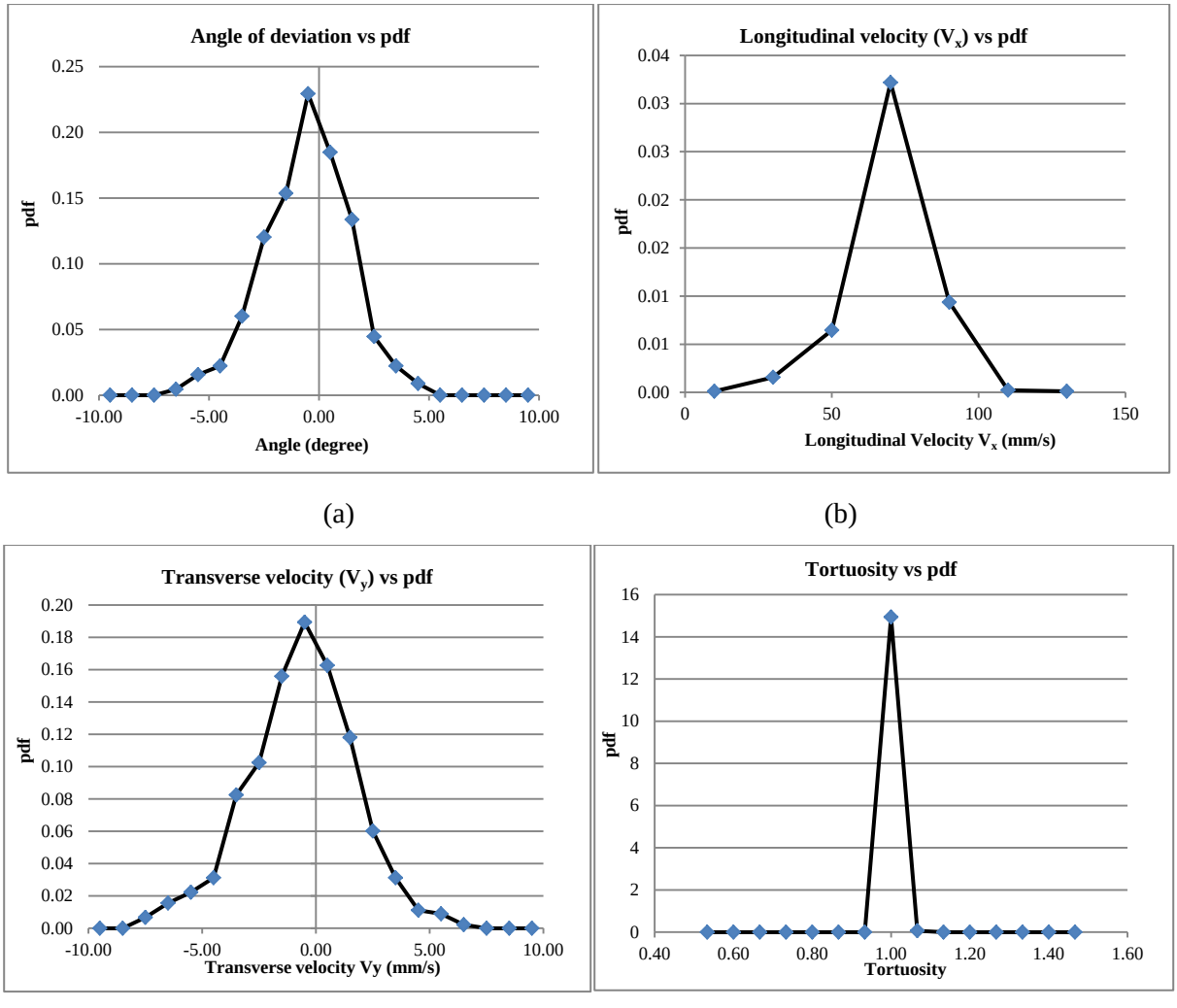


(a) (b)

(c) (d)

Figure 4.15: For discharge Q = 8 l/s; (a) Angle of deviation (degree) vs pdf; (b) Longitudinal

velocity vs pdf; (c) Transverse velocity vs pdf and (d) Tortuosity vs pdf.

It was observed that; for discharge 8.0 l/s the pdf's of angle of deviation, longitudinal velocity, transverse velocity and tortuosity are similar. For very less tortuosity the pdf of tortuosity became very sharp peak near 1.

### 4.2.2 pdf for discharge Q = 11.1 l/s

The probability distribution functions data of the considered variables for experimental discharge 11.1 l/s_1$^{st}$ group, 11.1 l/s_2$^{nd}$ group, 11.1 l/s_All.

It was observed that; for discharge 11.1 l/s, the pdf's of angle of deviation, transverse velocity and tortuosity for all groups of data are similar. For longitudinal velocity, the pdf was weakly right skewed so the tail in right was relatively longer than left. All the pdf's of tortuosity showed same behavior with sharp peak near 1.

#### 4.2.2.1 Q = 11.1 l/s _ 1$^{st}$ group

The probability distribution functions of the considered variables for experimental discharge 11.1 l/s_1$^{st}$ group are shown in figure 4.16.

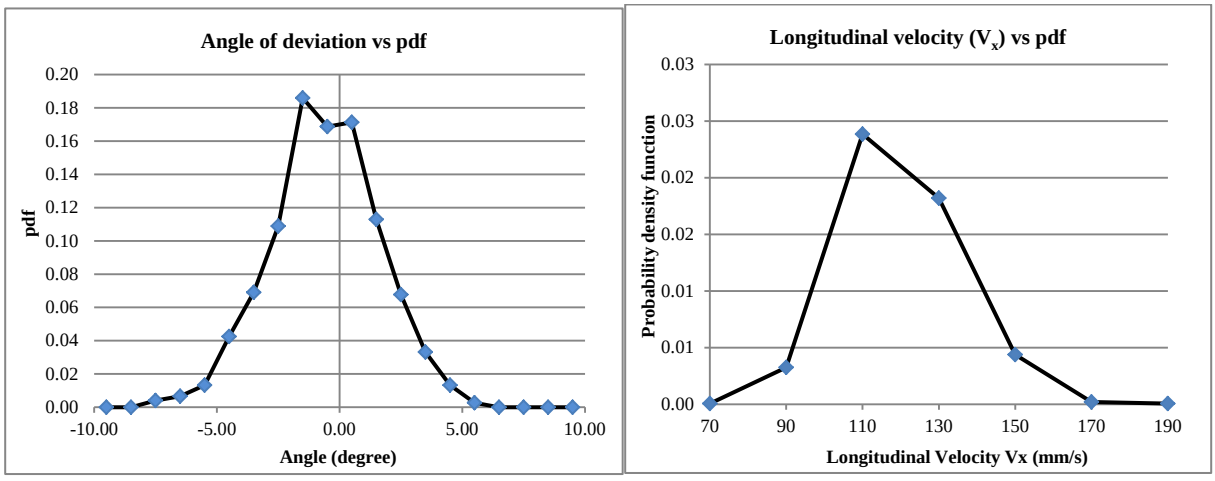


(a) (b)

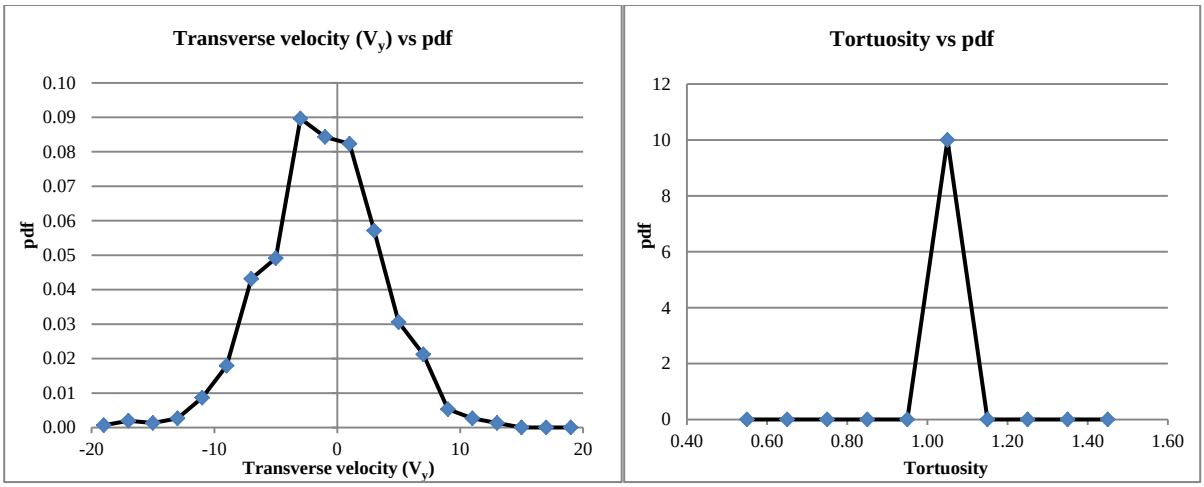


(c) (d)

Figure 4.16: For discharge Q = 11.1 l/s_1st group; (a) Angle of deviation (degree) vs pdf; (b) Longitudinal velocity vs pdf; (c) Transverse velocity vs pdf and (d) Tortuosity vs pdf.

### 4.2.2.2 Q = 11.1 l/s _ 2nd group

The probability distribution functions of the considered variables for experimental discharge 11.1 l/s_2nd group are shown in figure 4.17.

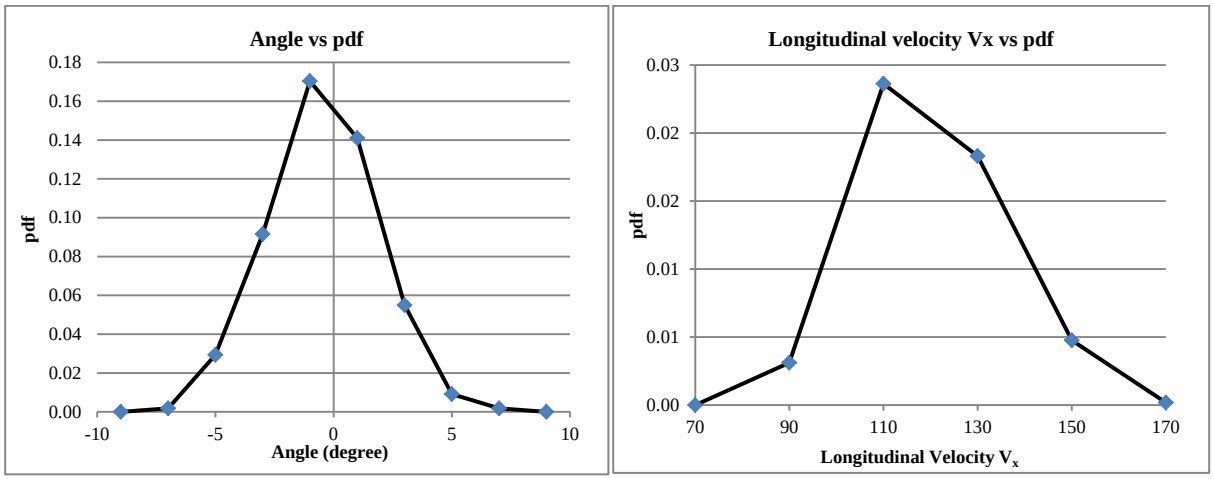


(a) (b)

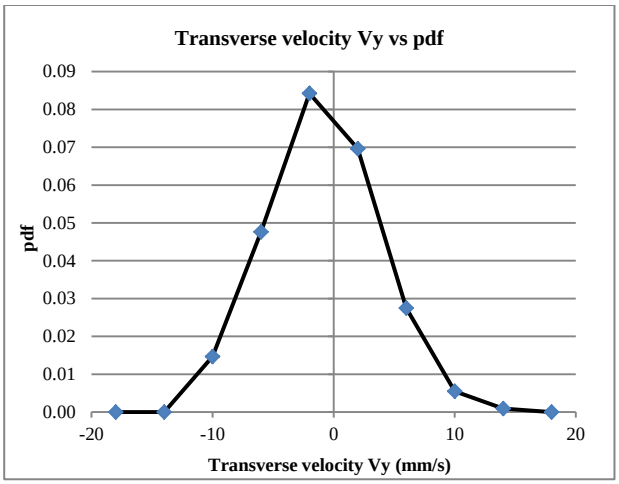


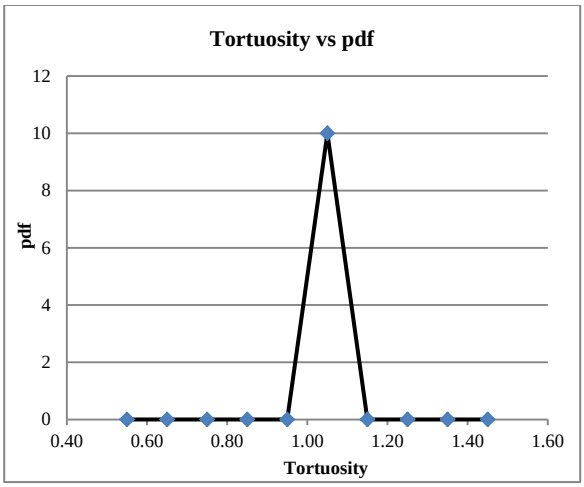


(c) (d)

Figure 4.17: For discharge Q = 11.1 l/s_2nd group; (a) Angle of deviation (degree) vs pdf; (b) Longitudinal velocity vs pdf; (c) Transverse velocity vs pdf and (d) Tortuosity vs pdf.

### 4.2.2.3 Q = 11.1 l/s _ All (combined both group)

The probability distribution functions of the considered variables for experimental discharge 11.1 l/s for combined group are shown in figure 4.18.

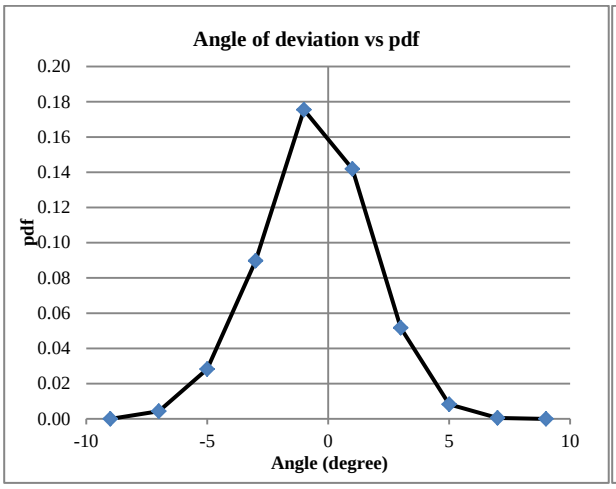


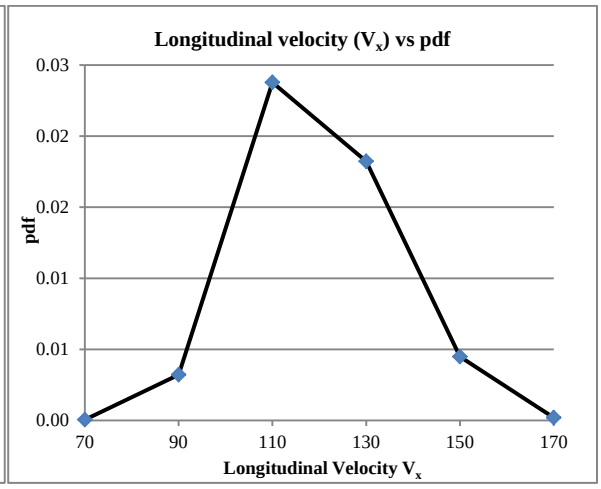


(a) (b)

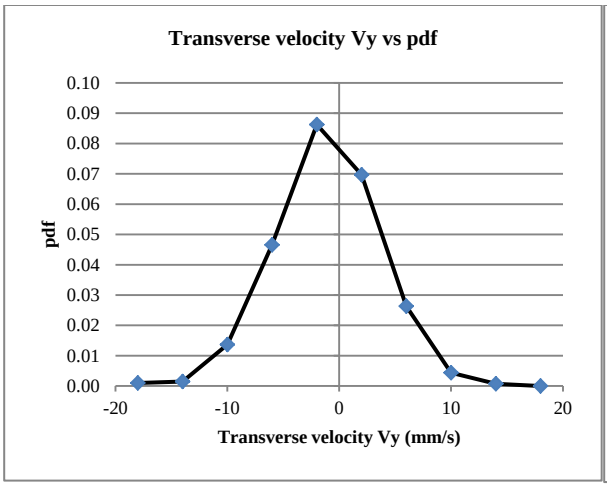


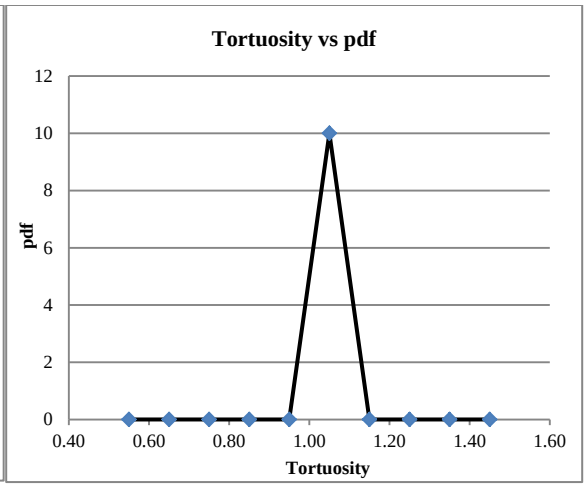


(c) (d)

Figure 4.18: For discharge Q = 11.1 l/s_All (combined both group); (a) Angle of deviation (degree) vs pdf; (b) Longitudinal velocity vs pdf; (c) Transverse velocity vs pdf and (d) Tortuosity vs pdf.

### 4.2.2.4 Comparison of all groups of data for Q = 11.1 l/s

The probability distribution functions of longitudinal velocity for all groups of data for experimental discharge 11.1 l/s are shown in figure 4.19.

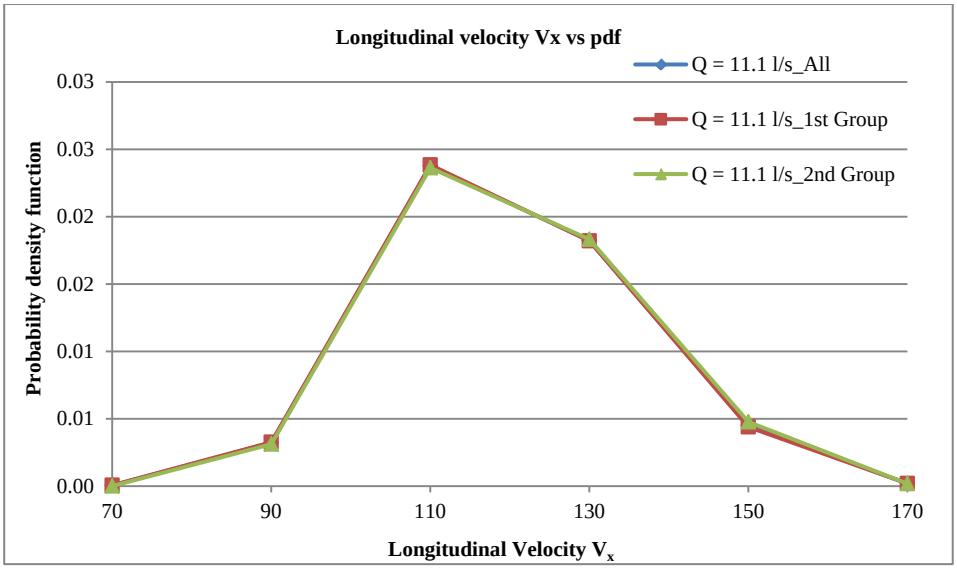


Figure 4.19: Longitudinal velocity vs pdf of all groups for discharge Q = 11.1 l/s.

It was observed that; for discharge 11.1 l/s, the pdf's of longitudinal velocities of different groups are same and weakly right skewed.

### 4.2.3 pdf for discharge Q = 13.0 l/s

The probability distribution functions data of the considered variables for experimental discharge 13.0 l/s_1st group, 13.0 l/s_2nd group, 13.0 l/s_All.

It was observed that; for discharge 13.0 l/s, the pdf's of angle of deviation, transverse velocity and tortuosity for all groups of data are similar. So for further analysis, combined group data were used as discharge 13.0 l/s data. For longitudinal velocity, the pdf was strongly right skewed so the tail in right was longer than left. Left tail was sharp to peak. All the pdf's of tortuosity showed same behavior with sharp peak near 1.

#### 4.2.3.1 Q = 13.0 l/s _ 1st group

The probability distribution functions of the considered variables for experimental discharge 11.1 l/s_1st group are shown in figure 4.20.

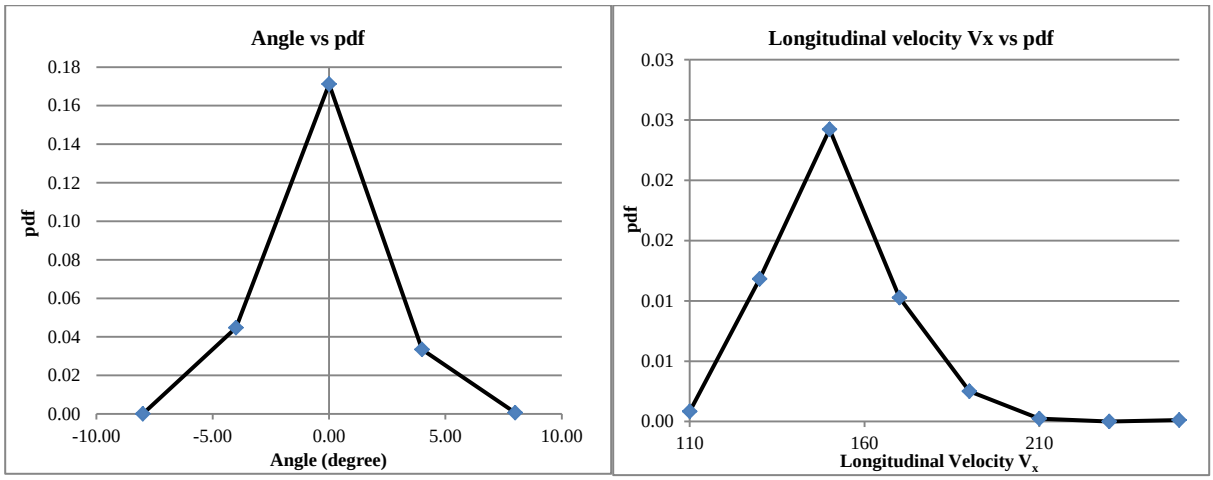


(a) (b)

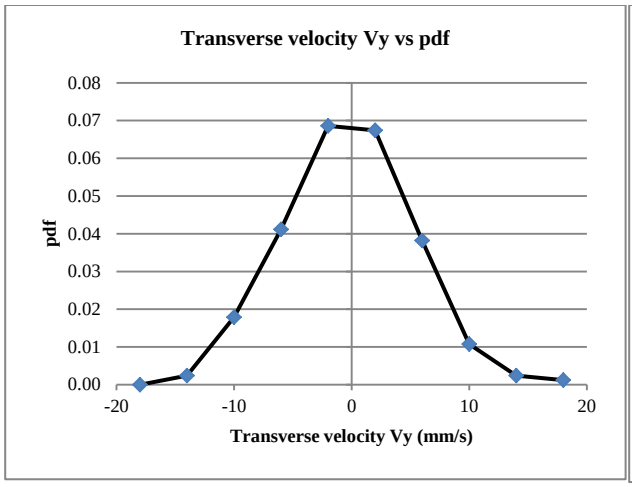


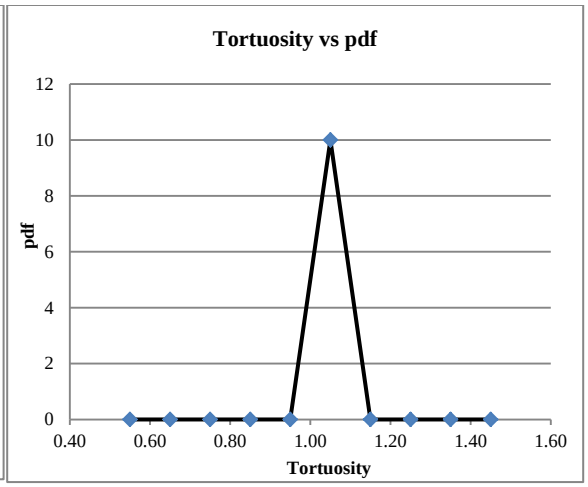


(c) (d)

Figure 4.20: For discharge Q = 13.0 l/s_1st group; (a) Angle of deviation (degree) vs pdf; (b) Longitudinal velocity vs pdf; (c) Transverse velocity vs pdf and (d) Tortuosity vs pdf.

### 4.2.3.2 Q = 13.0 l/s _ 2nd group

The probability distribution functions of the considered variables for experimental discharge 11.1 l/s_2nd group are shown in figure 4.21.

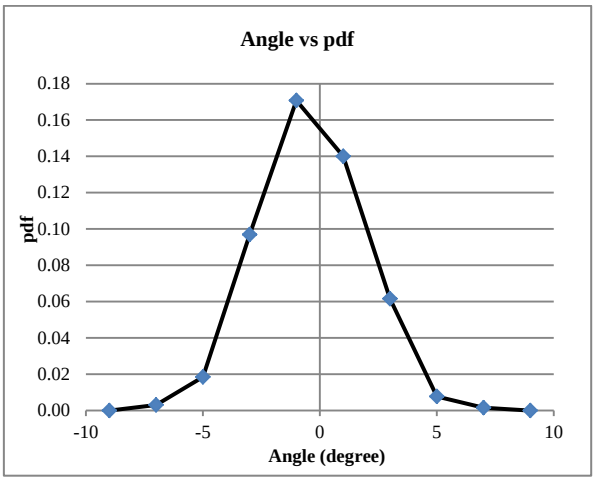


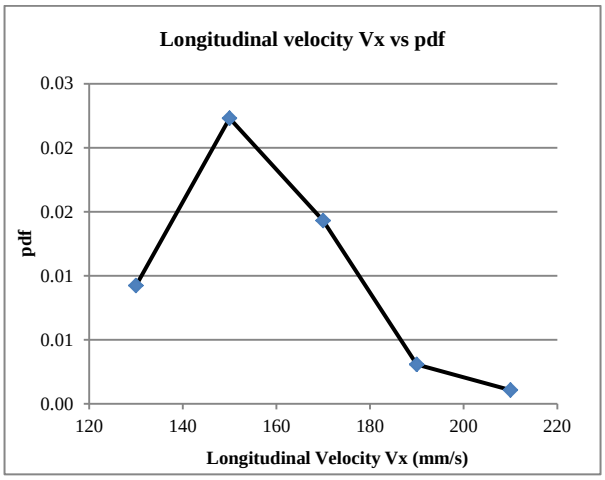


(a) (b)

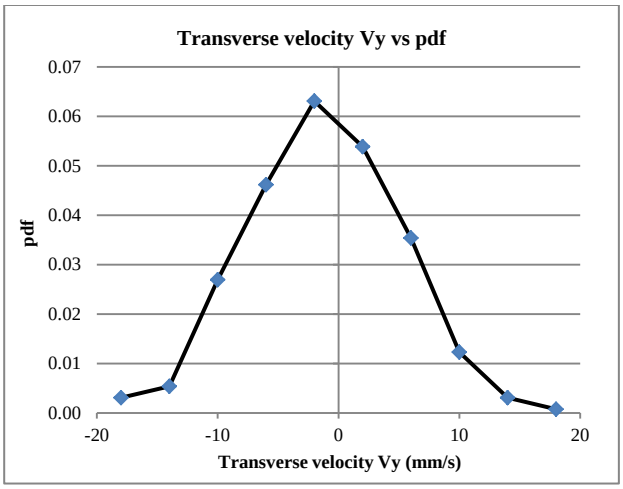


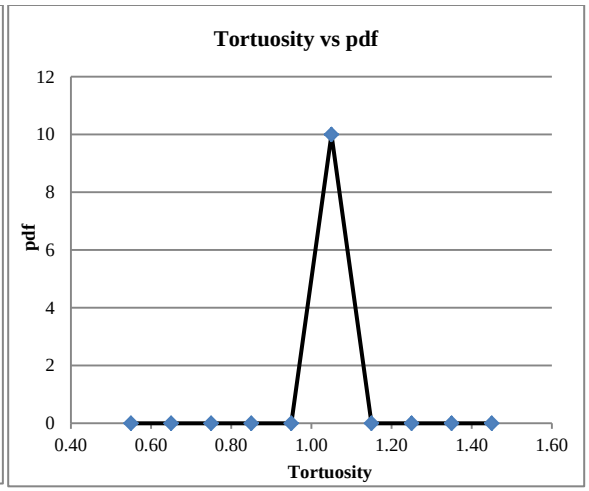


(c) (d)

Figure 4.21: For discharge Q = 13.0 l/s_2nd group; (a) Angle of deviation (degree) vs pdf; (b) Longitudinal velocity vs pdf; (c) Transverse velocity vs pdf and (d) Tortuosity vs pdf.

### 4.2.3.3 Q = 13.0 l/s _ All (combined both group)

The probability distribution functions of the considered variables for experimental discharge 13.0 l/s_all (combined group) are shown in figure 4.22.

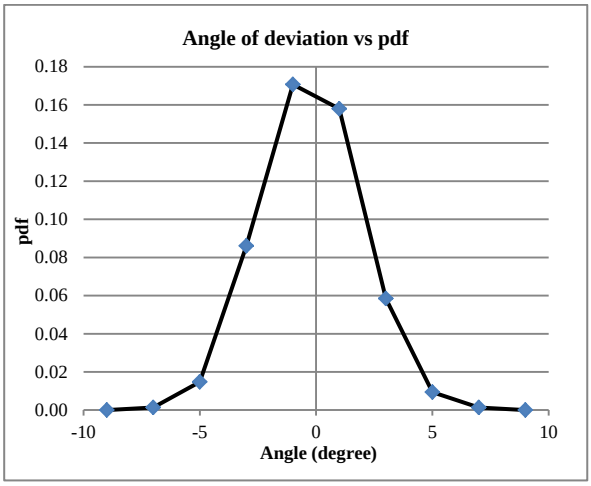


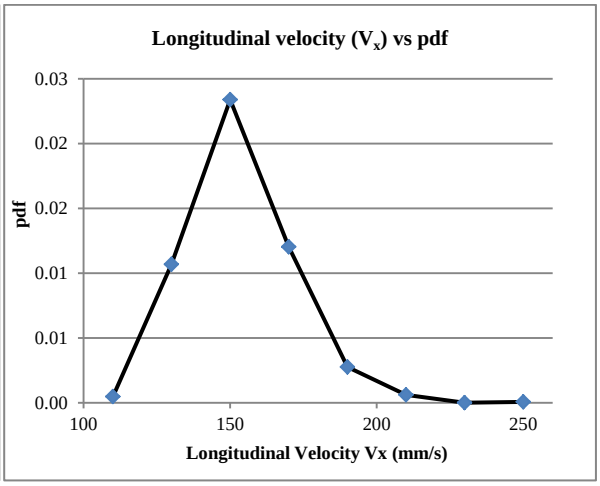


(a) (b)

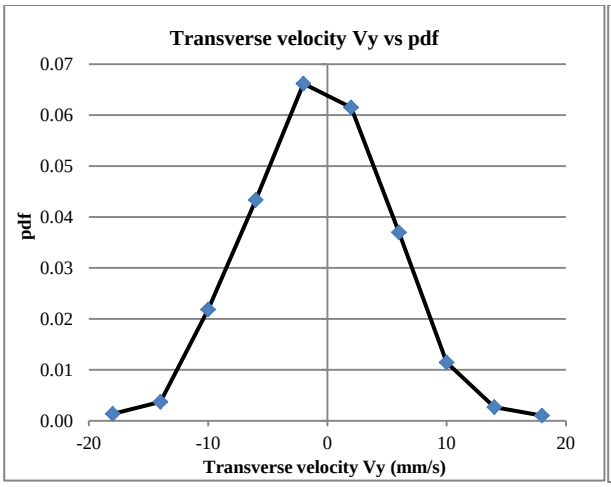


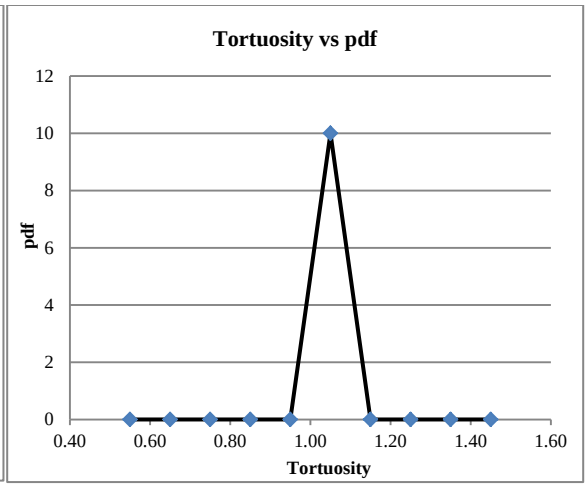


(c) (d)

Figure 4.22: For discharge Q = 13.0 l/s_All (combined both group); (a) Angle of deviation (degree) vs pdf; (b) Longitudinal velocity vs pdf; (c) Transverse velocity vs pdf and (d) Tortuosity vs pdf.

### 4.2.3.4 Comparison of all groups of data for Q = 13.0 l/s

The probability distribution functions of longitudinal velocity for all groups of data for experimental discharge 13.0 l/s are shown in figure 4.23.

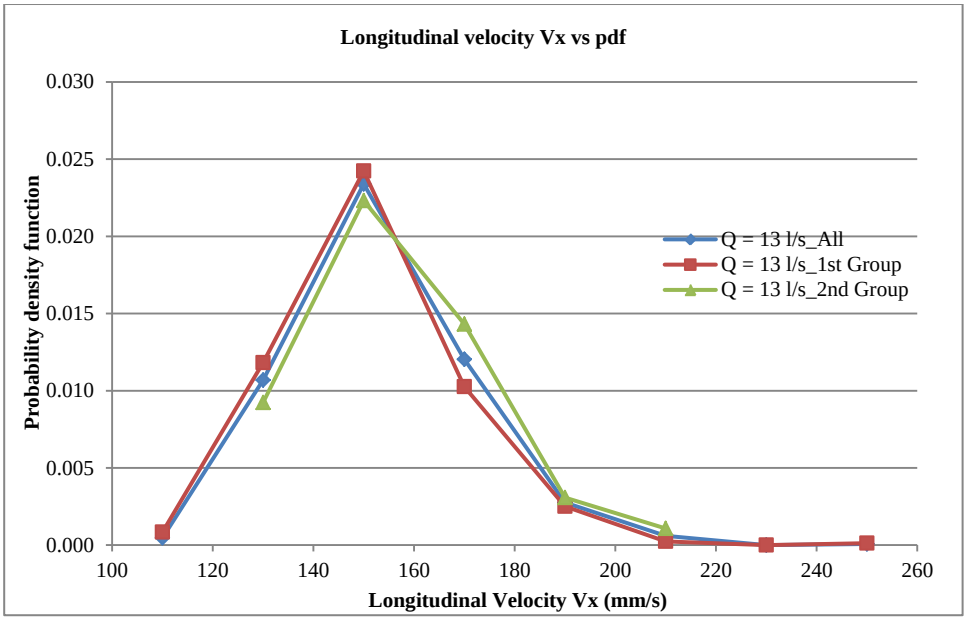


Figure 4.23: Longitudinal velocity vs pdf of all groups for discharge Q = 13.0 l/s.

It was observed that; for discharge 13.0 l/s, the pdf's of longitudinal velocities of different groups are similar and strongly right skewed. Right tail was longer than the left tail.

### 4.2.4 Comparison of longitudinal velocity ($V_x$)

The probability density functions of longitudinal velocity and dimensionless velocity for all discharges were compared to understand the velocity behavior of sediment movement in smooth bed configuration.

#### 4.2.4.1 Longitudinal velocity pdf for all discharges

The probability distribution functions of longitudinal velocity for all experimental discharges 8.0 l/s, 11.1 l/s & 13.0 l/s are shown in figure 4.24.

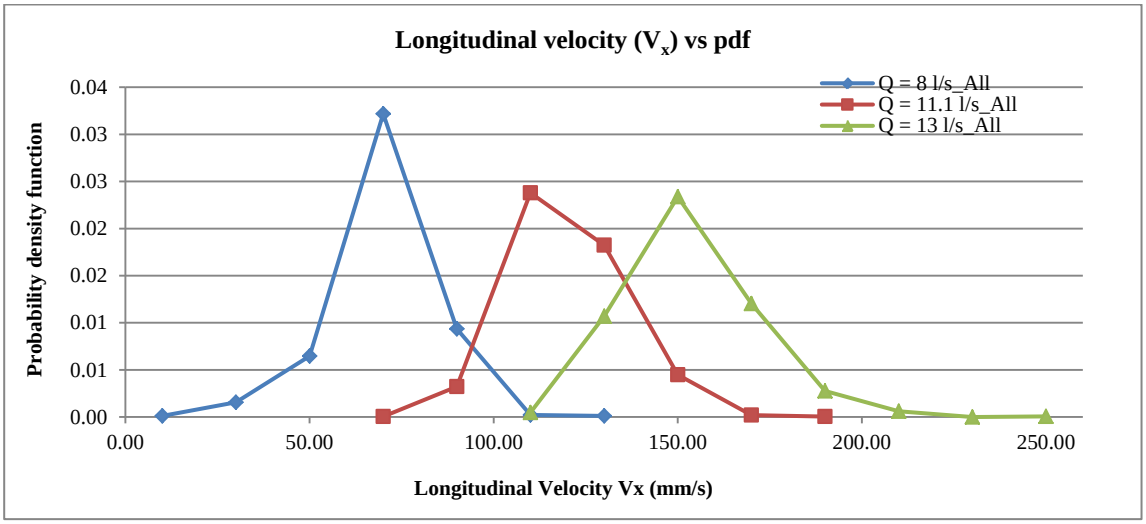


Figure 4.24: Longitudinal velocity vs pdf of all discharge Q = 8, 11.1 & 13.0 l/s.

It was observed that; longitudinal velocities were increased and peaks were decreased with increasing discharges. Also it skewed strongly with increasing discharges. In pdf comparison, right tail was becoming long with increasing discharges.

### 4.2.4.2 pdf with dimensionless velocity for all discharges

Dimensionless velocity was calculated with respect to the bulk velocity (U) and shear velocity ($U^*$) for all experimental discharges. The probability distribution functions of dimension less velocities ($V_x/U$ and $V_x/U^*$)for all experimental discharge 8.0 l/s, 11.1 l/s & 13.0 l/s are shown in figure 4.25.

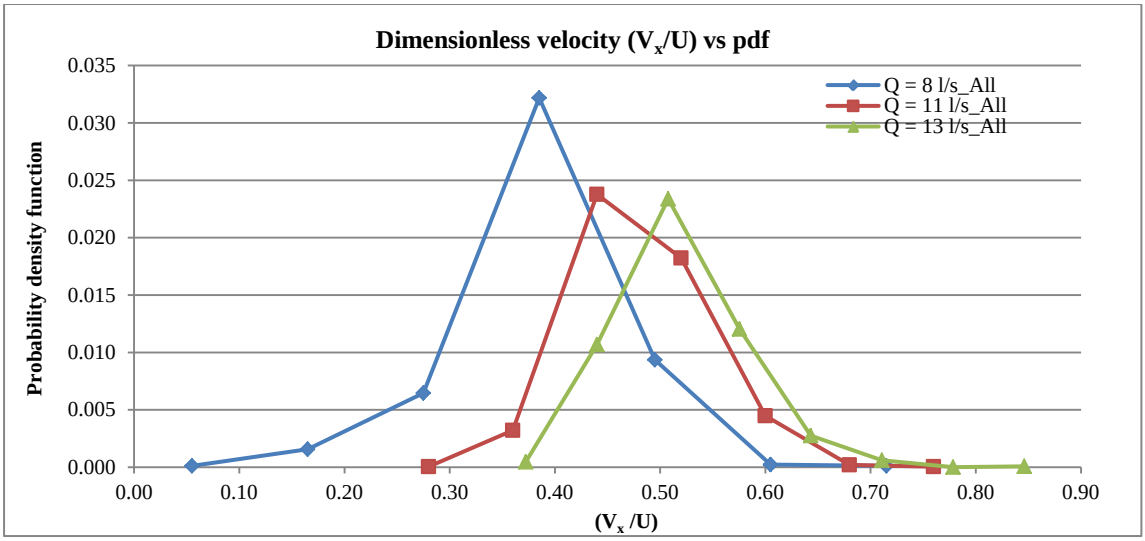


(a)

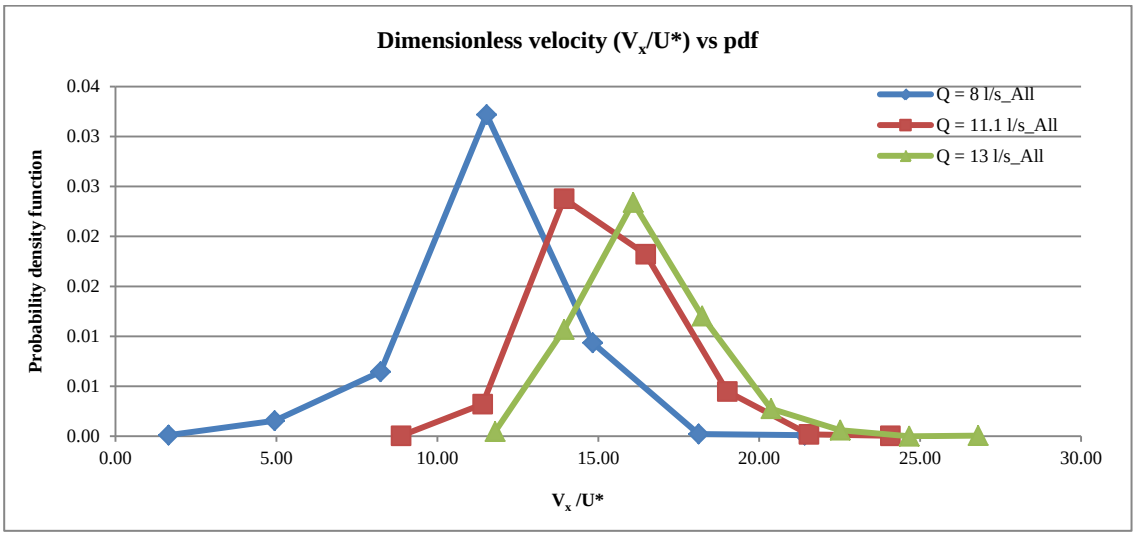


(b)

Figure 4.25: (a) Dimensionless velocity ($V_x/U$) vs pdf and (b) Dimensionless velocity ($V_x/U^*$) vs pdf for all discharge Q = 8, 11.1 & 13.0 l/s.

It was observed that; the dimensionless velocities ($V_x/U$) and $V_x/U^*$) are similar. The dimensionless velocities were increased with increasing discharges. The pdf's of dimensionless velocities for all discharges had the same characteristics like longitudinal velocities. It was also right skewed. Right tail was longer than the left tail.

## 4.3 Cumulative density functions (cdfs)

The cumulative distribution function (cdf) results of angle of deviation, longitudinal velocity, transverse velocity and tortuosity for all experimental discharges are shown below.

### 4.3.1 cdf for discharge Q = 8 l/s

The cumulative distribution functions of the considered variables for experimental discharge 8.0 l/s are shown in figure 4.26.

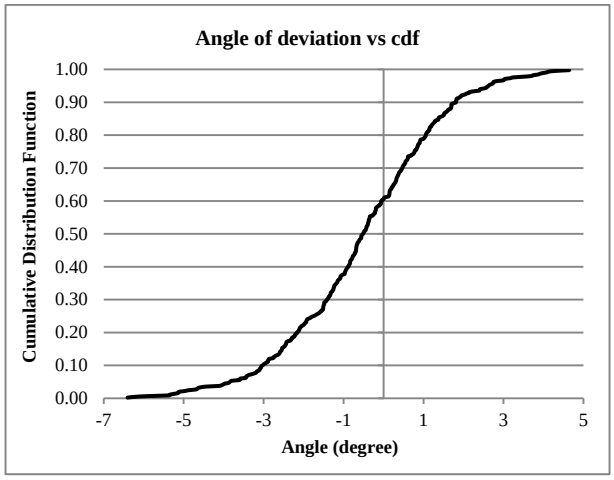


(a)

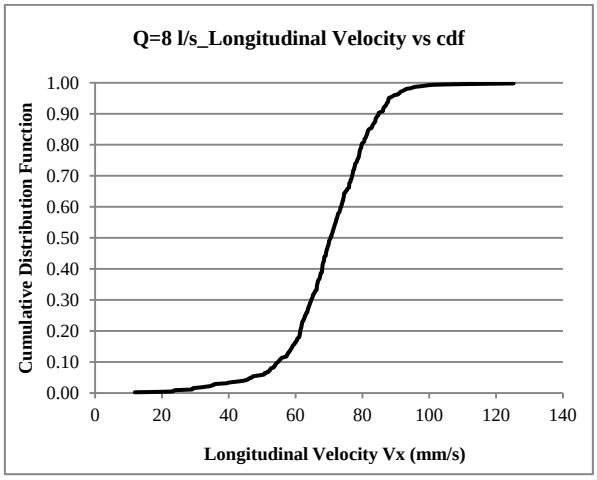


(b)

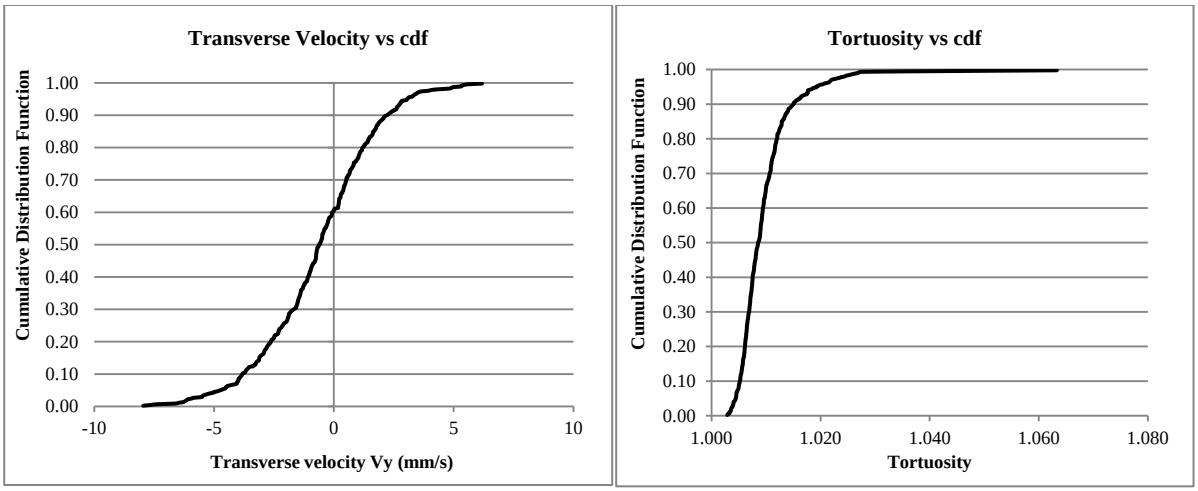


(c) (d)

Figure 4.26: For discharge Q = 8.0 l/s; (a) Angle of deviation (degree) vs cdf; (b) Longitudinal velocity vs cdf; (c) Transverse velocity vs cdf and (d) Tortuosity vs cdf.

It was observed that; the cdf's of longitudinal velocity for discharge 8.0 l/s were similar and the obtained experimental data are consistent, and transverse velocity was asymmetric with a bit long tail at left. The cdf of angle of deviation were also asymmetric with a longer tail at left because of camera position. 90% of longitudinal velocity frequencies were around 85 mm/s.

### 4.3.2 cdf for discharge Q = 11.1 l/s

The cdf's of the experimental groups of data for discharge 11.1 l/s; 1$^{st}$ group, 2$^{nd}$ group and all (combined group) have been shown in figure 4.27, 4.28 and 4.29 respectively.

It was observed that; the cdf's of longitudinal velocity for discharge 11.1 l/s were asymmetric; in this case right tail is longer and also the cdf's of transverse velocity for discharge 11.1 l/s were asymmetric; in this case left tail is longer. The cdf's of angle of deviation were not completely symmetrical; at right tail was a bit short because of the camera position. For three groups of data showed similar behavior. So combined group data can be used for discharge 11.1 l/s data.

### 4.3.2.1 Q = 11.1 l/s _ 1st group

The cumulative distribution functions of the considered variables for experimental discharge 11.1 l/s_1st group are shown in figure 4.27.

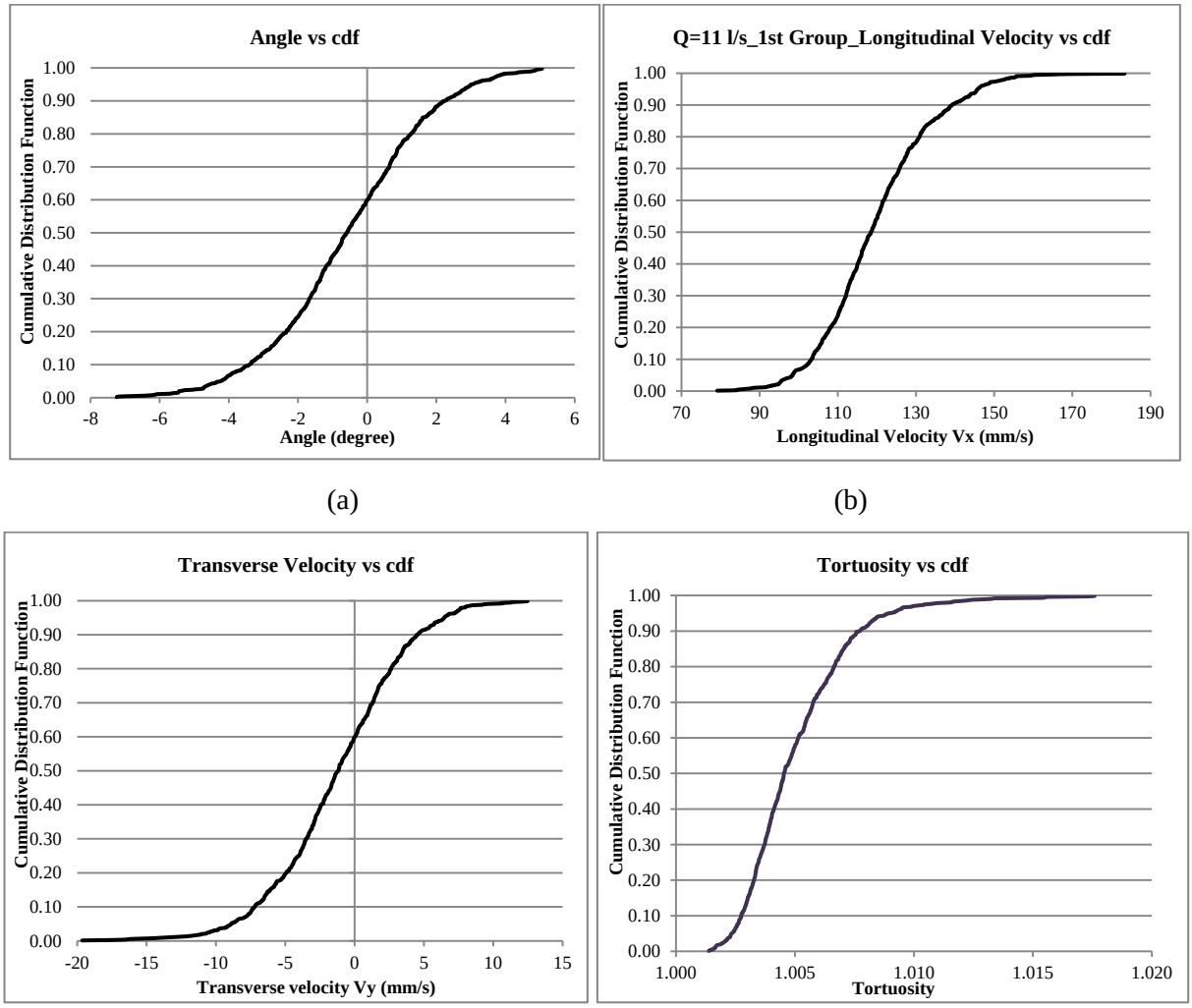


Figure 4.27: For discharge Q = 11.1 l/s_1st group; (a) Angle of deviation (degree) vs cdf; (b) Longitudinal velocity vs cdf; (c) Transverse velocity vs cdf and (d) Tortuosity vs cdf.

### 4.3.2.2 Q = 11.1 l/s _ 2nd group

The cumulative distribution functions of the considered variables for experimental discharge 11.1 l/s_2nd group are shown in figure 4.28.

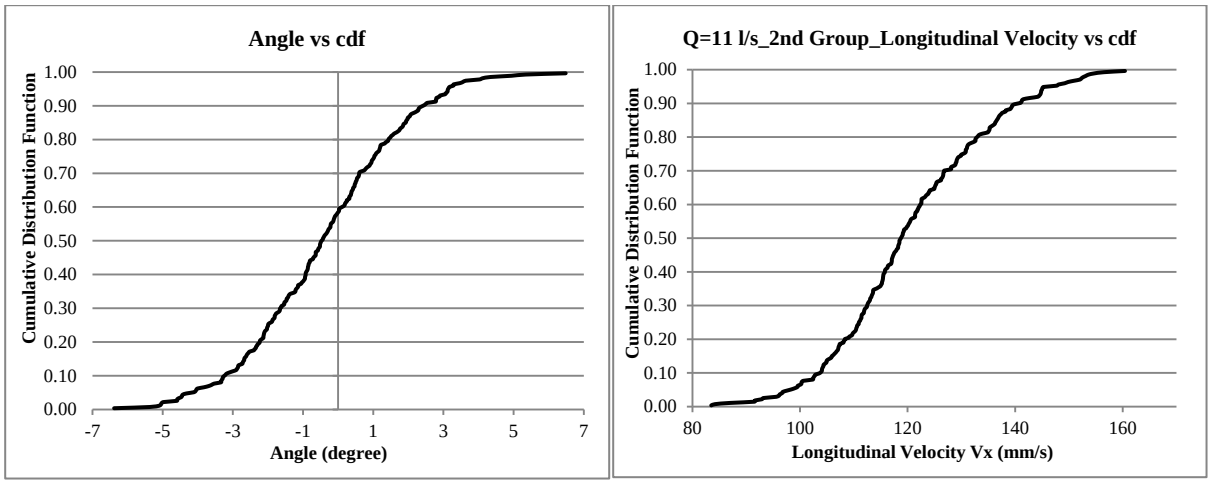


(a)




(b)

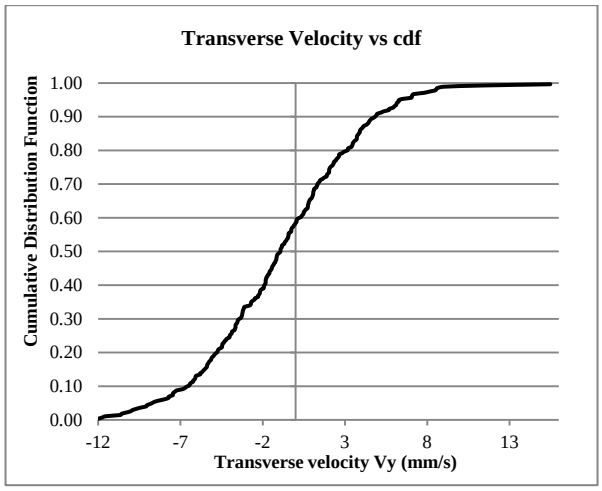


(c)

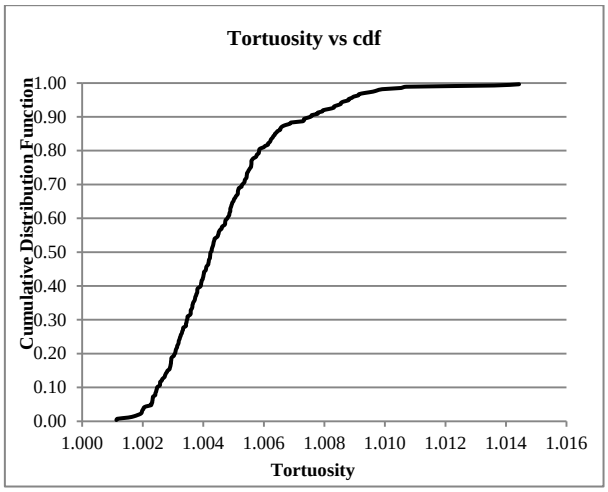


(d)

Figure 4.28: For discharge Q = 11.1 l/s_2nd group; (a) Angle of deviation (degree) vs cdf; (b) Longitudinal velocity vs cdf; (c) Transverse velocity vs cdf and (d) Tortuosity vs cdf.

### 4.3.2.3 Q = 11.1 l/s _ All (combined both group)

The cumulative distribution functions of the considered variables for experimental discharge 11.1 l/s_All (combined group) are shown in figure 4.29.

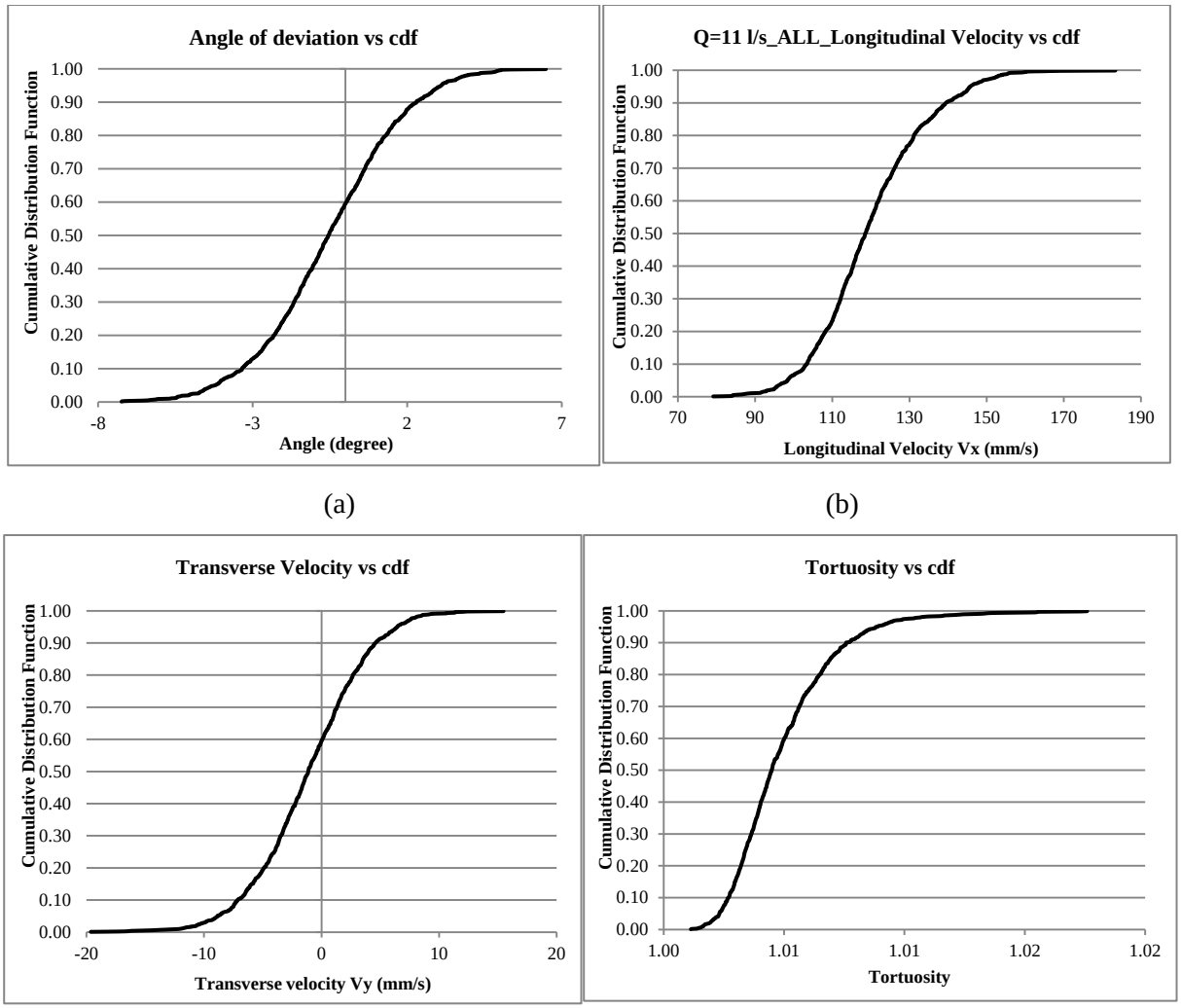


Figure 4.29: For discharge Q = 11.1 l/s_All (combined both group; (a) Angle of deviation (degree) vs cdf; (b) Longitudinal velocity vs cdf; (c) Transverse velocity vs cdf and (d) Tortuosity vs cdf.

### 4.3.2.4 Comparison of all groups of data for Q = 11.1 l/s

The cumulative distribution functions of longitudinal velocities for all groups of data for experimental discharge 11.1 l/s are shown in figure 4.30.

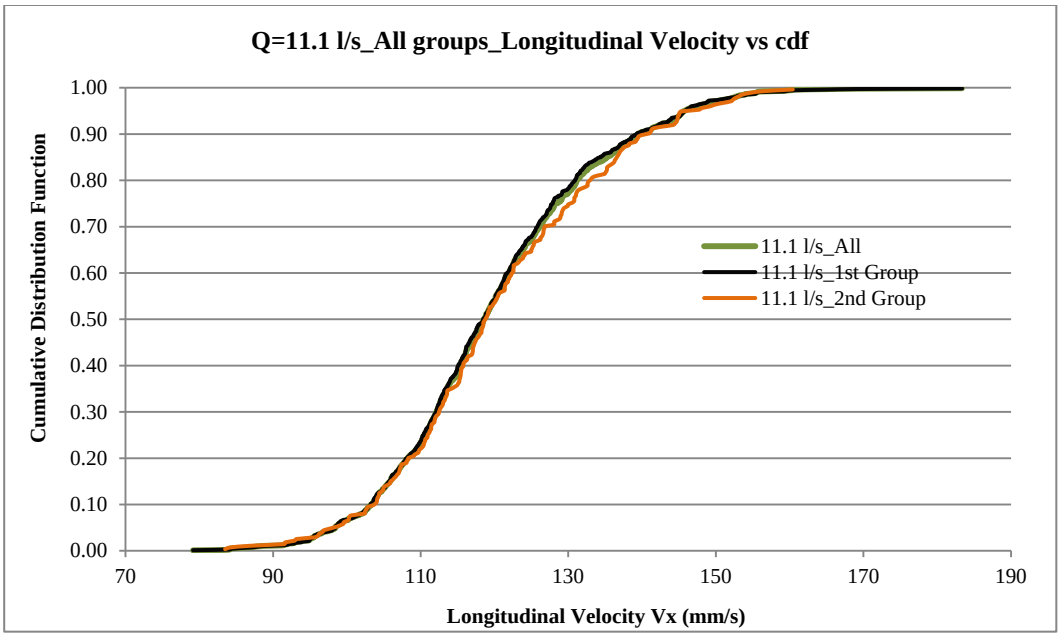


Figure 4.30: Longitudinal velocity vs cdf of all groups for discharge Q = 11.1 l/s.

It was observed that; cdfs of longitudinal velocities for all groups of data showed the same behavior. It was asymmetric as left tail is shorter than right one. 2$^{nd}$ group of data had a little variation from the combined one. Here 90% of longitudinal velocity frequencies were around 140 mm/s.

### 4.3.3 cdf for discharge Q = 13.0 l/s

The cdf's of the experimental groups of data for discharge 13.0 l/s; 1st group, 2nd group and all (combined group) have been shown in figure 4.31, 4.32 and 4.33 respectively.

It was observed that; the cdf's of angle of deviation and transverse velocity for discharge 13.0 l/s were becoming more similar with respect to lower discharges 8.0 l/s and 11.1 l/s. So the obtained experimental data are more consistent than low discharges. For three groups of data showed similar behavior. So combined group data can be used for discharge 13.0 l/s data. The cdfs of longitudinal velocity and transverse velocity for discharge 13.0 l/s of all groups showed asymmetry. Left tail was getting shorter to the right tail.

### 4.3.3.1 Q = 13.0 l/s _ 1st group

The cumulative distribution functions of the considered variables for experimental discharge 13.0 l/s_1st group are shown in figure 4.31.

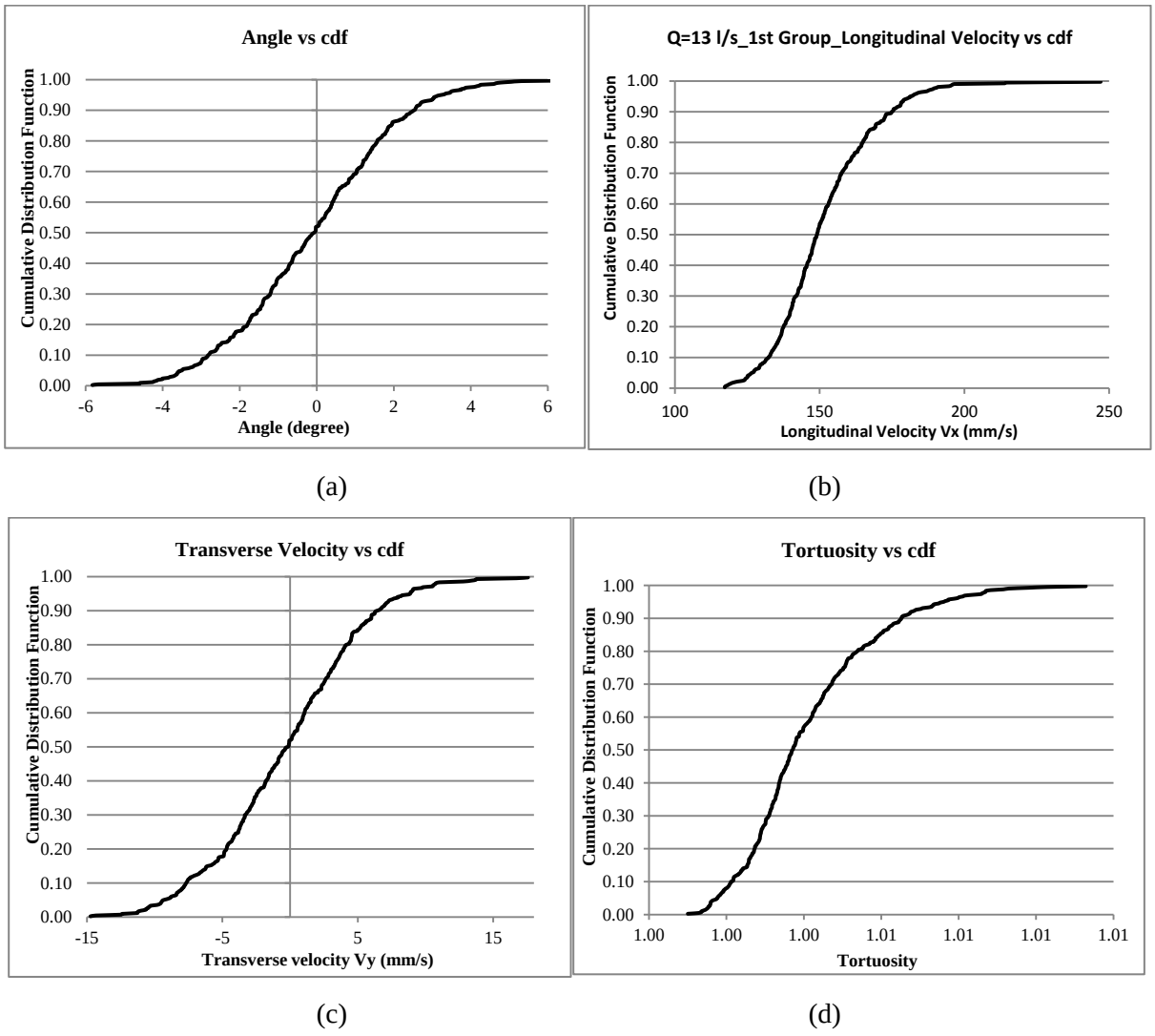


Figure 4.31: For discharge Q = 13.0 l/s_1st group; (a) Angle of deviation (degree) vs cdf; (b) Longitudinal velocity vs cdf; (c) Transverse velocity vs cdf and (d) Tortuosity vs cdf.

### 4.3.3.2 Q = 13.0 l/s _ 2nd group

The cumulative distribution functions of the considered variables for experimental discharge 13.0 l/s_2nd group are shown in figure 4.32.

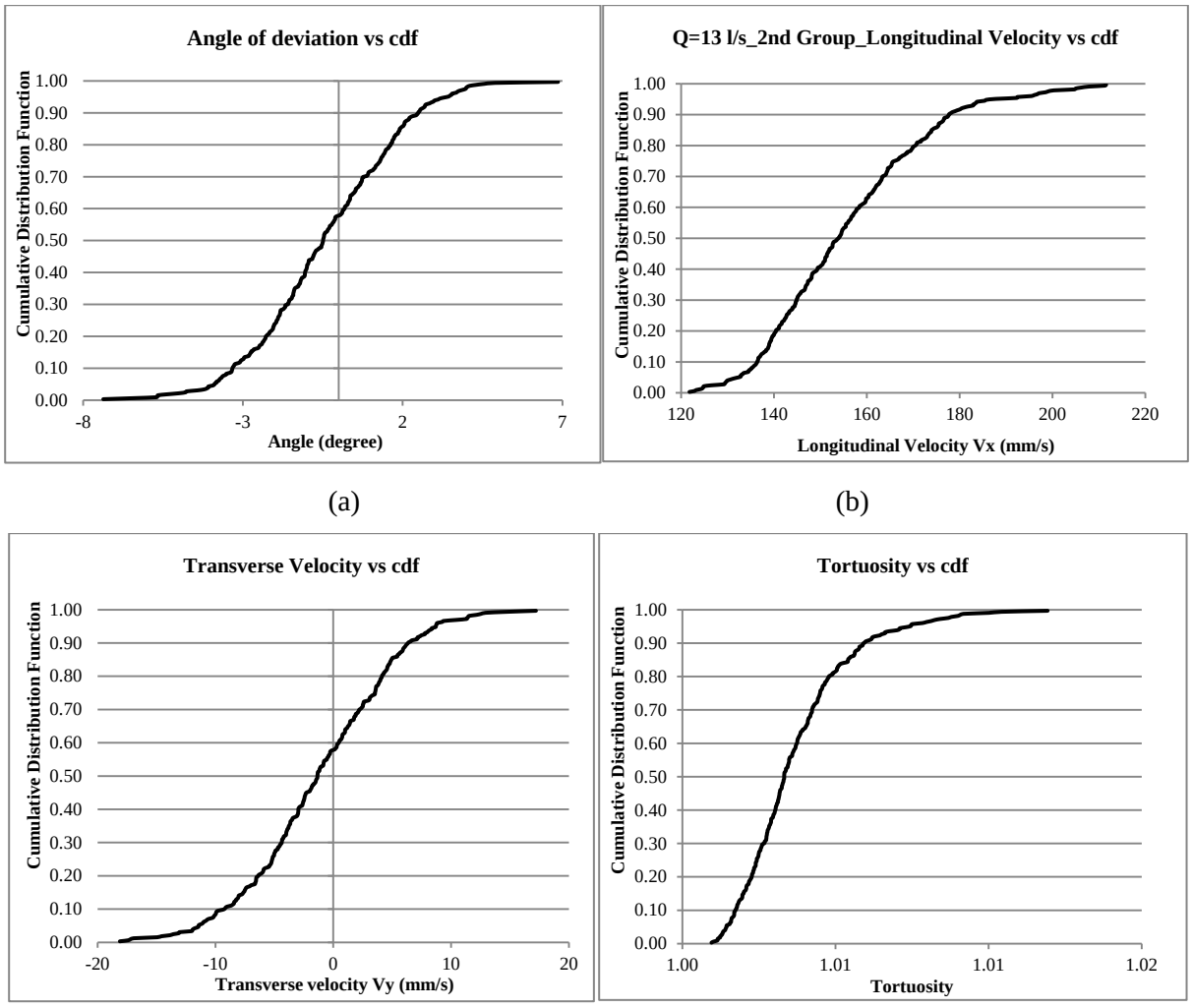


Figure 4.32: For discharge Q = 13.0 l/s_2nd group; (a) Angle of deviation (degree) vs cdf; (b) Longitudinal velocity vs cdf; (c) Transverse velocity vs cdf and (d) Tortuosity vs cdf.

### 4.3.3.3 Q = 13.0 l/s _ All (combined both group)

The cumulative distribution functions of the considered variables for experimental discharge 13.0 l/s_All (combined group) are shown in figure 4.33.

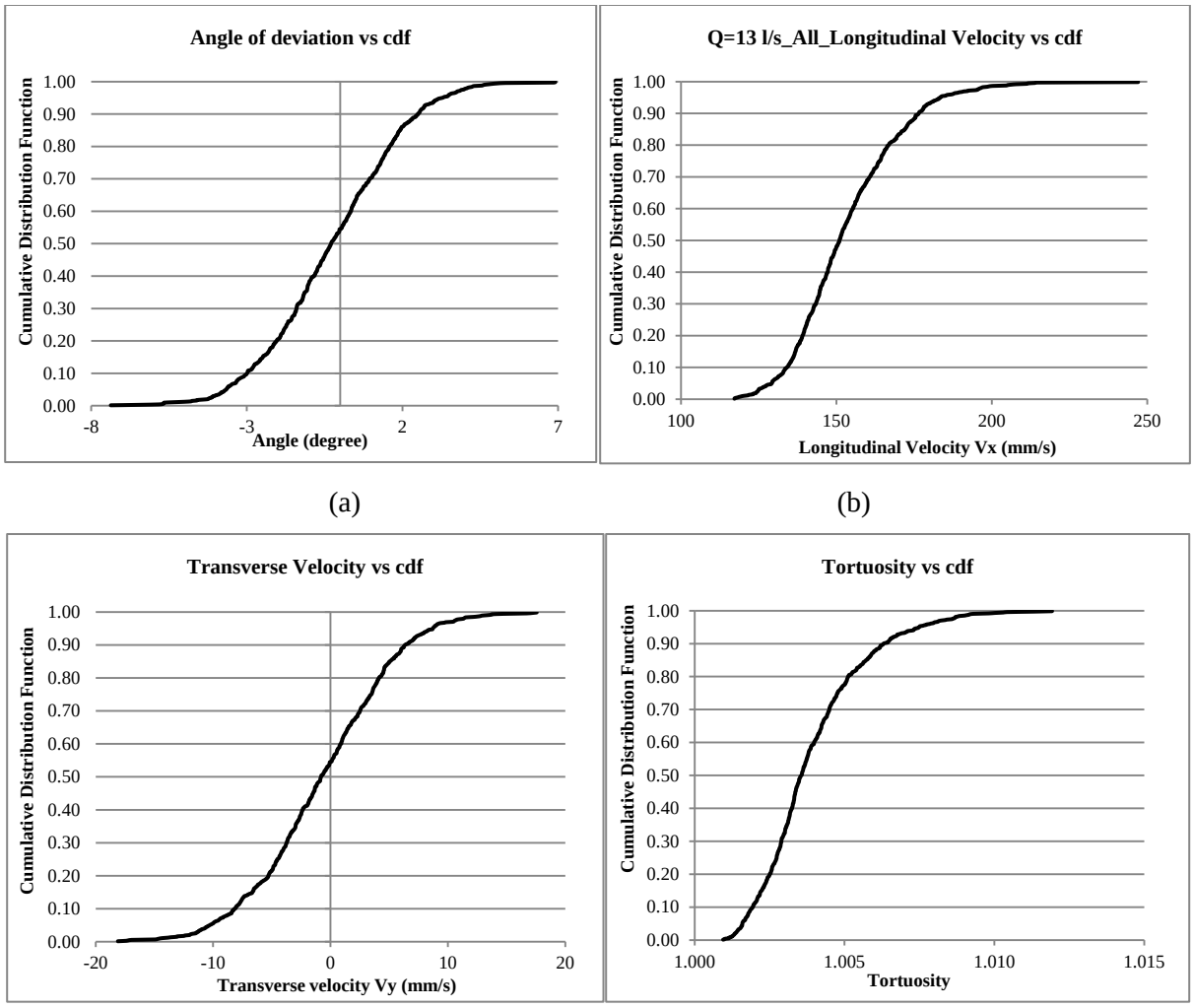


Figure 4.33: For discharge Q = 13.0 l/s_All (combined both group); (a) Angle of deviation (degree) vs cdf; (b) Longitudinal velocity vs cdf; (c) Transverse velocity vs cdf and (d) Tortuosity vs cdf.

### 4.3.3.4 Comparison of all groups of data for Q = 13.0 l/s

The cumulative distribution functions of longitudinal velocities for all groups of data for experimental discharge 13.0 l/s are shown in figure 4.34.

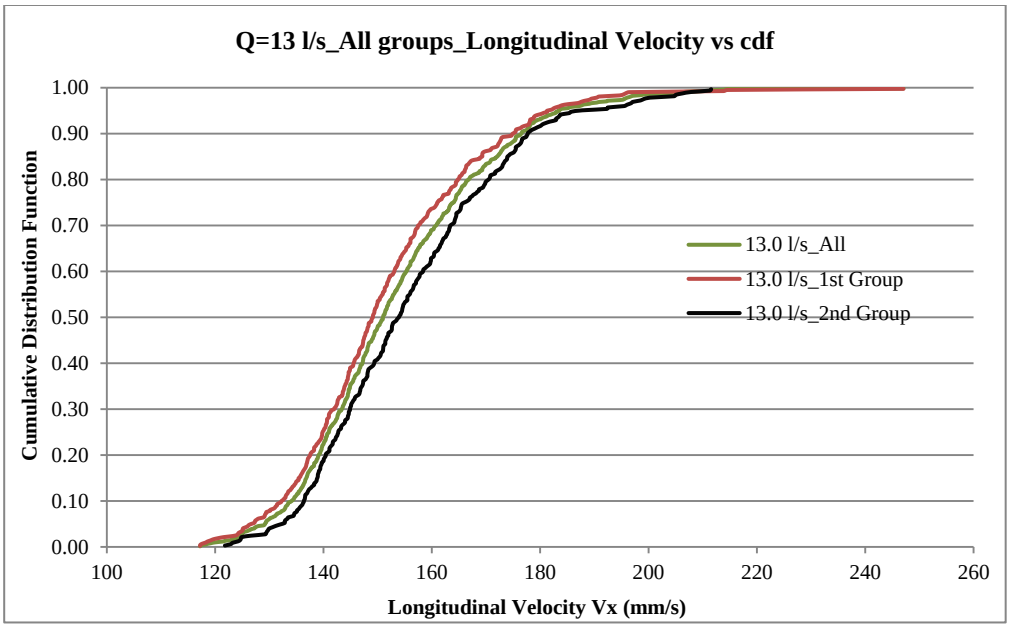


Figure 4.34: Longitudinal velocity vs cdf of all groups for discharge Q = 13.0 l/s.

It was observed that; cdfs of longitudinal velocities for all groups of data (discharge 13.0 l/s) showed a bit different behavior but similar among them. The combined group showed average shape of the other two. Individually, it was more asymmetric as left tail is shorter than right one than lower discharge 11.1 l/s. Here, 90% frequencies longitudinal velocities were around175 mm/s which was increasing with increasing discharge.

### 4.3.4 Comparison of longitudinal velocity ($V_x$)

The cumulative distribution functions have been compared with longitudinal velocity and dimensionless velocity with respect to all experimental discharges and dimensionless velocities.

#### 4.3.4.1 Longitudinal velocity cdf for all discharges

The comparison of cdfs and longitudinal velocities for all experimental discharges (8 l/s, 11.1 l/s and 13.0 l/s) is shown in figure 4.35.

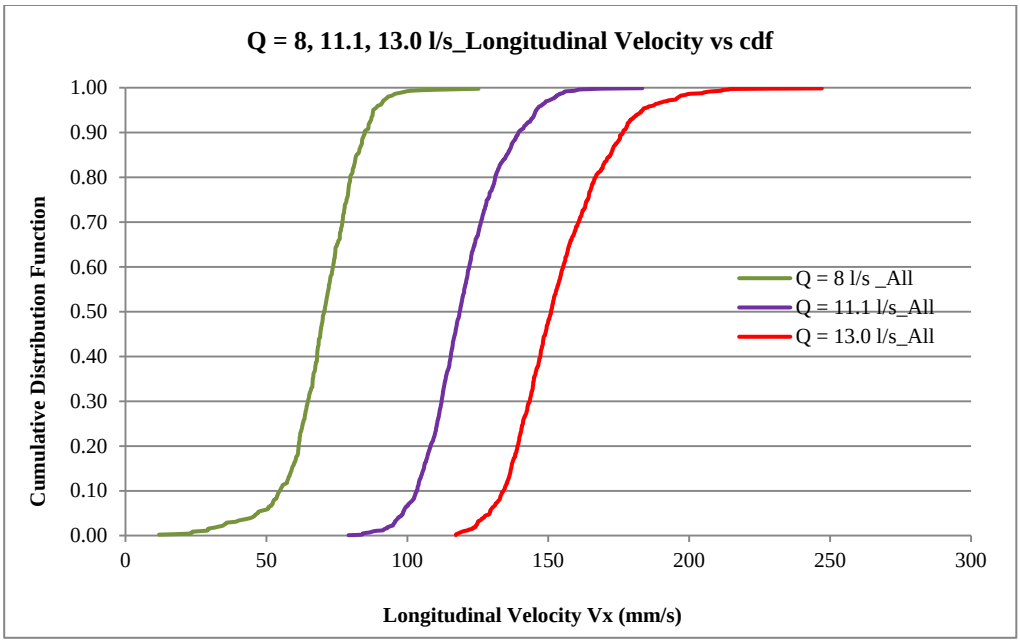


Figure 4.35: Longitudinal velocity vs cdf of all groups for all discharges.

It was observed that; cdf of longitudinal velocities became asymmetric with increasing discharge. Left tail became shorter with increasing discharge.

### 4.3.4.2 cdf with dimensionless velocity for all discharges

The comparison of cdfs and dimensionless velocities ($V_x/U$ and $V_x/U^*$) for all experimental discharges (8 l/s, 11.1 l/s and 13.0 l/s) is shown in figure 4.36.

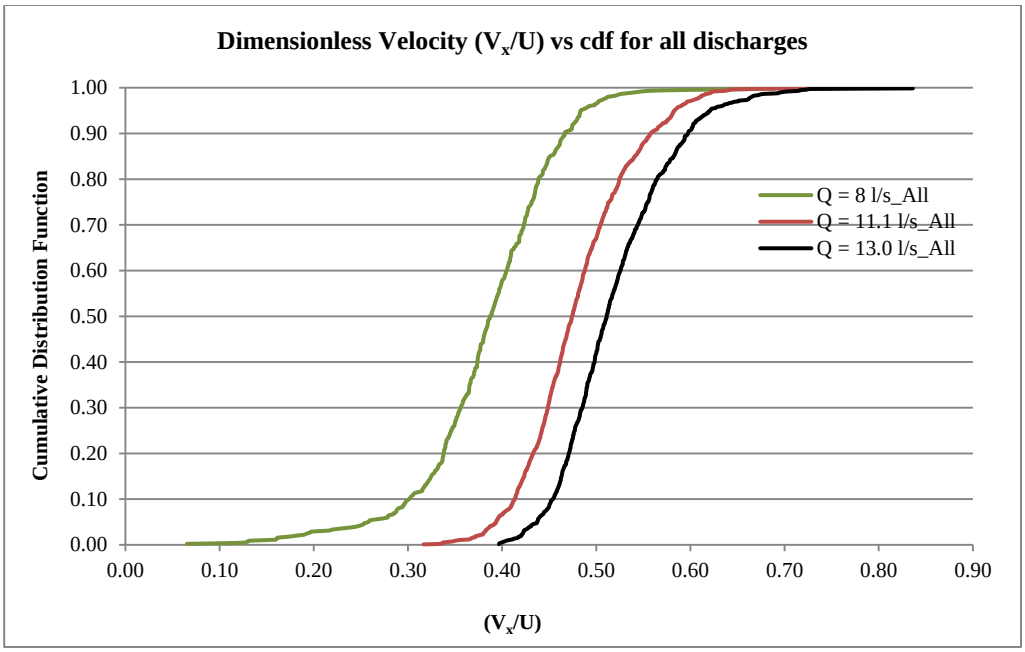


(a)

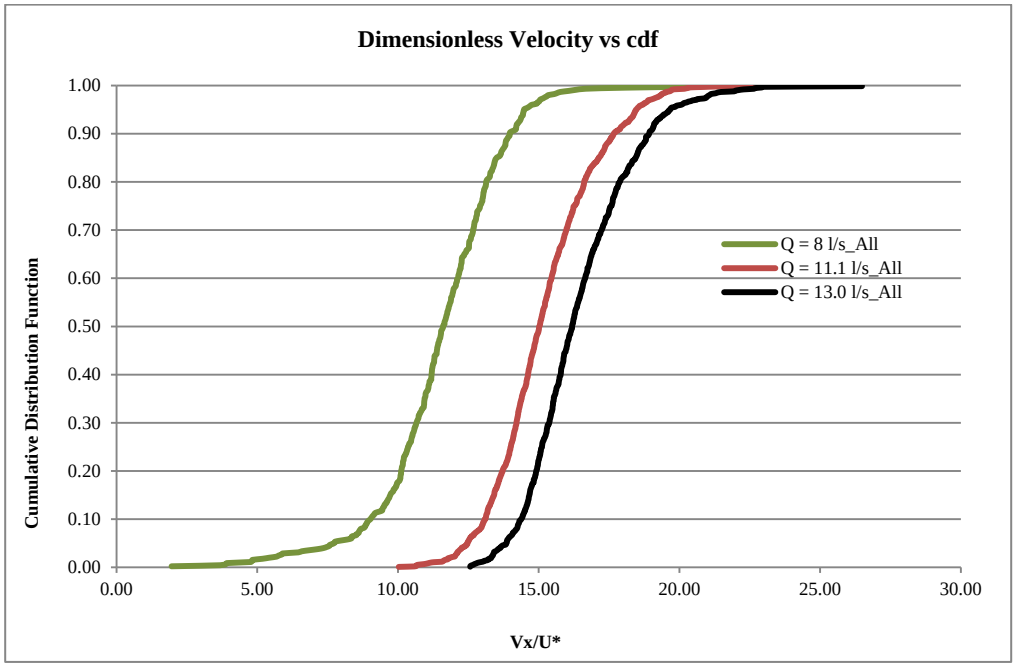


(b)

Figure 4.36: (a) Dimensionless velocity ($V_x$/U) vs cdf and (b) Dimensionless velocity ($V_x/U^*$) vs cdf for all discharge Q = 8, 11.1 & 13.0 l/s.

It was observed that; cdf for both dimensionless velocities showed the same behavior as longitudinal velocities. Left tail became shorter with increasing discharge.

# CONCLUSIONS

Extensive analysis has been performed of the characteristics of individual sediment particle motion on a smooth bed configuration, for comparison with corresponding characteristics in a rough bed configuration. The data used in this research work were obtained from an experimental campaign previously conducted at the Politecnico di Milano, using a pressure duct with transparent wall and lid, the duct being 5.8 m long with a cross section 40 cm wide and 11 cm high. Several bed conditions of the bed were used and appropriate parameters of the runs were controlled during the tests. A CCD camera with a frequency of 32 Hz was used to make movies.

The flow properties were estimated from data taken with Ultrasonic Velocity Profilers. The shear velocity for the discharge of 13.0 l/s was successfully computed, while some instrument malfunctioning prevented computation of the shear velocity for the two other discharges. These shear velocities were thus calculated assuming a linear relationship between shear velocity and bulk velocity after some assessment by the Moody diagram.

In total, for the smooth bed configuration 55 movies were processed for flow discharges of 8 l/s, 11.1 l/s and 13 l/s. Image processing has been used for particle tracking and to extract of the individual grain motion. Image filter background technique was used to avoid the background disturbance. The software Streams has been used in particle tracking; results of the latter were manually validated by superimposing the image frames and the measured particle trajectories. In total, 2219 trajectories were found and used for a statistical analysis. In post processing, the statistical parameters that have been analyzed are mean ($\mu$), standard deviation ($\delta$), coefficient of variation ($C_v$), skewness ($S_k$) and kurtosis ($K_u$) for the variables angle of deviation ($\alpha$), velocity along the flowing direction ($V_x$), velocity along the transverse direction of flow ($V_y$) and tortuosity ($T_{tor}$) as integral properties (meaning averaged over the entire length of the trajectory for which a particle was tracked). Whenever possible, a comparison with corresponding results for rough bed was performed.

Data for discharge 11.1 l/s and 13.0 l/s were apparently divided into two groups showing different properties, and have thus been analyzed separately. It was found that the difference between the two data was limited to the length of trajectory portions for

which particles had been observed, probably due to differences in lighting conditions. Following analyses of particle velocity showed no significant differences between the two groups, which could then be analyzed together.

The moving sediment angle of deviation ($\alpha$) and transverse velocity ($V_y$) had means with very small negative value, close to zero which was considered as zero, and tortuosity ($T_{tor}$) with a mean value of 1. The angle of deviation showing small negative values indicated that the camera was probably a bit skewed in comparison with the mean flow direction, but the angle was very small. The longitudinal velocity ($V_x$) was considered as the most significant property for smooth bed configuration.

From the pdf analysis with respect to dimensional and non-dimensional form, it can be concluded that, for discharge 8.0 l/s, 11.1 l/s and 13.0 l/s, the pdfs of longitudinal velocities were weakly right skewed and became more right skewed with increasing discharges. Within groups of data set for discharge 11.1 l/s, the pdfs of longitudinal velocities were same and weakly right skewed and for discharge 13.0 l/s, they were again similar and strongly right skewed. So, as previously mentioned, combined data set could be used for corresponding discharges.

The cdf analysis of longitudinal velocities with respect to dimensional and non-dimensional analysis obviously showed the same results obtained from the corresponding pdf, a cdf becoming asymmetric (with the left tail shorter than the right one) with increasing discharge.

In comparison of smooth bed analysis with rough bed configuration; it showed that shear velocity for both bed configurations increased with increasing discharge but because of higher roughness in rough bed it showed more shear velocity compared to smooth bed. As a result the mean longitudinal velocity was more in smooth bed configuration compared to rough bed. In rough bed the sediment movement on bed interrupted by bed roughness so bed longitudinal velocities were deviated more from the mean value and smooth bed velocities were more stable then rough bed data. As the sediments moved on a smooth bed, near bed velocity in smooth bed configuration was slowly increased with increasing discharges. Longitudinal velocity distribution in smooth bed configuration has a distinct peak near to mean value compare to normal distribution. It showed similar behaviour for dimensionless analysis. For rough bed

condition some particles were glued at bottom of bed to make the bed rough so the full diameter distance velocity in rough bed suddenly increased means the difference of full diameter distance velocity and half diameter distance velocity in rough bed was significantly more than the corresponding difference in smooth bed configuration. Also Rough bed velocities were more right skewed than smooth bed velocities.

As there are insufficient theoretical relationships available for prediction of the sediment particle motion, studies like that documented here can significantly contribute to advancement of knowledge. On the other hand, the analysis in this work was limited to the integral properties of moving sediments; such analysis can therefore be complemented by that of the instantaneous values of the kinematic properties of particles. In addition, exploring particle motion with different particles on different beds can support analysis of the influence that different agents (turbulence, bed roughness, other moving particles) have on sediment motion. Finally, measurement of particle motion in this work was just two dimensional (the movement of a sediment particle in the direction perpendicular to the bed plane was not considered), but the vertical movement could be included in the future to get more precise characteristics of the sediment motion.

REFERENCES


1. Achanta Ramakrishna Rao and Bimlesh Kumar; 'Friction Factor for Turbulent Pipe Flow' – Department of Civil Engineering, Indian Institute of Science, Bangalore-560012, India.
2. Zhaoding Xie; 'Theoretical and Numerical Research on Sediment Transport in Pressurized Flow Conditions' – student research, Department of Civil Engineering, University of Nebraska, Lincoln (7-19-2011).
3. Zhou Liu; 'Sediment Transport' - Laboratoriet for Hydraulik og Havnebygning, Instituttet for Vand, Jord og Miljøteknik, Aalborg Universitet (January 2001).
4. K. Whipple; 'Essentials of Sediment Transport' - 12.163/12.463 Surface Processes and Landscape Evolution. (September 2004).
5. Edward J. Hickin; 'River geomorphology', Chapter-6: River Hydraulics and Channel Form; Wiley 1995; University of California, 8 March 2009.
6. Courtney K. Harris; 'Sediment transport processes in coastal environments' - January 16, 2003.
7. Leo C, Van Rijn; 'Sediment transport; Part-ii: Bed load transport'- Journal of hydraulic engineering, Volume 110, No 11; November 1984 ASCE.
8. Dr David Apsley; 'Introduction to Sediment Transport' – Autumn 2013.
9. T.G., Drake, R.L. Shreve, W.E. Dietrich, P.J. Whiting, L.B. Leopold. Bedload transport of fine gravel observed by motion-picture photography, J. Fluid Mech., 192, 1998, 193-217 p.
10. Edward J. Hickin; 'River geomorphology', Chapter-4: Sediment Transport; Wiley 1995; University of California, 8 March 2009.
11. J. Campagnol, A. Radice, F. Ballio. Insight on how Bed Configuration Affects Properties of Bed Load Motion. Politecnico di Milano, Dept. I. I. A. R., 2012. (The abstract is sent and approved for conference, CSE6 Paris - August 27-31, 2012).
12. Nikora, V., H. Habersack, T. Huber, I. McEwan. On bed particle diffusion in gravel bed flows under weak bed load transport. American Geophysical Union, Water Resources. Research, Vol. 38, № 6, 2002, 17-26 p.
13. A. Radice, F. Ballio, R. Nokes. Preliminary results from an application of PTV to bed-load grains. River flow 2010 – Dittrich, Koll, Aberle & Geisenhainer, 2010, 1681 – 1686 p.
14. Alessio Radice, Vladimir Nikora, Jenny Campagnol, Francesco Ballio; Active interactions between turbulence and bed load: Conceptual picture and experimental evidence. - Water Resources Research,Volume 49, Issue 1, pages 90–99, January 2013.

15. Hans Albert Einstein; Sediment Transportation Research. Engineering and Science Monthly. August-September, 1944.
16. Einstein, H. A. (Hans Albert). Bed-load functions for sediment transportation in open channel flows. Washington, U.S. Dept. of Agriculture, 1937, 71p.
17. Nokes, R.; Streams, version 2.01: System Theory and Design, Department of Civil & Natural Resources Engineering, University of Canterbury, New Zealand, March 2013.
18. A. Radice, S. Malavasi, F. Ballio. Solid transport measurements through image processing, Exp. Fluids, 41, 2006 721-734 p.
19. Katherine Heays, Heide Friedrich and Bruce W. Melville; Re-evaluation of Image Analysis for Sedimentary Processes Research. Department of Civil and Environmental Engineering, The University of Auckland, Private Bag 92019, Auckland, New Zealand.
20. A. Radice, F. Ballio, V. Nikora. On statistical properties of bed load sediment concentration, Institute of Geophysics, Polish Academy of Sciences. vol. 58, no. 6, pp. 1072-1093 DOI: 10.2478/s11600-010-0020-y (2010).
21. E. Lajeunesse, L. Malverti, F. Charru. Bed load transport in turbulent flow at the grain scale: experiments and modeling. Journal of Geophysical research. Vol 115, F04001, 2001.
22. B. S. Kevin, A. Sam, W. Peter & E. Darren. The use of particle tracking in sediment transport studies: a review; Coastal and Shelf Sediment Transport. Special Publications, 274, 73–91. 0305-8719/07, The Geological Society of London 2007.
23. Bergami, G. (2012). Misura e analisi del moto dei sedimenti nel trasporto solido. B.Sc. Thesis, Politecnico di Milano, Milan, Italy.
24. Campagnol, J. (2012). Characterization of bed load sediment transport at the grain scale. Ph.D. Thesis, Politecnico di Milano, Milan, Italy.
25. Lescova, A. (2012). Effect of bed roughness on lagrangian properties of bed-load sediment transport. M.Sc. Thesis, Riga Technical University, Riga, Latvia.
26. Bulankina, V. (2012). Lagrangian analysis of bed-load particle motion. M.Sc. Thesis, Riga Technical University, Riga, Latvia.